Towards a purposeful construction of a new generation of artificial reefs : Comparative analyses of the intrinsic factors favouring their colonization from micro to macro-scale

Elisabeth Riera

▶ **To cite this version:**

Elisabeth Riera. Towards a purposeful construction of a new generation of artificial reefs : Comparative analyses of the intrinsic factors favouring their colonization from micro to macro-scale. Earth Sciences. Université Côte d'Azur, 2020. English. NNT : 2020COAZ4001 . tel-03000490

HAL Id: tel-03000490

https://theses.hal.science/tel-03000490v1

Submitted on 11 Nov 2020

HAL is a multi-disciplinary open access archive for the deposit and dissemination of scientific research documents, whether they are published or not. The documents may come from teaching and research institutions in France or abroad, or from public or private research centers.

L'archive ouverte pluridisciplinaire **HAL**, est destinée au dépôt et à la diffusion de documents scientifiques de niveau recherche, publiés ou non, émanant des établissements d'enseignement et de recherche français ou étrangers, des laboratoires publics ou privés.

UNIVERSITÉ CÔTE D'AZUR

ÉCOLE DOCTORALE
SCIENCES FONDAMENTALES ET APPLIQUÉES

THÈSE DE DOCTORAT

Vers une construction raisonnée d'une nouvelle génération de récifs artificiels : Analyses comparatives des facteurs intrinsèques favorisant leur colonisation de la micro à la macro-échelle

---

Towards a purposeful construction of a new generation of artificial reefs: Comparative analyses of the intrinsic factors favouring their colonization from micro to macro-scale

Elisabeth RIERA

UMR 7035 ECOSEAS / UMR 7802 BOREA

Présentée en vue de l'obtention du grade de Docteur en Sciences de L'environnement **de** l'Université Côte d'Azur
Dirigée par :
Patrice FRANCOUR (Pr., UCA)
Cédric HUBAS (HDR, MNHN-Paris)
Soutenue le : 21/01/2020

Devant le jury, composé de :
Philippe LENFANT, (Pr., UPVD)
Gérald CULIOLI (HDR, Université de Toulon)
Denis ALLEMAND (Pr., CSM)
Sylvain PIOCH (CM, Université Paul Valéry Montpellier III)
Paolo GUIDETTI (Pr., UCA)
Dominique LAMY (CM, UPMC)
Jacqueline Gautier Debernardi (Gestionnaire des AMP de Monaco)

ECOSEAS
ECOLOGY AND CONSERVATION SCIENCE FOR SUSTAINABLE SEAS

Vers une construction raisonnée d'une nouvelle génération de récifs artificiels : Analyses comparatives des facteurs intrinsèques favorisant leur colonisation de la micro à la macro-échelle

---

Towards a purposeful construction of a new generation of artificial reefs: Comparative analyses of the intrinsic factors favouring their colonization from micro to macro-scale

Elisabeth RIERA

UMR 7035 ECOSEAS / UMR 7802 BOREA

Présentée en vue de l'obtention du grade de Docteur en Sciences de L'environnement de l'Université Côte d'Azur

Dirigée par :

Patrice FRANCOUR (Pr., UCA)

Cédric HUBAS (HDR, MNHN-Paris)

Soutenue le : 21/01/2020

Devant le jury composé de :

Président :

Paolo GUIDETTI (Pr., UCA)

Rapporteurs :

Philippe LENFANT, (Pr., UPVD)

Gérald CULIOLI (HDR, Université de Toulon)

Examinateurs :

Denis ALLEMAND (Pr., CSM)

Sylvain PIOCH (CM, Université Paul Valéry Montpellier III)

Invités :

Dominique LAMY (CM, UPMC)

Jacqueline Gautier Debernardi (Gestionnaire des Aires Marine Protégés de Monaco)

RESUME

Les récifs artificiels sont des structures immergées posées délibérément sur le fond marin pour imiter certaines caractéristiques d'un habitat naturel, ils sont utilisés depuis des milliers d'années par les hommes dans le but d'améliorer leurs pratiques de pêches et depuis peu ils sont également employés pour la protection voire la restauration de certains habitats marins. Malgré ces divers objectifs, il réside encore un manque de fondements scientifiques pour déterminer la qualité de ces structures mises à l'eau afin d'en évaluer leur efficacité. Les présent travaux, focalisés sur l'étude de leurs caractéristiques intrinsèques, à savoir leurs matériaux et leurs structures

Un suivi conjugué du biofilm et du macrofouling sur différents matériaux, complété par une analyse de leur contenu en métaux lourds a permis de mettre en évidence la qualité de certains matériaux utilisé pour la construction de récifs artificiel. Le suivi simple du biofilm s'est révélé être un bon indicateur pour mettre en valeur ces différences de façon simple et rapide pour valider l'utilisation de tel ou tel matériau.

Par ailleurs, la mise au point d'une méthode destinée à évaluer la complexité et l'hétérogénéité des récifs artificiels a permis de donner une classification pertinente des différentes structures existantes. Cette méthode standardisée permettra d'évaluer *in situ* l'influence des paramètres structuraux des récifs artificiels sur le recrutement, l'abondance, la distribution et/ou la diversité. Une première étude à l'échelle microscopique a permis de révéler l'influence de la structure du matériau à la fois sur l'abondance du biofilm et sur l'activité photosynthétique de ces communautés.

L'ensemble de ces résultats permet d'offrir un cadre scientifique plus précis pour aborder la construction des récifs artificiels sur le choix de leurs matériaux et de leurs designs. De futures lignes directrices pourraient être émises afin d'optimiser l'efficacité de tout projet d'immersion de récifs artificiels.

Mots-clés : Récif artificiels, colonisation des récifs artificiels, matériaux des récifs artificiels, structure des récifs artificiels, biofilm, macrofouling, substances polymériques extracellulaires, métagénomique, chromatographie en phase liquide, contamination en métaux lourds, Imaging Pam, modèle numérique 3D CAD, Complexité, hétérogénéité

ABSTRACT

Artificial reefs are submerged structures deliberately placed on the seabed to mimic some characteristics of a natural habitat, they have been used for thousands of years by fishermen to improve their fishing practices and recently they are also used for the protection or even the restoration of certain marine habitats. Despite these various objectives, there is still a lack of scientific fundaments for determining the quality of these submerged structures in order to assess their effectiveness. The present works, focused on the study of their intrinsic characteristics, namely their materials and their structures.

A combined monitoring of the biofilm and the macrofouling on different substrates, supplemented by an analysis of their heavy metal content allowed to highlight the quality of certain substrates used for the construction of artificial reefs. Simple monitoring of the biofilm has proven to be an efficient indicator for highlighting these differences to validate the use of a particular substrate.

In addition, the development of a method to assess the complexity and heterogeneity of artificial reefs has enabled us to give a relevant classification of the various existing structures. This standardized method will allow to assess *in situ* the influence of structural parameters of artificial reefs on recruitment, abundance, distribution and/or diversity. A first study at the microscopic scale revealed the influence of substrate structure on both the abundance of biofilm and the photosynthetic activity of these communities.

A more precise scientific framework is now available to guide the construction of artificial reefs on the choice of materials and the design of artificial reef structures in order to optimize the effectiveness of artificial reef immersion project.

Keywords: Artificial reefs, colonisation of artificial reefs, artificial reef substrates, biofouling, , artificial reef structure, biofilm, macrofouling, extracellular polymeric substances, metagenomic, Hight performance liquid chromatography, heavy metals contamination, Imaging Pam, 3D CAD model, complexity, Heterogeneity.

AVANT-PROPOS

En 2010, la Société Boskalis, société néerlandaise d'assistance maritime aux travaux offshore spécialisée dans les travaux de dragage, travaille sur un projet d'implantation de récifs coralliens en Jamaïque. Madame Astrid KRAMER, ingénieur environnement, lance une étude sur les récifs artificiels et découvre un article présentant un inventeur italien, Monsieur Enrico DINI, Président de la Société Dini Engineering et concepteur d'une imprimante 3D qu'il utilise pour créer des récifs artificiels avec du sable. L'idée lui vient de réaliser des récifs avec du sable de dragage, un produit naturel plus adapté que le béton habituellement utilisé. Son projet remporte en 2014 le « Challenge de l'innovation » qui permet aux collaborateurs de la Société Boskalis de présenter des idées innovantes.

Peu de temps après, Son Altesse Sérénissime le Prince Albert II de Monaco en visite officielle aux Pays-Bas, accompagné de Son Excellence Monsieur Bernard FAUTRIER, Vice-Président de la Fondation Prince Albert II de Monaco, rencontre plusieurs industriels dont les représentants de la Société Boskalis qui présentent le concept de récifs artificiels réalisés avec une imprimante 3D. Le caractère innovant de ces récifs permet à la Société Boskalis de mettre en place dès 2015 un projet pilote à Monaco, coordonné par Madame Jamie LESCINSKI, ingénieur en océanographie, en partenariat avec la Fondation Prince Albert II de Monaco et Madame Jacqueline GAUTIER-DEBERNARDI, Directeur de l'Association Monégasque pour la Protection de la Nature (AMPN), gestionnaire des aires marines protégées de Monaco à qui revient le soin de mettre en œuvre ce projet dans l'aire marine protégée du Larvotto.

L'expertise du Professeur Patrice FRANCOUR (UMR ECOSEAS), spécialiste des populations de poissons et des récifs artificiels a permis d'imaginer le design des récifs en bénéficiant des avantages liés à la technologie de l'impression 3D. Un design complexe, proche de la réalité du milieu naturel, a offert la possibilité de reconstituer les habitats spécifiques d'espèces patrimoniales. Le Professeur Patrice FRANCOUR a par la suite lancé un programme de recherche sur l'étude de la structure des récifs artificiels. Ce programme a été complété par l'étude de la qualité du matériau en collaboration avec les Docteurs Cédric HUBAS et Dominique LAMY (UMR BOREA) à travers le travail de Master 2 et de Doctorat de Mademoiselle Elisabeth RIERA.


Jacqueline Gautier
Debernardi
S.E. Bernard
Fautrier
Cédric Hubas &
Dominique Lamy
Elisabeth Riera
Patrice Francour
BOREA
ECOSEAS
Astrid Kramer &
Jamie Lescinski
Enrico Dini
Boskalis
d-shape

A Patrice

L'Invitation au voyage

Mon enfant, ma sœur,
Songe à la douceur
D'aller là-bas vivre ensemble !
Aimer à loisir,
Aimer et mourir
Au pays qui te ressemble !
Les soleils mouillés
De ces ciels brouillés
Pour mon esprit ont les charmes
Si mystérieux
De tes traîtres yeux,
Brillant à travers leurs larmes.

Là, tout n'est qu'ordre et beauté,
Luxe, calme et volupté.

Des meubles luisants,
Polis par les ans,
Décoreraient notre chambre ;
Les plus rares fleurs
Mêlant leurs odeurs
Aux vagues senteurs de l'ambre,
Les riches plafonds,
Les miroirs profonds,
La splendeur orientale,
Tout y parlerait
À l'âme en secret
Sa douce langue natale.

Là, tout n'est qu'ordre et beauté,
Luxe, calme et volupté.

Vois sur ces canaux
Dormir ces vaisseaux
Dont l'humeur est vagabonde ;
C'est pour assouvir
Ton moindre désir
Qu'ils viennent du bout du monde.
– Les soleils couchants
Revêtent les champs,
Les canaux, la ville entière,
D'hyacinthe et d'or ;
Le monde s'endort
Dans une chaude lumière.

Là, tout n'est qu'ordre et beauté,
Luxe, calme et volupté

Baudelaire (1821-1867), Les Fleurs du Mal (1857)

CLAUDE LORRAIN : MATIN DANS LE PORT (II) – 1640S -CONSERVE AU MUSEE DE L'HERMITAGE A SAINT PETERSBOURG

REMERCIEMENTS

L'aventure de cette thèse est une conjugaison de belles rencontres, d'émotions fortes et d'une solidarité sans relâche avec l'ensemble des personnes qui ont parcouru ce chemin à mes côtés de loin ou de près. J'ai eu la chance de pouvoir changer d'atmosphère dans les deux coins les plus extrêmes de la France : Nice-Concarneau = 875 km à vol d'oiseau. Malgré la variété des modes de transport en commun et d'escales que j'ai pu tester, je n'ai toujours pas trouvé le moyen de traverser la France en moins de 8h. Mais le voyage en valait la peine. J'ai pu apprécier la sympathie des bretons, la danse gracieuse des phoques dans les laminaires, les paysages lunaires des fonds granitiques, l'eau glaciale et vivifiante de l'Atlantique (ton astuce des cailloux réchauffés avant la marée montante, je n'y crois pas Cédric !), le caramel au beurre salé, les crêpes de chez Masson et les maisons aux atmosphère étranges… Merci à Franck et Marie de m'avoir sauvée des griffes de la sorcière de Concarneau !

Comme il est de coutume, je m'essaie à l'exercice des remerciements en sachant qu'il est inévitable que j'oublie certain(e)s d'entre vous. Au-delà de la coutume, ces remerciements sont des plus sincères car sans votre soutien à tous je ne serais pas en train d'écrire ces dernières lignes qui clôturent l'écriture de mon manuscrit.

Je voudrais tout d'abord remercier Patrice Francour qui de son vivant et après son départ m'a portée pour devenir la chercheuse que je suis aujourd'hui. Depuis les années de licence, c'est à travers ses cours que mon parcours jusqu'à la thèse s'est dessiné. Son aura, qui se passe de parole, a toujours suscité en moi un profond respect à son égard. Ses encouragements m'ont poussée à partir à Paris pour poursuivre mes études au MNHN où j'ai rencontré Cédric Hubas, mon co-directeur. Durant ces trois années passées aux côtés de Patrice, j'ai pu développer mon esprit scientifique, engager des collaborations, construire des projets. En l'observant sous l'eau, j'ai appris à être plus économe, plus observatrice, à gagner en confiance tout en restant vigilante, à trouver des solutions méthodologiques dans ce milieu particulier qui restreint bien souvent les possibilités. Ses gestes calmes et précis m'ont toujours apaisée, la mer était son milieu. J'aime l'idée d'imaginer Patrice dans le grand bleu, entouré d'un cortège de mérous près de la Gabinière, savourant paisiblement son souffle éternel. Il reste près de moi à travers ce travail. Je sais que notre amour commun pour la Méditerranée me liera à lui pour toujours.

Mes pensées se tournent évidemment vers Jacqueline Gautier-Debernardi, sa compagne et mon amie. J'admire ta force de caractère et ta détermination pour continuer. Sans toi, toute cette aventure n'existerait pas, sans toi il n'y aurait pas ce brin de folie pour décoincer nos esprits un peu trop rigides de scientifiques. Malgré la tempête, tu continues à être enthousiaste et curieuse, tu gardes ton beau sourire et ton sens de l'humour. C'est cette belle étincelle qui ne faiblit jamais qui a sûrement séduit ta saupe. Je suis si heureuse de pouvoir continuer à travailler à tes côtés pour poursuivre tout ce que nous avons mis en place ensemble avec Patrice. Je te remercie également pour ton aide dans cette dernière ligne droite, sans toi la qualité de ce manuscrit serait largement réduite. Je t'embrasse avec mes milliers de ventouses de Poulpinette.

Malgré la distance de 875 km à vol d'oiseau qui nous sépare, le soutien de mon co-directeur, a été sans relâche. Cédric, je te remercie pour ton écoute et pour tes mots qui ont toujours su me ramener à l'essentiel tout en considérant mes difficultés. Je te remercie pour ta confiance lorsque je t'ai proposé le sujet du stage de Master 2. Merci d'avoir cédé à mon obsession de la microtopographie du matériau en trouvant des moyens de tester cette hypothèse à travers le projet LIMIT. Merci pour ton accueil à Concarneau et pour ce jogging sur le sentier des douaniers que j'ai pris comme une épreuve symbolisant le chemin vers la soumission du manuscrit. Le parcours a été rude, mais j'ai enfin réussi toutes les étapes tel un padawan à tes côtés ! J'espère que notre collaboration se poursuivra au-delà de la thèse, car j'aime beaucoup travailler avec toi. J'admire la rigueur et l'intégrité de ta démarche scientifique, teintée d'un désir de créer des liens avec diverses disciplines. Avec toi, le champ des possibles semble toujours pouvoir s'élargir.

Merci à tous mes collègues d'ECOSEAS, votre bienveillance dans le contexte particulier de ma fin de thèse m'a apporté beaucoup de courage et de joie. Merci à Paolo pour ton soutien à la fin de mon parcours, tes mots envers Patrice m'ont tant touchée. Merci à ceux qui m'ont prêté main forte lors de mes périodes de terrain (je pense à Virginie, Marie-Jeanne, Jean-Michel en particulier). Merci à Natacha qui a rendu toutes mes tâches administratives plus fluides, merci pour ton écoute et ta gentillesse. Merci à Martina pour tes fous rires et tes pièces de théâtre improvisées, tu vas nous manquer ! Merci à Benoît pour toutes tes initiatives ''écoterroristes'', ton dynamisme est un vrai moteur dans le labo. Merci également pour le 38 rue André Theuriet, un vrai petit nid douillet ! Merci à Francesca pour ta confiance pour

poursuivre ensemble le projet de recherche sur les récifs artificiels initié avec Patrice. Merci à Claudia, Emna, Sylvaine, Patricia, Elena, Margalida, Alexis, Eugenio, Alexandre, Antonio & Antonio, votre présence a rendu cette expérience bien plus amusante. Mes poulettes et ma cocotte, sans vous au labo, c'est un peu moins rigolo, (heureusement le copain marseillais est encore là, Marseille en force !!!!), mais je sais qu'au-delà des distances notre amitié reste forte. Merci pour votre douceur, votre écoute et vos rires.

Special Thanks to Elena, the thesis gave me the gift to meet you. Together in the same storm we encourage each other to accomplish all the baby steps that lead us to the creation of our fantastic little lizard. You have been the closest to me even if you were so far away.

Merci à mes collègues de BOREA avec qui j'ai partagé de beaux moments au labo et sur Paris. Votre accueil a toujours été des plus chaleureux. Je pense plus particulièrement à Dominique qui a beaucoup participé à l'élaboration de mon projet de thèse depuis le Master 2. Merci pour ta douceur et ta compréhension. Merci à Tarik pour tes dattes, tes jujubes et tes paroles ensoleillées lorsque je venais vous rendre visite. Merci à Najet pour ton accueil, ton franc-parler, heureusement que tu étais là pour veiller sur moi lorsque j'étais all by myself dans le labo. Merci à Guillaume, Sylvia et Franck pour les échanges toujours intéressants que nous avons eus lorsque nous nous sommes retrouvés.

Merci à mes stagiaires.

À Thomas Gutierrez qui n'était pas loin de ressembler à un lapin atteint de myxomatose à la suite des séances d'identification. J'admire ton abnégation à vouloir identifier le turf, ton travail a été de qualité, je te remercie mille fois.

À Axel Munerol, pour avoir réalisé mon rêve de l'étude de la microtopographie et de son influence sur les communautés de biofilm. Merci pour tout ce travail de fourmi sur le repositionnement des patchs.

À Emma Faveau, qui a amorcé les premières digestions et analyses des contenus en métaux lourds dans les pièges à sédiments.

Merci à l'équipe de Thierry Virolle, de l'IBV, sans qui je n'aurais pas pu conserver mes centaines d'échantillons, et qui a mis à ma disposition tout le matériel nécessaire afin que je puisse appliquer certains de mes protocoles sur le biofilm.

Merci à Stéphane Jamme et Jérôme Espla d'avoir immortalisé des scènes insolites de ma vie subaquatique en compagnie de mes collègues et de Patrice.

Maman, je pense que lorsque tu m'apprenais à dessiner des maisons selon la perspective, tu m'as inoculé une vision tridimensionnelle qui a sûrement eu une influence majeure sur ma façon d'aborder la complexité de la structure des habitats. Ta voix d'architecte devait me parlait tout bas pour orienter ma manière d'aborder mon sujet de thèse. Merci pour ton écoute quand ça n'allait pas, merci d'avoir toujours été là pour m'aider dans les étapes charnières de ma vie.

Papa, quand tu m'as mis pour la première fois un masque et un tuba sur la tête et des petites palmes aux pieds, tu ne te doutais pas que ce premier baptême dans les eaux claires de la lagune de Gaou allait déterminer la passion qui m'a menée jusqu'à ce projet de thèse. C'est en vous suivant, toi et Frédéric, à l'Estagnol, à Hyères, à Sète, dans tous les coins que tu connaissais, que mon amour pour la Méditerranée a grandi. Merci de m'avoir appris à lire et à comprendre la nature à tes côtés.

Merci à vous deux d'avoir cru en moi et de m'avoir donné la possibilité de m'engager même tardivement dans cette voie scientifique.

Mon frère, ton influence sur mon parcours est incontestable, je ne serais jamais allée si loin sans toi. Tu m'as entraînée dans ta soif de connaissance et ton besoin de comprendre le vivant, l'humain, les étoiles, la terre. Tout sujet que tu abordes est pour toi une source inépuisable de questions et un terrain de jeu pour ton esprit analytique et créatif. J'admire l'intelligence et la sensibilité de ton esprit. Ton soutien dans mes phases de doute a toujours su me ramener à celle que je suis, car tu me connais mieux que personne. Merci Piquick.

Merci au plus méchant des méchants qui depuis des années me supporte et me pousse à persévérer dans cette voie malgré les sacrifices que cela engage sur notre couple. Je t'ai rencontré sous l'eau, il n'y a pas de signe plus clair pour décrire l'évidence de notre union. La réussite de ce projet te revient aussi. Tu as constamment veillé à ce que je ne "mange pas des pierres", dans mes rêves ton corps a été le cobaye de mes calculs de la dimension fractale et ton brin de folie a su apaiser mes angoisses. Sans toi, je me serais probablement transformée en méchant Gremlins. Ta patience est sans limite. Merci ce Chat.

Alain, tu serais très fier de celle que je suis devenue. Merci d'avoir éveillé en moi le besoin d'aller toujours chercher de nouvelles perspectives.

Merci à Toutoune, tu as toujours cru en moi. Ton attention et ta bienveillance m'ont poussée à poursuivre mes rêves.

Papi Lili et Mamie Odile, de là où vous êtes je vous envoie toute ma reconnaissance et je vous remercie pour les belles valeurs que vous nous avez inculquées.

Merci à Antoine, tu m'as appris le sens de l'abnégation et de la rigueur. Je n'en serais pas là sans ton aide.

Merci à mes caillettes de Marseille, vous avez toujours cru en mes projets, votre soutien m'a toujours été extrêmement précieux. Même si la vie rend nos retrouvailles de plus en plus rares, je vous sens toujours près de moi.

Merci à l'association de Plongée IEMANJA et à Serge Vermillac, mon formateur en plongée loisir. Merci pour ta bienveillance et ta formation de qualité, tu m'as donné la confiance et la vigilance essentielles pour aborder la plongée dans le monde professionnel.

Thanks to the Plan Blue team for the nice moments spent underwater with the hyperspectral camera, and the others to come.

‹°)))>< <°)))>< ‹°)))>< ‹°))>< ‹°)))><

J'en viens maintenant à adresser des remerciements plus formels à toutes les parties prenantes ainsi qu'à tous ceux qui ont collaboré à ce projet :

Les gestionnaires des aires marines protégées de Roquebrune Cap Martin et de Monaco qui ont facilité mes expérimentations in situ.

Le Conseil d'Administration de l'AMPN sans qui ce projet n'aurait pu voir le jour. Merci pour votre confiance et votre bienveillance à mon égard. Merci d'avoir mis à ma disposition vos moyens à la mer et vos locaux pour conduire mes travaux sur le terrain. Je remercie également les adhérents qui m'ont régulièrement prêté main forte.

La Société Boskalis dont l'implication depuis le début du projet et la générosité ont permis de développer la base de mes travaux de recherche sur le suivi du biofouling en mettant notamment à disposition les multiples échantillons de matériaux nécessaires aux diverses analyses.

Monsieur Enrico Dini, Président de la Société Dini Engineering et concepteur de l'imprimante 3D utilisée pour les récifs immergés en Principauté de Monaco, dont la maîtrise de la technologie de l'impression 3D à grande échelle et la conscience de son intérêt pour créer des récifs artificiels innovants, le conduit aujourd'hui à poursuivre notre collaboration dans le cadre d'un prochain programme de recherche.

Les Sociétés Créocéan et Geolab dont le savoir-faire et la méthodologie en matière de modélisation par photogrammétrie sous-marine m'ont permis de tester ma méthode d'évaluation de la structure de l'habitat sur le milieu naturel, et dont les résultats ont été présentés lors de la 5ème conférence européenne sur la plongée scientifique en avril 2019 à l'Institut d'Océanologie de l'Université des Sciences de Sopot (Pologne).

L'équipe de THALASSA Marine research & Environmental awareness pour leur professionnalisme, leur disponibilité, leur soutien et leur bonne humeur durant tous les suivis mis en place sur le terrain.

Le Gouvernement Princier de Monaco pour avoir permis la réalisation du projet d'immersion des récifs et avoir facilité la mise en œuvre de mes travaux de recherche.

Les mécènes privés qui, par le soutien apporté aux projets mis en place par l'AMPN depuis la création des aires marines protégées de Monaco, ont permis de mener à bien les différents axes de recherche sur les récifs artificiels.

La Fondation Prince Albert II de Monaco qui est à l'origine du projet d'immersion à Monaco de récifs artificiels réalisés avec une imprimante 3D et s'est engagée dans un programme de financement visant à valoriser les travaux de recherche qui en découlent.

© Stéphane Jamme – Les Aquanautes

TABLE DES MATIERES

RESUME **4**

ABSTRACT **5**

AVANT-PROPOS **7**

REMERCIEMENTS **12**

TABLE DES MATIERES **20**

TABLE DES TABLES **24**

TABLE DES ILLUSTRATIONS **25**

I. INTRODUCTION GENERALE **32**

1. CONTEXTE GLOBAL 33
2. HISTORIQUE ET DEFINITION DES RECIFS ARTIFICIELS 34
3. ETAT DE L'ART DES CARACTERISTIQUES INTRINSEQUES DES RECIFS ARTIFICIELS 39
4. COLONISATION DES RECIFS ARTIFICIELS 41
5. INFLUENCE DES CARACTERISTIQUES INTRINSEQUES DES RECIFS ARTIFICIELS SUR LA COLONISATION 44
6. HYPOTHESES 47

II. CHAPTER 1: BIOFILM MONITORING AS A TOOL TO ASSESS THE EFFICIENCY OF ARTIFICIAL REEFS AS SUBSTRATES: TOWARD 3D PRINTED REEFS **49**

RESUME 50

ABSTRACT 51

1. INTRODUCTION 52
2. MATERIALS & METHODS 55
   - *2.1. Sampling and site of monitoring* *55*
   - *2.2. Pigment analysis* *56*
   - *2.3. Extraction of Polymeric substances* *56*
   - *2.4. Quantification of carbohydrate concentration by colorimetric assay* *57*
   - *2.5. Amino acid composition of polymers by HPLC* *58*
   - *2.6. Data analysis* *59*
3. RESULTS 60
   - *3.1. Pigment analysis* *60*
   - *3.2. Sugar and protein concentration dynamics on the different substrates* *63*
   - *3.3. Amino acid composition* *64*

3.4. Principal Component Analysis 66
4. DISCUSSION 68
CONCLUSIONS 72
III. CHAPTER 2: COLONISATION OF ARTIFICIAL REEF SUBSTRATES: "THE HABIT DOES NOT MAKE THE MONK." 74
RESUME 75
ABSTRACT 77
1. INTRODUCTION 78
2. MATERIALS & METHODS 80
2.1. Substrates 80
2.2. Monitoring and sampling 80
2.3. Biofilm analysis 83
2.4. Macrofouling identification 84
2.5. Heavy metals analyses 85
2.6. Statistical analyses 86
3. RESULTS 89
3.1. Temperature and sedimentation rates during the monitoring 89
3.2. Structure of the biofilm microbial communities 90
3.3. Sugars and proteins content in the Extracellular Polymeric Substances (EPS) of the biofilm 95
3.4. Macrofouling communities 97
3.5. Heavy metals in sinking and suspended POM and virgin substrates 102
4. DISCUSSION 106
CONCLUSION 111
IV. CHAPTER 3: STUDY THE COMPLEXITY OF ARTIFICIAL REEFS FROM THE MICRO TO THE MACRO SCALE 113
PART 1: TOWARD A PURPOSEFUL DESIGN OF ARTIFICIAL REEFS: A FIRST METHOD TO ASSESS THEIR STRUCTURAL COMPLEXITY AND HETEROGENEITY 114
RESUME 115
ABSTRACT 116
1. INTRODUCTION 117
2. MATERIAL & METHOD 120
2.1. The numerical object of artificial reefs and fictive objects 120

2.2. Normalization of the 3D CAD models and process of the input. 122
2.3. Point clouds and normals 123
2.4. Combination of modules 124
2.5. Evaluation of the structure 124
2.6. Data analysis 128
3. RESULTS 129
3.1. 3D fictive 3D CAD models 129
3.2. Evaluation of the structure of the AR modules 130
3.3. Combination of modules 135
4. DISCUSSION 136
CONCLUSION 139
PART 2: LINK BETWEEN MICROTOPOGRAPHY AND PHOTOSYNTHETIC BIOFILM PHYSIOLOGY AT DIFFERENT SCALES 140
RESUME 141
ABSTRACT 142
1. INTRODUCTION 143
2. MATERIEL & METHOD 144
2.1. Substrates of artificial reefs and natural rock 144
2.2. Characterization of the surface topography 144
2.3. Analyse of biofilm activity by Imaging PAM 146
2.4. scale 148
3. RESULTS 149
3.1. Characterisation of the surface of substrates at the global scale 149
3.2. Characterisation of the biofilm activity with Imaging PAM and correlation with complexity indexes 150
4. DISCUSSION 153
CONCLUSION 155
V. DISCUSSION GENERALE 157
CONCLUSION 164
RÉFÉRENCES 169
ANNEXES 185

TABLE DES TABLES

Table II-1:Composition of the solutions used in the modified LOWRY assay protocol . 57

Table II-2: HPLC solvents for amino acid detection..... 58

Table II-3: Mean proportion of pigments over time on each substrate (Cg: grey concrete, Ds: dolomite Sorel cement, Cw: white concrete) 62

Table II-4: Means of sugar to protein ratio over time on each substrate (Cg: grey concrete, Ds: dolomite Sorel cement, Cw: white concrete) 64

Table II-5: Mean proportion of amino acids over time on each substrate (Cg: grey concrete, Ds: dolomite Sorel cement, Cw: white concrete) 65

Table IV-1:Indexes computed on the 3D fictive 3D CAD models and evaluation of the global complexity (C) 129

Table IV-2: Indexes computed on the artificial reef's modules and evaluation of average values for all the modules..... 130

Table IV-3: Index and score of the different combinations of artificial reefs..... 135

Table IV-4: Mean of the complexity indices on the three substrates (concrete, dolomite, rock) on the total surface 149

TABLE DES ILLUSTRATIONS

Figure I-1 :Illustration japonaise représentant l'utilisation de gabions en bambou ('jakagos') remplis de pierres utilisés pour lutter contre l'érosion des rivières au VIIIe siècle et comme récifs artificiels au XVIIe siècle (source : http://kmcenter.rid.go.th/kcdesign/dblog/wp-content/uploads/2009/10/history-and-method-of-Gabion1TCNPF-o-Compatibility-Mode.pdf) 34

Figure I-2 : Dispositifs de concentration de poissons "Kannizzati", destinés à fournir de l'ombre aux poissons, utilisés dans la partie méridionale du bassin central de la Méditerranée, à Malte et en Sicile (source : Bombace 1989)..... 35

Figure I-3 : Illustration de diverses structures artificielles déployées dans les mers européennes : a) Languedoc-Roussillon, France; b), c) Nienhagen, Allemagne (bouches d'égout, d'après NICKELS et al., 2006); d), e) Grèce; f) Sicile, Italie; g) Réserve du Larvotto, Monaco (www.gouv.mc), h) Nordfjorden, Norvège (d'après HARTVIG, 2007); i), j) Algarve, Portugal; k) Odessa, Ukraine (de COLLINS, www.soes.soton.ac.uk), l) Pool Bay, Royaume-Uni (de COLLINS, www.soes.soton.ac.uk) (source : Fabi et al. 2011) 36

Figure I-4 : Exemple de récifs artificiels conçus par impression 3D : a) conception D-Shape, immergé en 2010 à Bahreïn (source : https://d-shape.com/artificial-reefs/) b) conception Reef Design Lab, immergé en 2013 aux Maldives (source : https://www.reefdesignlab.com/) c) conception Sea-Boost/X-Tree, immergé en 2019 au Parc national des Calanques à Marseille (http://www.xtreee.eu/project-rexcor-artificial-reef/). ... 37

Figure I-5 : Illustration des étapes du projet d'immersion de récifs artificiels conçus par impression 3D (Boskalis/D-Shape) en Principauté de Monaco : a) impression du récif, b) état du module après impression et excavation du matériau excédent, c) immersion d'un module en Principauté de Monaco, d) état d'un module après quelques jours d'immersion, e) f) état d'un module après 2 ans d'immersion (crédit photos : Boskalis, Patrice Francour, Jean-Michel Mille-AMPN, Stéphane Jamme-Les Aquanautes)..... 38

Figure I-6 :Illustration de récifs artificiels réalisés à partir de pneus : a) projet Tire Artificiel Reefs (TAR) immergés en 1997 à Hong Kong (source :

https://www.maoandpartners.com/tyre-artifical-reefs/), b) pneus immergés dans les années 1970 à Fort Lauderdale (Floride) dans le but de créer un récif artificiel (source : http://www.geologyin.com/2015/10/floridas-tire-reef-has-turned-into.html) 40

Figure I-7 : Illustration du biofouling : a) schéma illustrant le processus de colonisation du biofilm en cinq étapes: 1) phase d'attachement réversible, 2) phase d'attachement irréversible avec production de la matrice extracellulaire, 3) croissance verticale du biofilm 4) biofilm mature, 5) dispersion du biofilm (source : Bixler & Bhushan 2012), b) paysage d'un biofilm microbien colonisant un environnement sédimentaire, la structure des colonies est fonction des flux (en agrégat au niveau des flux lents, en filament au niveau des flux rapides) créant des micro-perturbations qui induisent une dispersion des organismes (source : Battin et al. 2007), c) topographie 3D d'un biofilm composé principalement de diatomées (Amphora sp. Et Navicula sp.) sur des panneaux immergés pendant 3 semaines à Southampton (Royaume-Uni). Le trait pointillé blanc indique la section illustrée en d) représentant la topographie de la surface du biofilm (source : (Salta et al. 2013), e) surface en bois immergée à Southampton (Royaume-Uni) pendant 20 mois avec une communauté complexe de macrofouling comprenant des algues corallines, des vers turbicoles, des éponges et des algues. (source : (Salta et al. 2013) 42

Figure I-8 : Illustration de l'arrangement des récifs artificiels selon l'échelle du module (source : Cépralmar 2015) 46

Figure II-1: Variation of pigment concentration over time on the different substrates (dashed line: grey concrete Cg, solid line: dolomite Sorel cement Ds, dotted line: white concrete Cw). (Van-der-Waerden test on substrates: p= 0.867) 60

Figure II-2: Variation of (A) sugar concentration (equivalent glucose) and of (B) protein concentration (equivalent BSA) over time on the different substrates (dashed line: grey concrete Cg, solid line: dolomite Sorel cement Ds, dotted line: white concrete Cw). (Van-der-Waerden test on substrates: sugar: p = 0.0315; proteins: p = 0.322) 63

Figure II-3: Principal component analysis: A) Ordination of the samples according to sampling time (d01: first day, d07: 1 week, d14: 2 weeks, d28: 4 weeks, d35: 5 weeks) and substrates (red star: grey concrete, green triangle: dolomite Sorel cement, brown circle: white

concrete). B) Correlation circle of the pigments variables (Carotens: Carot., Chl.a: Chlorophyll a, Chl.b: Chlorophyll b, Chl.c: Chlorophyll c, Pheo.: Pheopigments, Anth.: Antheraxanthin, Diadino.: Diadinoxanthin, Diato.: Diatoxanthin, Fuc.: Fucoxanthin, Hex.fuc.: Hex-fucoxanthin, Pras.: Prasinophyte, Zea.: Zeaxanthin) and supplementary variables (sugar and protein concentrations)..... 66

Figure III-1: Map of the two Marine Protected Areas (MPA) selected for the sampling design: The Larvotto reserve (Monaco) with a highly artificialized coast and Roquebrune Cap Martin (France) with a natural coast 81

Figure III-2: Sampling design for the monitoring of the biofilm and macrofouling on 3 different substrates (Concrete, Dolomite, Rock) in two different Marine Protected Area (Larvotto MPA of Monaco, and MPA of Roquebrune Cap Martin), and analyses related to both monitoring 82

Figure III-3: A) Average temperature of the sea, B) average sedimentation rate during biofilm and macrofouling monitoring at Monaco and Roquebrune. 89

Figure III-4: A) PcoA computed on the Bray Curtis dissimilarity matrix of the relative abundance of the bacterial classes ≥ 1 % sequencing in the biofilm over the monitoring period (D07, D14, D21, D28), at both sites (Monaco and Roquebrune), and on each substrate (concrete, dolomite, rock). Samples are ordinated according to clusters determined by cascade Kmean (5 clusters: Calinski Criterion 84.20, SSE: 4.23). B) The relative abundance of bacterial classes ≥ 1% of each cluster and its hierarchical classification 92

Figure III-5: A) PcoA computed on the Bray Curtis dissimilarity matrix of the relative abundance of pigments detected by HPLC in the biofilm over the monitoring period (D07, D14, D21, D28), at both sites (Monaco & Roquebrune), and on each substrate (concrete, dolomite, rock). Samples were ordinated according to clusters determined by cascade Kmean (4 clusters: Calinski Criterion 89.1, SEE: 6.09), B) Relative abundance of the type of pigments of each cluster and its hierarchical classification 94

Figure III-6: Mean concentration of sugars (glucose equivalence) and proteins (BSA equivalence) detected by colorimetry at each sampling period (T07, T14, T21, T28), at both sites

(Monaco and Roquebrune) and on each substrate (concrete, dolomite, rock). Grey zone corresponds to the confidence interval 96

Figure III-7: Mean total macrofouling dry weight (mg.cm^{-2}) over time, on both sites and on the three different substrates. Grey zone corresponds to smoothed conditional means .. 97

Figure III-8: A) Venn diagrams representing the taxa for each season: B) substrates, C) and sites. Gamma diversity computed with specific richness, Shannon index and Pielou index of equitability for each season, site, and substrate 99

Figure III-9: PcoA computed on the Bray Curtis dissimilarity matrix of the relative abundance of the dry weight of macrofouling taxa family from Aug. 2017 to Apr. 2018, on each substrate (concrete, dolomite, rock): A) Monaco community, B) Roquebrune community. Samples are ordinated according to clusters determined by cascade Kmean (Monaco: 2 clusters: Calinski Criterion: 30.60, SEE: 29.52; Roquebrune: Calinski Criterion 84.20, SSE: 4.23), C) Relative abundance of Families of each cluster 101

Figure III-10: Heavy metals concentration (ppm) in the biofilm, the macrofouling, the 3 virgin substrates and suspended material in sinking during biofilm and macrofouling monitoring 102

Figure III-11: Principal component analysis on the percentage of heavy metals within the biofilm, the sinking material and the virgin substrates used for the biofilm monitoring at D28 on both sites (Monaco and Roquebrune): A) Correlation circle of the variables, B) and ordination of the samples on the first two dimensions 104

Figure III-12: Principal component analysis on the percentage of heavy metals within the macrofouling, the marine POMl and the virgin substrates in April 2018 on both sites (Monaco and Roquebrune): A) Correlation circle of the variables, B) and ordination of the samples on the first two dimensions 105

Figure IV-1: Fictive 3D CAD models generated on Tinkercad. The surface of a simple cube has been refolded three times, and tree different cavities have been added 120

Figure IV-2: Samples of Artificial reef modules from Tessier et al.2015 generated on Tinkercad and model from Boskalis (scales are not respected)..... 121

Figure IV-3: BOSK module and its bounding box computed on MeshLab..... 122

Figure IV-4: Representation of the point cloud of BOSK modules. on the left: the 3D CAD model with vertices highlighted in yellow, on right: the 3D CAD model with the normal of each vertex computed in blue..... 123

Figure IV-5: Values of SDnz (A) and Dn (B) computed on the fictive model with different density of point clouds (points per unit squared: 1, 5, 10, 15 and 20)..... 129

Figure IV-6: K-means cascade on the AR modules according to computed with Euclidean distance on the scaled value of the complexity variables (Dn, SDnz, Topo, and Poro), and Calinski criterion, groups ranging between 2 and 8: A)Comparison of the k-means repartitions of the AR modules according to the number of groups in each partition, B) and their value of the Calinski criterion 132

Figure IV-7:Principal component analysis: A) correlation circle of the variable of complexity (Dn, SDnz, Topo, and Poro) and supplementary quantitative variable the index of complexity "C", B) and the factor map of the artificial reef's modules, C) coloured ordination according to the optimal clustering computed by K-means cascades with Calinski criterion. 134

Figure IV-8: Example of a light curve (A) fited with the model of Eilers and Peeters (B) used to find the values of Ek and ETRmax 148

Figure IV-9: Surface scan image of the different substrates (from left to right: dolomite, concrete, rock)..... 149

Figure IV-10: Absorbance of the biofilm by imaging PAM on the different substrates (concrete, dolomite & rock)..... 150

Figure IV-11: Different Imaging PAM-parameters on cobblestone number 3 of concrete 151

Figure IV-12: Correlogram of the microtopography complexity indices and the Imaging Pam indices on the three substrates (concrete, dolomite, rock) according to the three scale scales studied (Small, medium, big), the gradient scale corresponds to the correlations, from the red to blue from negative to positive, framed values show significant correlations at p <0.05 152

I. INTRODUCTION GENERALE

1. Contexte global

Les activités anthropiques des cinquante dernières années conduisent à un déclin sans précédent de la nature et de la biodiversité à toutes les échelles (Mace et al. 2005). Les derniers rapports de la plateforme intergouvernementale sur la biodiversité et les services écosystémiques (IBPES) sont alarmants et nous révèlent les conséquences de ce déclin sur l'ensemble des services écosystémiques dont nous dépendons. En Méditerranée, de nombreuses espèces marines sont menacées en raison de la surpêche, de la réduction de leurs aires de répartition liée à la pollution et la destruction de leurs habitats, des impacts du changement climatique, ou encore de la progression des espèces exotiques envahissantes. Aujourd'hui, 74% des habitats benthiques méditerranéens sont menacés (Clemens et al. 2018). De plus, l'ensemble des pratiques traditionnelles autour de la mer, telles que la pêche artisanale, sont menacées par les nouvelles technologies permettant d'obtenir des rendements de pêche plus élevés.

Malgré ces sombres constats, des « changements transformateurs » économiques, sociétaux, politiques et technologiques peuvent nous permettre de conserver et de restaurer la nature. Il est donc de première nécessité de mettre au service de cette transformation l'ensemble des connaissances scientifiques disponibles pour orienter notre système socio-écosystème mondial vers une utilisation durable des services écosystémiques que la nature nous offre. Outre la protection des zones côtières/marines qui passe par la mise en place d'aires marines protégées, des solutions de restauration ou d'aménagement visant à valoriser et soutenir les pratiques d'exploitation durable de la mer sont aussi à envisager. Il est important d'identifier les usages autour de ces territoires menacés et d'apporter des améliorations à leur mise en place et à leur suivi afin de concilier protection de la nature et services rendus aux populations.

2. Historique et définition des récifs artificiels

Les récifs artificiels sont à ce titre utilisés depuis des milliers d'années par les hommes pour améliorer leurs pratiques de pêches. En immergeant des structures, les pêcheurs attirent des espèces présentant un fort intérêt et améliorent ainsi leurs prises. Aux Etats Unis, les premières installations référencées remontent aux années 1830 ; des assemblages de bûches et de pierres avaient été placés dans des bras de mer au sud de la Californie pour remplacer des arbres morts et favoriser la pêche de sparidés (Stone 1985). Au Japon, les premières pratiques remontent au XVIIème siècle ; des pêcheurs de l'île d'Awaji, près de Köbe, dans la mer de Seto eurent l'idée de remplacer une vielle épave très productive – délabrée par un typhon – par un assemblage de gabions composé de paniers en bambou remplis de pierres (Thierry 1988, Figure 2-1). En Europe, et plus particulièrement dans la partie méridionale du bassin central de la Méditerranée, l'utilisation de dispositifs de concentration de poissons (DCP) remonte à la Rome antique. Ces DCP appelés *"Kannizzati"* à Malte ou *"Incannizati"* en Sicile sont encore utilisés aujourd'hui (Bombace 1989, Figure 2-2).

Figure I-1 :Illustration japonaise représentant l'utilisation de gabions en bambou ('jakagos') remplis de pierres utilisés pour lutter contre l'érosion des rivières au VIIIe siècle et comme récifs artificiels au XVIIe siècle (source : http://kmcenter.rid.go.th/kcdesign/dblog/wp-content/uploads/2009/10/history-and-method-of-Gabion1TCNPF-o-Compatibility-Mode.pdf)

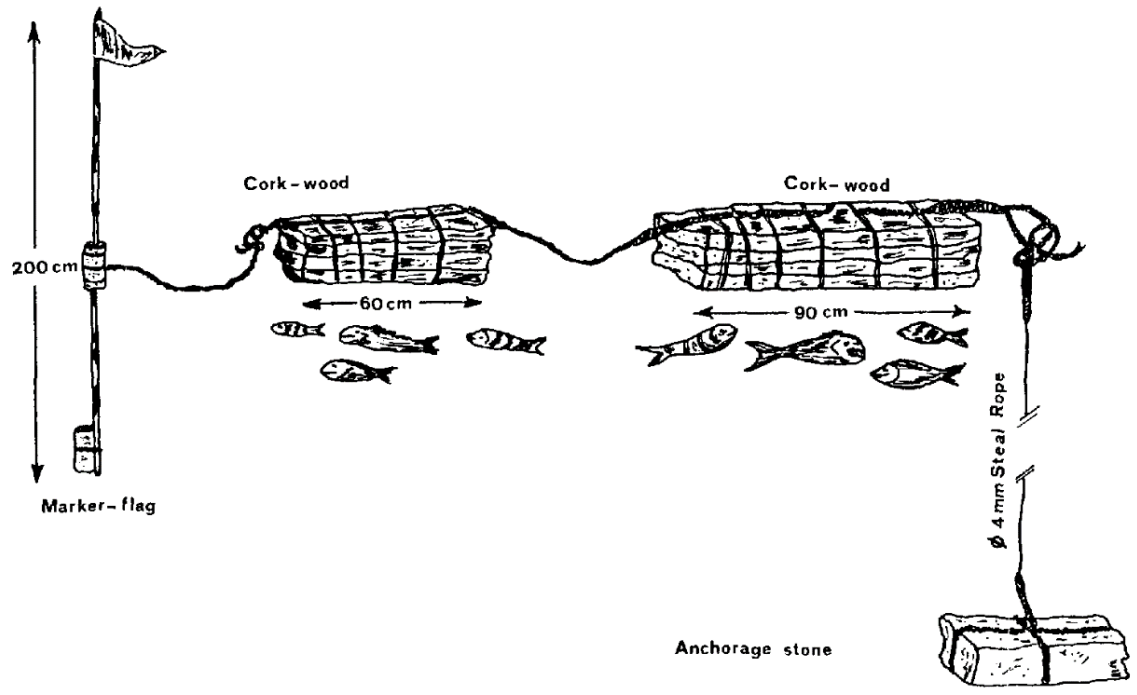

Figure I-2 : Dispositifs de concentration de poissons "Kannizzati", destinés à fournir de l'ombre aux poissons, utilisés dans la partie méridionale du bassin central de la Méditerranée, à Malte et en Sicile (source : Bombace 1989)

A partir des années 1960, l'immersion de structures artificielles s'est multipliée partout dans le monde selon des initiatives locales, sans suivi ni cadre scientifique. L'usage de matériaux de recyclage (ex : vieux pneus, carcasses de voitures, épaves de bateaux) a progressé sans se soucier des impacts sur l'environnement en termes de pollution (Pickering et al. 1998, Tessier et al. 2015). Au cours des années 70/80, ces initiatives se sont structurées et des programmes spécifiques ont été développés (Figure I-3). En 1974, l'organisation de la première *International Conference on Artificial Reef and Related Aquatic Habitats* (CARAH) au Texas (USA) a permis d'initier l'échange d'informations et d'attirer l'attention de la communauté internationale sur le potentiel des récifs artificiels dans la gestion de la pêche. A cette époque, l'Europe était encore peu impliquée dans ce consortium international. Ce n'est qu'après la cinquième conférence du CARAH (California (USA), 1991) qu'un groupe de scientifiques européens s'est organisé pour fonder le *European Artificial Reef Research Network* (EARRN) en 1994 (Jensen et al. 2000).

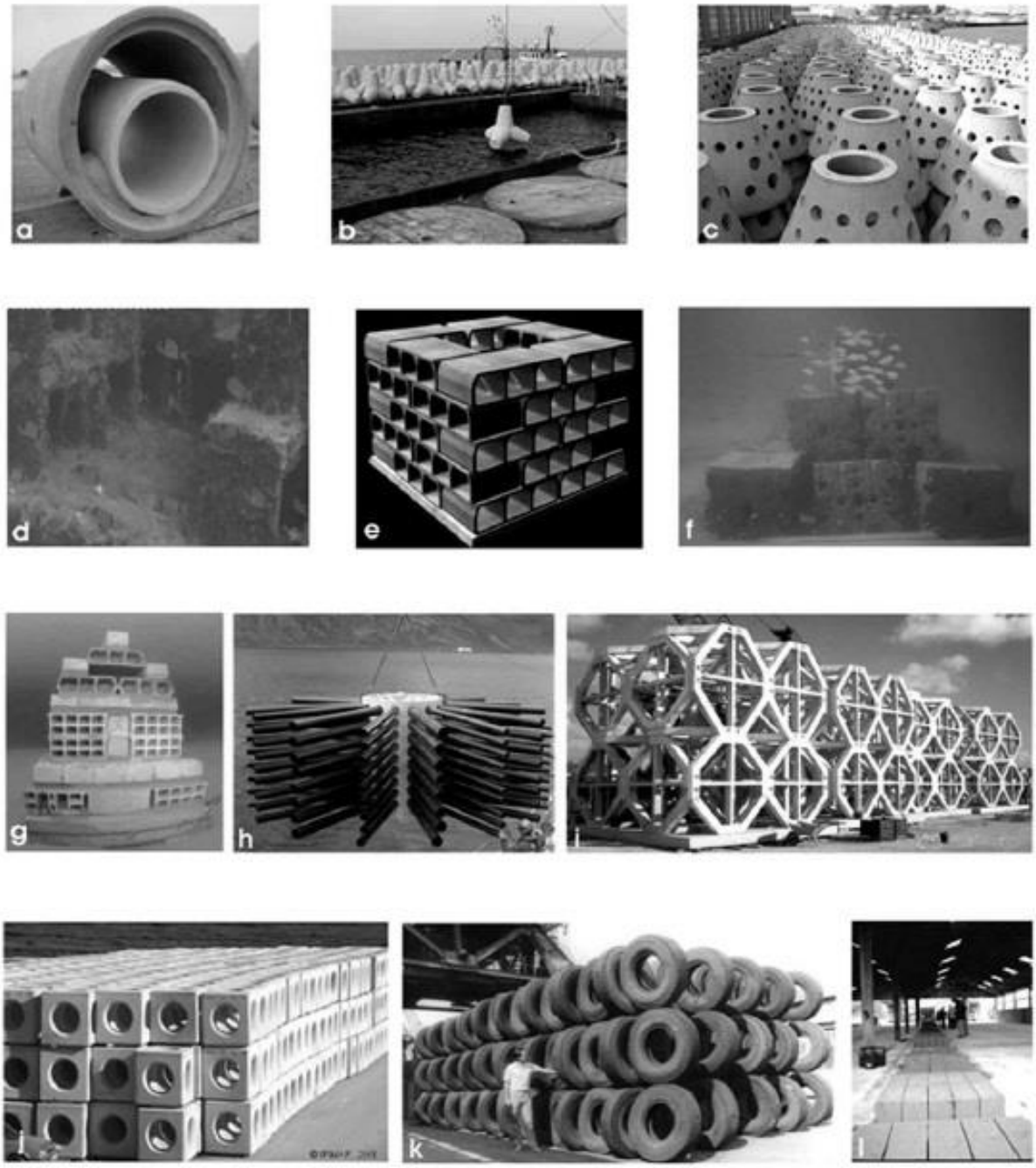

Figure I-3 : Illustration de diverses structures artificielles déployées dans les mers européennes : a) Languedoc-Roussillon, France; b), c) Nienhagen, Allemagne (bouches d'égout, d'après NICKELS et al., 2006); d), e) Grèce; f) Sicile, Italie; g) Réserve du Larvotto, Monaco (www.gouv.mc), h) Nordfjorden, Norvège (d'après HARTVIG, 2007); i), j) Algarve, Portugal; k) Odessa, Ukraine (de COLLINS, www.soes.soton.ac.uk), l) Pool Bay, Royaume-Uni (de COLLINS, www.soes.soton.ac.uk) (source : Fabi et al. 2011)

Enfin, c'est au cours des années 2000 que des premières lignes directrices ont été publiées par le programme des Nations Unies pour l'environnement, donnant une définition claire des récifs artificiels et de leurs objectifs (UNEP MAP 2005, UNEP 2009) :

« Un récif artificiel est une structure immergée posée délibérément sur le fond marin pour imiter certaines caractéristiques d'un récif naturel telles que la protection, la régénération, la concentration et/ou l'amélioration des populations de ressources marines vivantes.

Les objectifs d'un récif artificiel peuvent également inclure la protection, la restauration et la régénération des habitats aquatiques, ainsi que la promotion de la recherche, des possibilités de loisirs et de l'utilisation éducative de la région.

Le terme n'inclut pas les structures submergées délibérément placées pour remplir des fonctions non liées à celles d'un récif naturel - telles que brise-lames, amarre, câbles, pipelines, appareils de recherche marine ou plates-formes - même si, de manière incidente, elles imitent certaines fonctions d'un récif naturel. »

Figure I-4 : Exemple de récifs artificiels conçus par impression 3D : a) conception D-Shape, immergé en 2010 à Bahreïn (source : https://d-shape.com/artificial-reefs/) b) conception Reef Design Lab, immergé en 2013 aux Maldives (source : https://www.reefdesignlab.com/) c) conception Sea-Boost/X-Tree, immergé en 2019 au Parc national des Calanques à Marseille (http://www.xtreee.eu/project-rexcor-artificial-reef/).

A la suite de ces directives et grâce au progrès technologique, une nouvelle génération de récifs artificiels a vu le jour avec l'utilisation d'imprimantes 3D de grande taille permettant de proposer un design plus complexe que les modules des générations précédentes aux formes simples et géométriques (Figure I-3, Figure I-4). Un projet en particulier, mené en Principauté de Monaco, a proposé un design mimant la complexité naturelle des habitats rocheux et s'est

efforcé de développer un matériau se rapprochant des propriétés chimiques du milieu marin (Figure I-5).

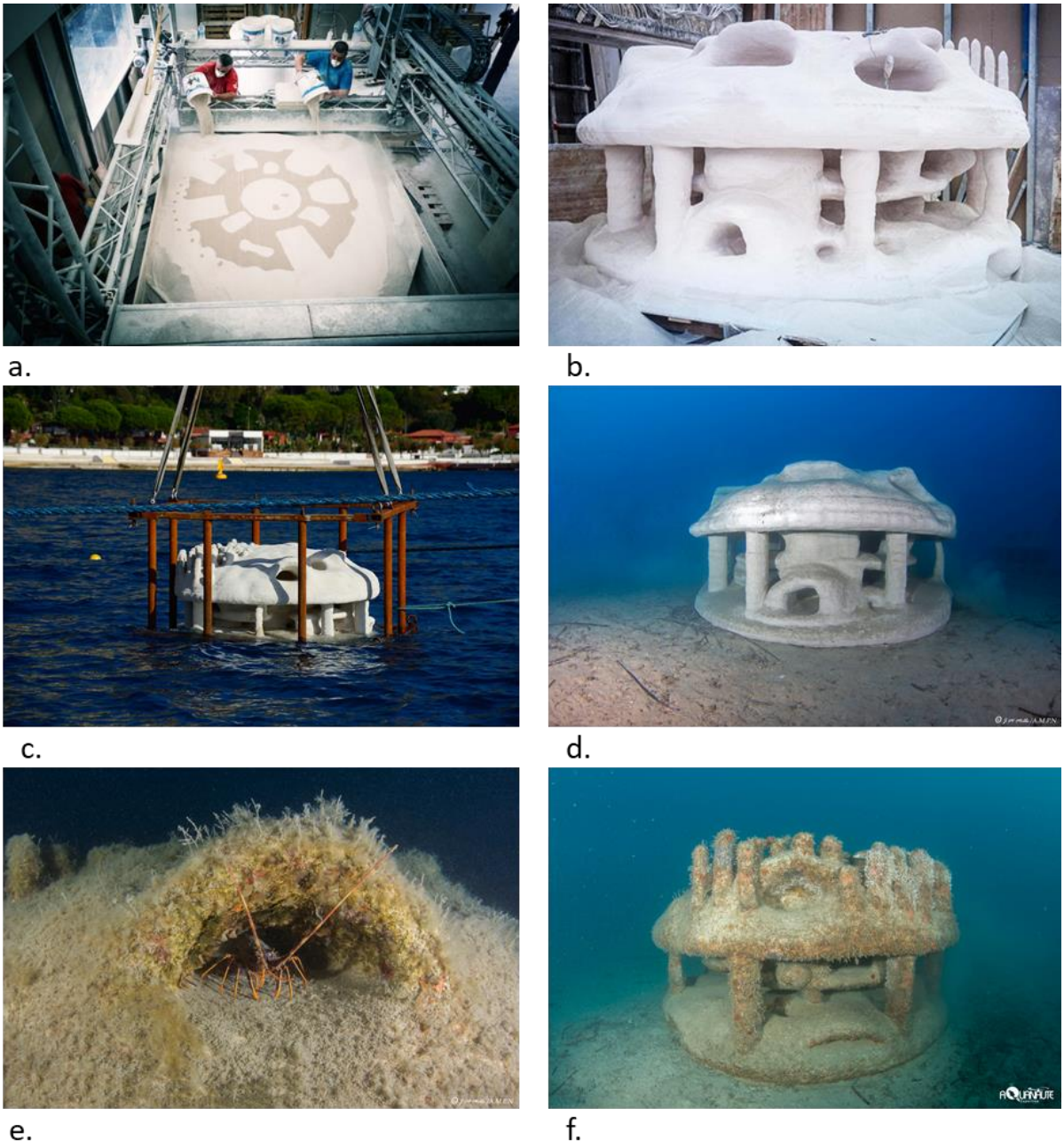

Figure I-5 : Illustration des étapes du projet d'immersion de récifs artificiels conçus par impression 3D (Boskalis/D-Shape) en Principauté de Monaco : a) impression du récif, b) état du module après impression et excavation du matériau excédent, c) immersion d'un module en Principauté de Monaco, d) état d'un module après quelques jours d'immersion, e) f) état d'un module après 2 ans d'immersion (crédit photos : Boskalis, Patrice Francour, Jean-Michel Mille-AMPN, Stéphane Jamme-Les Aquanautes).

3. Etat de l'art des caractéristiques intrinsèques des récifs artificiels

Ces directives ont permis d'établir un cadre plus précis définissant 3 critères principaux à considérer lors d'un programme de déploiement de récifs artificiels. Il s'agit de l'emplacement, déterminant les caractères extrinsèques des récifs artificiels ainsi que des matériaux et de la structure tridimensionnelle, déterminant les caractères intrinsèques des récifs artificiels. Concernant ces dernières caractéristiques, la construction de récifs artificiels doit être faite à partir de matériaux inertes n'engendrant pas de pollution des écosystèmes par lessivage, altération physique ou chimique, et/ou activité biologique, afin de ne pas entraîner une exposition accrue des contaminants nuisibles aux organismes. Ces matériaux peuvent être naturels, recyclés ou préfabriqués. Les principaux matériaux recommandés pour la construction de récifs artificiels sont la roche naturelle, le béton ou l'acier, excluant tous matériaux constituant des déchets. Par ailleurs, les structures utilisées doivent tout d'abord offrir un design correspondant à leurs objectifs et avoir des dimensions et des formes pouvant favoriser le recrutement de la vie marine à sa surface et aux alentours. Tout en remplissant ces fonctions premières, les structures doivent avoir une résistance mécanique suffisante afin qu'elles ne soient pas déplacées ou renversées par des engins de dragage, et qu'elles puissent résister aux conditions marines (vagues, courant ou processus d'érosion). De plus, toute structure mise à l'eau doit remplir ses objectifs avec une occupation minimale de l'espace et doit pouvoir être retirée si nécessaire (UNEP MAP 2005, UNEP 2009).

Malgré la mise en place de ces lignes directrices, il existe à l'heure actuelle un manque de fondements scientifiques pour l'ensemble des initiatives. Les matériaux utilisés sont choisis principalement pour leur faible coup et leur robustesse. Cependant, leur résistance à la bio-érosion ne fait pas l'objet d'études à ce jour. Le cas le plus inquiétant a été l'utilisation de pneus encouragée lors de la première conférence du CARAH en 1974 et leur usage a même été sponsorisé aux USA par le géant Goodyear (Lizarraga-Partida 1974, Figure 3-1). Suite à ces encouragements, leur immersion s'est répandue dans le monde entier (Pickering et al. 1998) en dépit des études qui commençaient à montrer leur potentiel impact sur l'environnement (Collins et al. 1995). En effet, les pneus s'avèrent être des vecteurs de bioaccumulation de métaux lourds dans les tissus de certains bivalves (Risso-de Faverney et al. 2010) et une source de pollution des sédiments (Taneez et al. 2018).

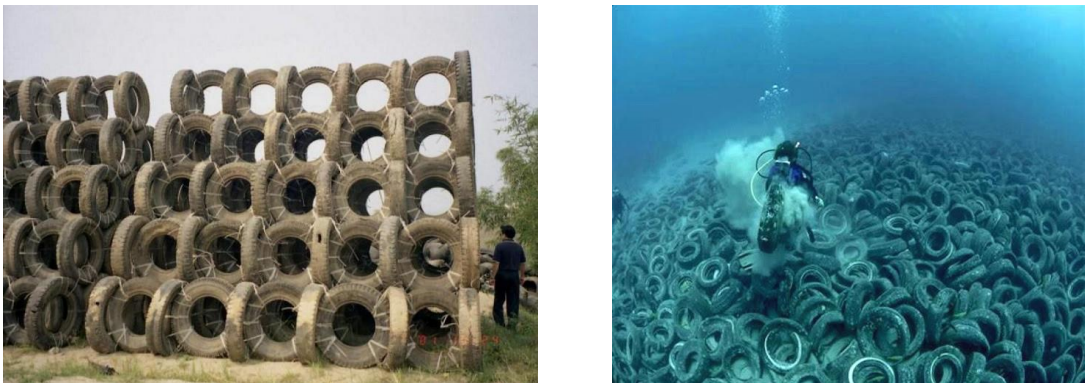

Figure I-6 :Illustration de récifs artificiels réalisés à partir de pneus : a) projet Tire Artificiel Reefs (TAR) immergés en 1997 à Hong Kong (source : https://www.maoandpartners.com/tyre-artifical-reefs/), b) pneus immergés dans les années 1970 à Fort Lauderdale (Floride) dans le but de créer un récif artificiel (source : http://www.geologyin.com/2015/10/floridas-tire-reef-has-turned-into.html)

De nos jours, la plupart des structures sont construites en béton, dont la base en ciment est souvent chargée de métaux lourds en raison de l'utilisation de déchets industriels pour la cuisson du clinker (Achternbosch & Bräutigam 2003). Bien que le béton soit considéré comme un matériau très inerte et conservant bien ses composants face à la lixiviation, sa résistance à la bio-érosion a déjà été remise en cause (Javaherdashti et al. 2009). Par ailleurs, le pH très alcalin (proche de pH 13) de ces matériaux peut également avoir un impact non négligeable sur la physiologie des espèces colonisant ces structures. De la même manière que l'utilisation des pneus, le béton pourrait se révéler être un matériau polluant. Il existe cependant des moyens permettant de limiter la présence de métaux lourds dans la confection des ciments mais aussi de diminuer le pH du béton.

Par ailleurs, l'efficacité des récifs artificiels se focalise principalement sur les assemblages de poissons et de la faune mobile qui représentent les espèces d'intérêt pour la pêche et leur efficience dépend directement du design. Les structures sont conçues selon le jugement d'expert sans méthode standardisée pour évaluer leur design (Tessier et al. 2015). De nombreuses approches de post-complexification de certaines structures sélectionnées selon des dires d'expert ont d'ailleurs été mises en place pour améliorer leur efficacité de production et attirer une plus grande diversité d'espèces (Charbonnel et al. 2001, Bodilis et al. 2011). En effet, à la suite de complexifications sur des récifs BONNA, effectuées par Charbonnel et associés (2002), la diversité a été multipliée par 2 et la biomasse globale par 4. De manière générale, l'efficacité des récifs artificiels avance par processus d'essai/ échec. La plupart des études publiées sur les récifs artificiels sont descriptives alors que de par la nature

manipulatoire des récifs artificiels elles pourraient être exploratoires en s'axant sur les processus écologiques permettant d'atteindre leurs objectifs et d'améliorer les chances de succès dans la réalisation de tout objectif d'ingénierie écologique lié aux récifs artificiels (Miller 2002).

4. Colonisation des récifs artificiels

Afin de répondre à ces critères, il faut tout d'abord comprendre les mécanismes de colonisation des récifs artificiels. Au regard du vocabulaire fleurissant permettant de déterminer les communautés fixées, il semble important d'en faire une courte synthèse afin de se tenir à une définition et une terminologie identique au cours des prochains chapitres. Le périphyton, l'épibiose ou encore le biofouling sont des terminologies utilisées pour définir les communautés d'organismes se fixant sur des surfaces immergées. L'épibiose est davantage utilisée pour des surfaces naturelles, et plus particulièrement sur des organismes, impliquant ainsi une relation entre deux organismes. Cependant, cette terminologie est également utilisée dans le cadre de l'étude de la colonisation des récifs artificiels (Svane & Petersen 2001). Le terme périphyton, peut être utilisé aussi bien pour des surfaces naturelles qu'artificielles, mais cette terminologie définit davantage des communautés photosynthétiques composées d'algues, de cyanobactéries, de champignons et de microbes hétérotrophes pouvant favoriser le recrutement d'invertébrés sessiles (Falace & Bressan 2000). Enfin le biofouling, ou bio-encrassement, est principalement utilisé pour définir la couche se développant sur la coque des bateaux. Le biofouling entraine un ralentissement des cargos et des coûts de carburant importants, raison pour laquelle tout un panel de recherche explore les moyens d'en limiter l'apparition (e.g. : Wahl 1989, Holmström & Kjelleberg 1994, Callow & Callow 2006, Qian et al. 2007, Bixler & Bhushan 2012, Briand et al. 2012, 2017, Myan et al. 2013, Salta et al. 2013). Malgré le caractère négatif de cette définition, ce terme semble le plus complet car il inclut deux compartiments : le biofilm qui constitue les premières communautés unicellulaires se formant à la surface du substrat et qui facilitent le recrutement et l'adhésion des larves d'invertébrés constituant alors le macrofouling (Salta et al. 2013). Nous utiliserons donc le terme biofouling pour déterminer les communautés se fixant sur les récifs artificiels. Lorsque la distinction sera nécessaire, le biofilm sera utilisé pour définir les premières communautés unicellulaires se développant à la surface et le macrofouling sera utilisé pour définir les communautés pluricellulaires s'installant dans un second temps (Figure I-7).

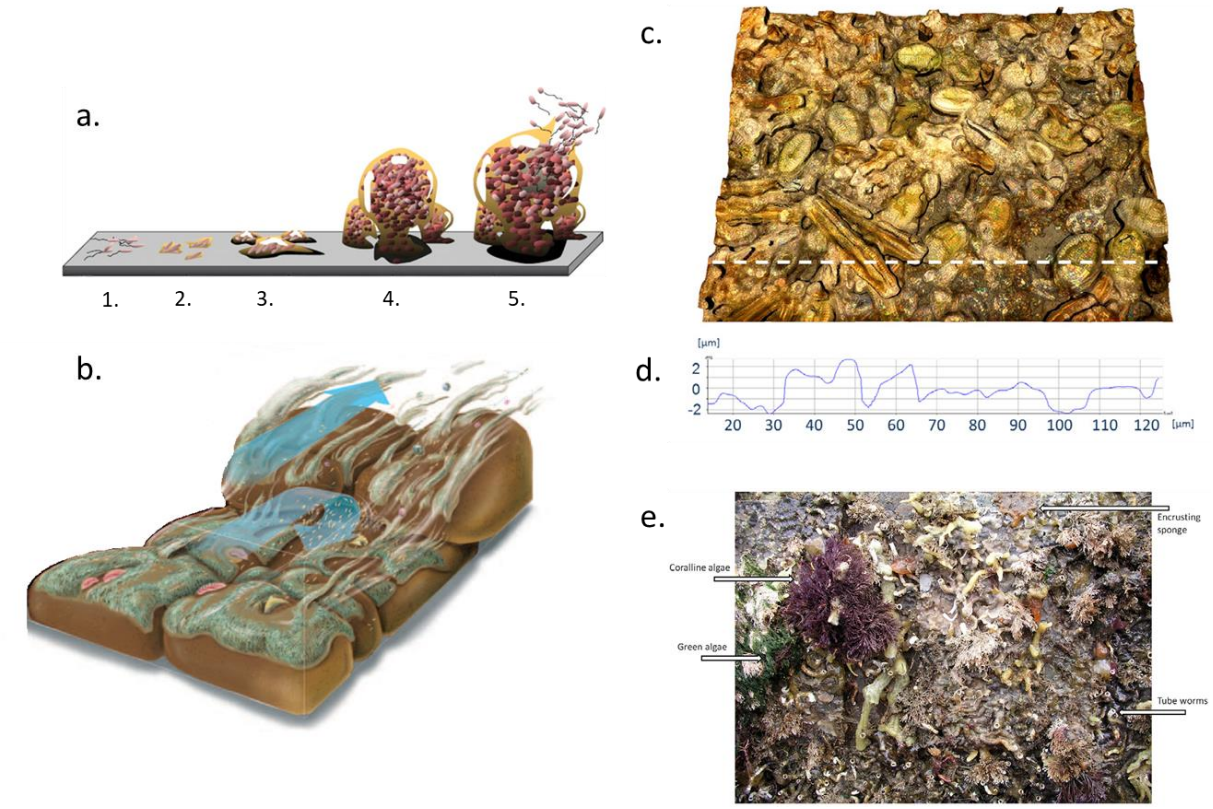

Figure I-7 : Illustration du biofouling : a) schéma illustrant le processus de colonisation du biofilm en cinq étapes: 1) phase d'attachement réversible, 2) phase d'attachement irréversible avec production de la matrice extracellulaire, 3) croissance verticale du biofilm 4) biofilm mature, 5) dispersion du biofilm (source : Bixler & Bhushan 2012), b) paysage d'un biofilm microbien colonisant un environnement sédimentaire, la structure des colonies est fonction des flux (en agrégat au niveau des flux lents, en filament au niveau des flux rapides) créant des micro-perturbations qui induisent une dispersion des organismes (source : Battin et al. 2007), c) topographie 3D d'un biofilm composé principalement de diatomées (Amphora sp. Et Navicula sp.) sur des panneaux immergés pendant 3 semaines à Southampton (Royaume-Uni). Le trait pointillé blanc indique la section illustrée en d) représentant la topographie de la surface du biofilm (source : (Salta et al. 2013)*, e) surface en bois immergée à Southampton (Royaume-Uni) pendant 20 mois avec une communauté complexe de macrofouling comprenant des algues corallines, des vers turbicoles, des éponges et des algues. (source :* (Salta et al. 2013)

Actuellement, l'étude de la colonisation des récifs artificiels se focalise principalement sur la faune mobile et rarement sur le biofouling. Au sein de ce dernier compartiment, le biofilm constitue la base du processus de colonisation, mais il est pourtant très rarement étudié dans le cadre des récifs artificiels (Salamone et al. 2016, Liu et al. 2017, Riera et al. 2018). Il définit pourtant la première forme de vie entrant en interaction avec le récif artificiel une fois immergé, et peut donner des informations sur la structure des communautés et leur physiologie en peu de temps.

Les biofilms sont définis comme des assemblages microbiens adhérant les uns aux autres et se liant à une surface immergée (Costerton et al. 1995, Hall-stoodley et al. 2004). En milieu marin, le biofilm est composé de microbes tels que bactéries, archées, microalgues, champignons microscopiques, flagellés hétérotrophes et ciliés. L'abondance relative de ces taxons varie en fonction des conditions environnementales, mais les diatomées et les cyanobactéries sont les taxons majoritairement représentés (Wahl 1989, Callow & Callow 2006, Salta et al. 2013, Dang & Lovell 2016). Ces micro-organismes vivent d'abord une phase planctonique, puis se fixent sur tous types de surfaces immergées recouvertes de molécules adsorbées formant un film de conditionnement avant la fixation des cellules microbiennes (Dang & Lovell 2016). Cette première étape implique des interactions physico-chimiques avec la surface et le film primaire, puis dans une seconde phase les communautés s'adaptent physiologiquement à la surface en produisant une matrice de polymères extracellulaires (EPS) composée de macromolécules telles que des polysaccharides, des protéines, des acides nucléiques, des lipides et d'autres composés polymériques (Wahl 1989, Flemming & Wingender 2010, Sheng et al. 2010). Ces EPS constituent une matrice donnant une structure dynamique tridimensionnelle au biofilm et induisant chez les microorganismes qui les produisent l'expression d'un phénotype permettant d'améliorer l'accès aux nutriments, une meilleure colonisation et une résistance plus robuste de la communauté aux contraintes environnementales (Salta et al. 2013). Les EPS des biofilms sont très hétérogènes et varient spatialement, chimiquement et physiquement selon les gradients environnementaux (e.g. : pH, température, oxygène) (Costerton et al. 1995) (Figure I-7).

La colonisation ultérieure par le macrofouling est globalement déterminée par l'environnement biologique local, sous l'influence de l'établissement du biofilm (Svane & Petersen 2001, Hamer 2002, Lam et al. 2003, Patel et al. 2003, Dahms et al. 2004, Dobretsov & Qian 2006, Qian et al. 2007, Zardus et al. 2008, Bixler & Bhushan 2012, Wahl et al. 2012). Les algues sont les premières recrutées, s'ensuit une association plus diverse au bout de 6 à 8 semaines composée d'hydroïdes, de polychètes serpulides, de balanes et de mollusques (Ardizzone et al. 2000). L'équilibre de la communauté suit un processus interactif et dynamique régi par les conditions environnementales et la compétition interspécifique de l'assemblage (Svane et Petersen, 2001) (Figure I-7).

5. Influence des caractéristiques intrinsèques des récifs artificiels sur la colonisation

De nombreuses études ont mis en avant le rôle du substrat sur le recrutement du biofilm (Dang & Lovell 2000, 2002, Huang & Hadfield 2003, Jones et al. 2007, Dang et al. 2008, Chung et al. 2010) puis du macrofouling (Brown 2005, Lakshmi et al. 2012, Myan et al. 2013, Xiao 2014), ainsi que l'influence combinée du biofilm et du substrat sur le recrutement de ces derniers colonisateurs (Faimali et al. 2004, Huggett et al. 2009, Dobretsov et al. 2013, Salta et al. 2013). Ces communautés peuvent donc potentiellement présenter des assemblages différents selon le matériau utilisé pour la construction de récifs artificiels. Par ailleurs, si le matériau utilisé n'est pas inerte et présente des composés polluants, il est possible que le biofouling soit le vecteur de bioaccumulation depuis le biofilm (Späth et al. 1998, Bhaskar & Bhosle 2006, Pal & Paul 2008, Muhamed & Saly 2011, Dash et al. 2013, S. Morin et al. 2016, de Carvalho 2018) jusqu'au macrofouling (Antsulevich 1994, Das et al. 2008, Risso-de Faverney et al. 2010, Rouane-hacene et al. 2015). Ceci pourrait engendrer des conséquences sur l'ensemble du réseau trophique, impactant potentiellement la faune mobile et notamment les espèces d'intérêt économique et écologique (Camacho-Chab et al. 2016).

Outre les implications que peut avoir la qualité chimique du substrat sur la faune mobile, la structure tridimensionnelle de la texture du substrat jusqu'à la forme globale joue quant à elle un rôle essentiel sur le recrutement de ces espèces (Bohnsack 1991). En effet, la topographie du substrat peut influencer la diversité et l'abondance du biofouling et indirectement de la faune mobile s'en nourrissant (Bohnsack & Sutherland 1985, Bohnsack 1989, 1991, Svane & Petersen 2001, Tessier et al. 2015). Concernant le design global, il dépend avant tout de l'objectif du récif. Dans le cadre d'un récif récréatif ou de protection, l'attraction des communautés passe en second plan. Par contre, lorsqu'il s'agit d'un récif de production ou de restauration, l'aspect de la structure globale est de première importance afin de pouvoir imiter au plus près un habitat naturel et ses fonctions. Quelques recommandations sont données sur la hauteur et la largeur des arrangements, sur l'ouverture des modules et le volume vide des modules unitaire qui peut atteindre 98% du récif chez les structures japonaises, sans pour autant définir de véritables consensus (Bohnsack 1989). L'échelle à laquelle la complexité est étudiée implique des réponses différentes selon les espèces cibles (Bohnsack 1991).

Il découle en définitive que le design global doit être pensé selon l'environnement direct du site d'immersion qui déterminera quels types d'espèce peuvent être recrutées (UNEP 2009, Tessier et al. 2015). Cependant, il n'apparait pas de méthode quantitative pour évaluer les différents paramètres de la structure des récifs artificiels et vérifier leurs implications sur le recrutement des espèces cibles. Dans le milieu naturel, l'étude de la structure de l'habitat en lien avec l'abondance et la diversité des espèces est un sujet récurrent (e.g. : MacArthur & MacArthur 1961, MacArthur et al. 1962, McCoy et al. 1991, Kovalenko et al. 2012). En se basant sur la définition proposée par McCoy & Bell (1991), la structure de l'habitat se définit selon trois dimensions :

- La complexité, définie par la forme mesurée selon divers paramètres (quelques exemples des plus utilisés : rugosité, dimension fractale, porosité).
- L'hétérogénéité, définie par l'abondance relative des différentes formes (quelques exemples : indice de Shannon, écart type)
- L'échelle à laquelle les deux précédents paramètres sont étudiés.

Selon ces trois dimensions, il est possible de poser les bases d'une méthode d'évaluation des récifs artificiels depuis l'aspect de leur surface jusqu'à leur arrangement global qui suit un modèle identique de par le monde (Bohnsack 1989, Cépralmar 2015, Tessier et al. 2015, Charbonnel et al. 2011, Figure 5-1)

- Les modules sont assemblés en agrégat ou récif unitaire (*"set"* pour les anglophones). La distance entre chaque module peut varier d'une dizaine de centimètres à quelques mètres.
- Un ensemble de récifs unitaires forme un village (*"group"*) dont la distance varie d'une dizaine de mètres à 500 mètres selon la taille des agrégats.
- Enfin, un ensemble de villages forme un champ (*"complex"*) sous-entendu l'étendue globale du projet de déploiement des récifs. La distance entre les villages peut atteindre 3 km.

Ainsi, la complexité peut être évaluée au niveau du module unitaire, l'hétérogénéité au niveau des différents arrangements (agrégat, village, champ) et ces paramètres peuvent faire l'objet d'études à l'échelle globale de la structure ainsi qu'à l'échelle de la surface afin de donner une base d'évaluation à toutes les échelles possibles.

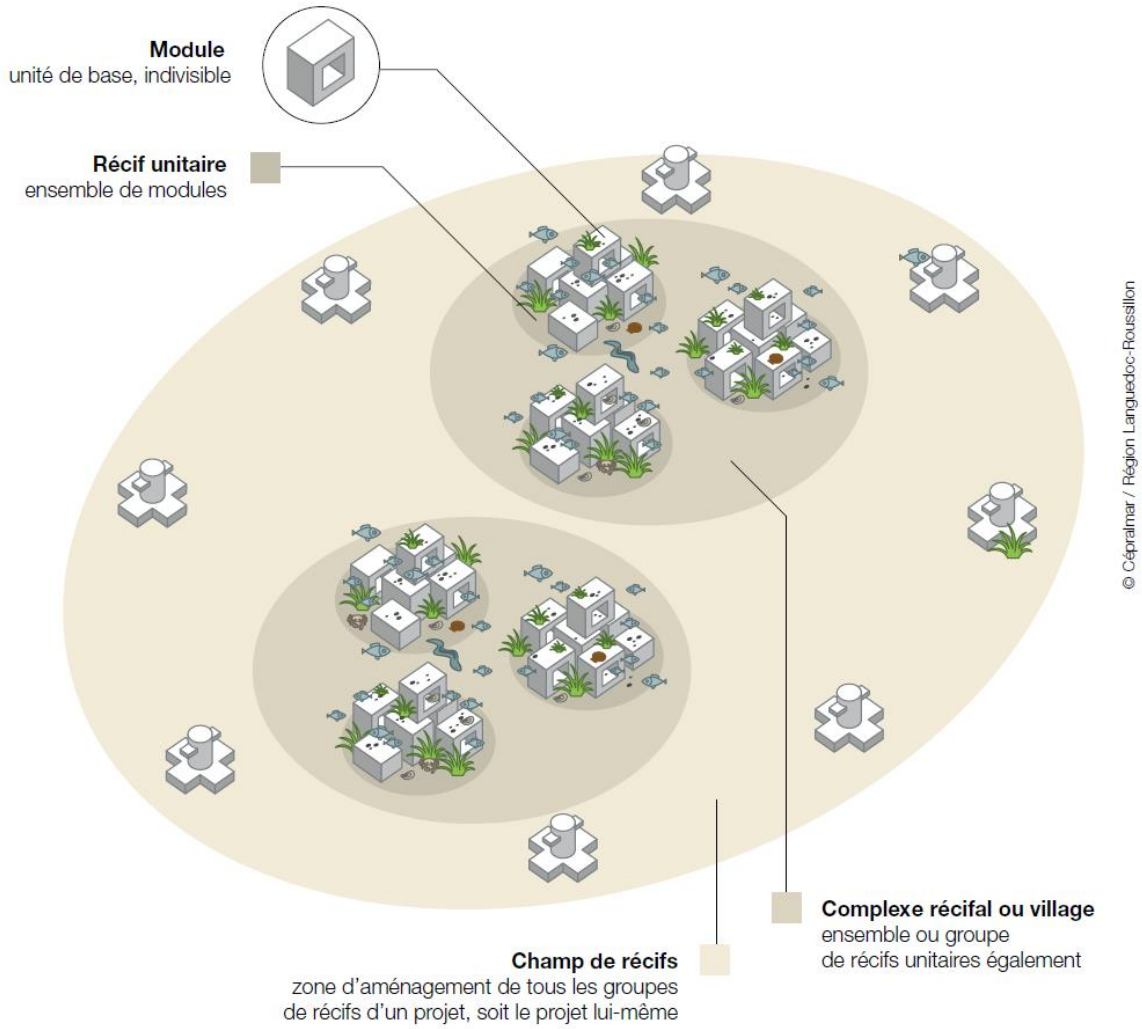

Figure I-8 : Illustration de l'arrangement des récifs artificiels selon l'échelle du module (source : Cépralmar 2015)

6. Hypothèses

Sur la base de ces différents postulats énumérés dans les paragraphes précédents, les études menées durant cette thèse visent à tester les hypothèses suivantes : (i) la nature du matériau influence la structure et les sécrétions des premières communautés microbiennes recrutées sur les récifs, (ii) la nature du matériau influence la structure des communautés de macrofouling sur le long terme, (iii) la nature du matériau influence la séquestration de métaux lourds présents dans l'environnement ou dans les matériaux eux-mêmes, (iv) l'efficacité des différents types de récifs artificiels peut reposer sur l'élaboration d'une méthode d'évaluation de leur structure de la micro à la macro-échelle, (iv) la structure tridimensionnelle influence la physiologie des communautés de biofilm.

Afin d'offrir un cadre scientifique à l'étude des caractéristiques intrinsèques des récifs artificiels, nous mettrons en place des moyens d'évaluer leurs matériaux et leurs structures.

Le premier chapitre se focalisera sur l'étude de la structure des communautés photosynthétiques du biofilm ainsi que sur leurs sécrétions d'EPS afin de mettre au point une méthode pouvant définir un indicateur de la qualité des matériaux utilisés pour la construction des récifs artificiels.

Le deuxième chapitre approfondira et validera ces premiers résultats en menant un suivi conjugué du biofilm et du macrofouling sur le long terme, complété par une analyse de leur contenu en métaux lourds afin de contrôler l'inertie des matériaux utilisés.

La première partie du troisième chapitre sera consacrée à l'élaboration d'une méthode destinée à évaluer la structure globale des récifs artificiels.

Enfin, la partie suivante permettra d'adapter cette méthode à l'échelle microscopique pour déterminer l'influence de la microtopographie du matériau à la fois sur l'abondance du biofilm et sur l'activité photosynthétique de ces communautés.

II. CHAPTER 1: BIOFILM MONITORING AS A TOOL TO ASSESS THE EFFICIENCY OF ARTIFICIAL REEFS AS SUBSTRATES: TOWARD 3D PRINTED REEFS.

Published in Ecological Engineering
Received 8 February 2018; Received in revised form 17 May 2018; Accepted 3 June 2018
0925-8574/ © 2018 Elsevier B.V. All rights reserved.

Authors: Riera E., Lamy D., Goulard C., Francour P. & Hubas C.

Résumé

Ce premier chapitre introduit les travaux préliminaires sur l'évaluation de la qualité d'un nouveau matériau à base de ciment Sorel et de sable des Dolomites utilisé pour concevoir une nouvelle génération de récifs artificiels (RA) réalisés à l'aide d'imprimantes 3D de grande taille. Jusqu'alors, l'évaluation de l'efficacité des RA s'était principalement concentrée sur les communautés de poissons et les espèces présentant un intérêt écologique et/ou socio-économique. Les communautés de biofilm avaient été totalement ignorées, bien qu'elles soient déterminantes dans la construction du premier maillon du réseau trophique d'un récif artificiel. Nous avons posé l'hypothèse que le matériau était susceptible d'influencer la qualité du biofilm, aussi bien au niveau de la structure des communautés que de leurs sécrétions.

Une étude comparative a été menée entre ce nouveau matériau et deux types de béton couramment utilisés pour la construction des RA. La structure des communautés photosynthétiques a été identifiée à l'aide de biomarqueurs pigmentaires et leur production de polymères extracellulaires (EPS) a été analysée en termes de concentrations totales en sucres, en protéines et en acides aminés.

Nous n'avons trouvé aucune différence significative entre les communautés de microalgues développées sur les différents matériaux. Le même constat s'applique aux protéines et aux acides aminés. Cependant, le matériau utilisé s'est révélé déterminant concernant la sécrétion de polysaccharides. En effet, les sécrétions sont plus abondantes sur les bétons gris et blancs que sur le ciment Sorel conçu à base de sable des Dolomites pour la construction de récifs artificiels par impression 3D.

Les raisons pour lesquelles ces sécrétions sont moins importantes sur le nouveau matériau restent encore à élucider. Il est important de déterminer si ces sécrétions, qui constituent un substrat organique, seront déterminantes dans le recrutement des macro-organismes sessiles qui s'installeront par la suite.

Ecological Engineering 120 (2018) 230–237

Contents lists available at ScienceDirect

Ecological Engineering

journal homepage: www.elsevier.com/locate/ecoleng

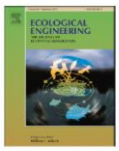

Biofilm monitoring as a tool to assess the efficiency of artificial reefs as substrates: Toward 3D printed reefs

Elisabeth Riera[a,b,*], Dominique Lamy[b], Christophe Goulard[c], Patrice Francour[a], Cédric Hubas[b,d]

https://doi.org/10.1016/j.ecoleng.2018.06.005

Abstract

Habitat destruction is one of the main causes of the decline of biodiversity and of fishery resources in the marine environment. An artificial reef (AR) could be a tool for protecting or restoring these habitats and their declining biodiversity, and also help to enhance sustainable fisheries. The goal is to design non-polluting structures that best mimic the complexity of natural habitats in order to improve their service to the community. To date, the assessment of reef performance has been mostly focused on fish assemblages and species of ecological and/or socio-economic interest, and has disregarded the biofilm communities that determine the first level of an AR's trophic network. In this work, we used biofilm formation to compare the quality of substrates used as building parts for an AR, in order to optimize an eco-friendly material that will be used to design a new generation of ARs produced by giant 3D printers. The structure of the photosynthetic communities has been identified using pigment biomarkers and their production of exudates has been analysed. These polymeric substances were quantified in terms of total sugar and protein concentrations. They were further analysed in terms of amino acid content. We found no significant differences between the micro-algae communities developed on different substrates. These photosynthetic communities were mainly composed of diatoms, prasinophytes, haptophytes, and dinoflagellates. However, we showed that the material for ARs is crucial for biofilm development, especially with regard to its secretions of sugar. The choice of an appropriate substrate for AR construction is thus of particular importance since biofilm secretions determine the organic substrate on which sessile macro-organisms will settle.

Keywords: biofilm, bio-indicator, photosynthetic pigments, extracellular polymeric substances, artificial reef substrates.

1. Introduction

Artificial reefs (ARs) have been defined as "submerged structures placed on the seabed deliberately to mimic some characteristics of natural reefs" (Pickering et al. 1999). The main goal is to protect, regenerate and increase marine resource production, to help measure conservation in the protection and restoration of habitat and to enhance fisheries (UNEP 2009). The first ARs were made with recycled waste materials, then since the mid-1970s, innovative trends shifted towards purpose-designed reef structures (Pickering et al. 1998, Barnabé et al. 2000, Tessier et al. 2015). In the USA, various depolluted waste materials were used, such as wrecks of oil and gas production platforms or charter vessels (Pickering et al. 1998), while in Europe and Japan since the 1980s, concrete blocks have been virtually exclusively used (Pickering et al. 1998, Barnabé et al. 2000, Tessier et al. 2015). In comparison to wrecks, AR design using concrete blocks limits the spatial heterogeneity and cannot mimic the high three-dimensional complexity of natural rocky habitats.

To date, the assessment of reef performance has focused mostly on fish assemblages and species of commercial value, and has underestimated the development of epibiosis (or biofouling) (Svane & Petersen 2001; Tessier et al. 2015). Moreover, material characteristics that affect larval settlement and recruitment have seldom been taken into account (Svane & Petersen 2001). ARs are colonized as a consequence of the immersion of vacant hard substratum (Wahl 1989, Svane & Petersen 2001, Salta et al. 2013); holes and structures provide shelter for motile organisms and the surface is colonized ultimately by epibionts. The establishment of epibiosis is a complex process. It follows the same basic pattern of an initial biochemical conditioning film formed by the ambient water chemistry, followed by early colonisers such as bacteria and unicellular eukaryotes which form a matrix biofilm that composes the living substratum necessary for the successive colonisation by multicellular eukaryotes (Wahl 1989; Svane & Petersen 2001; Callow & Callow 2006; Salta et al. 2013). The biofilm is, therefore, a key element in the subsequent colonisation of ARs and the development of their trophic network.

The biofilm is described as a matrix of microbial assemblages bonding with a biological or non-biological immersed surface (Costerton et al. 1994, Hall-stoodley et al. 2004). In the marine environment, biofilm is composed of microbes such as bacteria, archaea, microalgae;

microscopic fungus, heterotrophic flagellates, and ciliates that previously lived as plankton. The relative abundance of these taxa varies according to environmental conditions, but diatoms and cyanobacteria are those mainly represented (Wahl 1989, Callow & Callow 2006, Salta et al. 2013). Absorption and adherence of bacteria to the surface involves physical and chemical interactions and secretion that form the primary film, then unicellular eukaryote settles several days later, dominated by diatoms that are attached to the surface by mucus secretion (Wahl 1989). The unicellular eukaryote and bacterial secretions, called extracellular polymeric substances (EPS), are composed of macromolecules such as polysaccharides, proteins, nucleic acids, lipids and other polymeric substances (Flemming & Wingender 2010). Those EPS constitute a matrix giving a tri-dimensional structure to the biofilm and express a particular phenotype of the microorganisms, giving them better access to nutrients, stronger colonisation capability and greater resistance to the environmental pressure (Salta et al. 2013). The EPS are heterogeneous and vary spatially, chemically and physically within the matrix according to environmental gradients (pH, temperature, oxygen, light, etc.; Costerton et al. 1995). To date, only two studies have focused on characterizing the biofilm community of the ARs (Salamone et al. 2016, Liu et al. 2017), but no investigation dealing with the biochemical characterisation of the biofilm has been undertaken to evaluate the nutritional quality of biofilm exudates that may have a function in ARs' trophic network.

Recently, D-shape (3D giant inkjet printing company for building construction) and Royal Boskalis Westminster N.V (Netherlands-based Company that provides services relating to the construction and maintenance of maritime infrastructure on an international basis) proposed a new way to build ARs using a giant 3D printer and an eco-friendly material, dolomite Sorel cement (84% dolomite sand and 16% magnesium oxide). 3D printing enables the building of more complex artificial structures, closer to the complexity of natural rocky habitat. As part of the evaluation of the quality of this new generation of ARs, and to assess the quality of various kinds of substrate used for ARs, we developed a method to monitor the first stage of biofilm colonisation that constitutes the living substrate for epibiont settlement. A comparative study has been performed on different substrate types: grey concrete (which is commonly immersed in Europe), white concrete (that contains less metallic oxide than grey concrete, Telford 1999; BETOCIB 2000), and dolomite Sorel cement (used to build the 3D printed ARs). Samples of these substrates were immersed in the Larvotto marine reserve (Principality of Monaco) over a 35-

day period in order to determine the colonisation of biofilm from the early phase to maturation and to identify potential biological and biochemical variations of biofilm composition between the substrates. We hypothesised that the substrate type is likely to induce differences (i) in microbial diversity during the colonisation process and (ii) in the composition of biofilm secretion.

2. Materials & methods

2.1. Sampling and site of monitoring

Biofilm communities were monitored on different substrates for 35 days in the coastal waters of the Larvotto reserve (Monaco: 43.743950°N, 7.434700°E). The reserve is a protected marine area managed by the AMPN (*Association Monaco pour la Protection de la Nature*). Samples were retrieved one day after immersion to analyse the initiation phase, and then every week (during 4 weeks) to follow the maturation of communities. However, a storm occurred the third week of monitoring which delayed the sampling by one week. The five sampling dates are thus unevenly distributed, and sampling finally took place 1, 7, 14, 28 and 35 days after immersion. The samples were immersed at 18 m depth, 2 meters above a sandy bottom. They were fixed on 5 different 1m² plastic frames (1 frame for each sampling date), suspended from a 10 liters buoy and anchored by concrete blocks. The depth was selected in order to facilitate monitoring by scuba divers and corresponds to the depth at which ARs are commonly immersed in the French Mediterranean Sea (Tessier et al. 2015).

Cobblestones of 5*2*2 cm were cut within large slabs of dolomite Sorel cement (Ds), standard grey concrete (Cg) and white concrete (Cw). Three replicates of each substrate were dedicated for 3 different analyses (Pigment, EPS, and 16S ribosomal DNA analyses) at each sampling time (i.e. 3 replicates x 3 substrates x 3 analyses x 5 times = 135 samples). Unfortunately, after extraction, the quantity of DNA compared to the PCR inhibitory products was not sufficient to follow the analysis by amplicon sequencing.

Immersion, installation and sampling were done by scuba divers. The retrieval of the plastic frames with the attached cobblestone samples lasts for ca. 2 min from the bottom to the boat. We therefore consider that new irreversible settlement of planktonic microorganisms during the retrieval was very unlikely. Samples were then packed in falcon tubes and immediately frozen with liquid nitrogen. Samples were stored at -80°C before analysis.

2.2. Pigment analysis

The photosynthetic communities have been analysed by the quantification of pigments by High Performance Liquid Chromatography (HPLC) according to Brotas & Plante-Cuny (2003). Pigments were extracted by scraping the biofilm from the substrate using a scalpel and fiber glass filter (GF/F) with 6 mL of 95 % cold buffered MeOH (2 % ammonium acetate) for 4 hours at 4°C, in the dark. Extracts were then filtered (0.2 µm) immediately before HPLC analysis. Pigment extracts were analysed using an Agilent 1260 Infinity HPLC composed of a quaternary pump (VL 400 bar), a UV-VIS photodiode array detector (DAD 1260 VL, 190 to 950 nm), and a 100 µL sample manual injection loop (overfilled with 250 µL). Chromatographic separation was carried out using a C18 column for reverse phase chromatography (Supelcosil, 25 cm long, 4.6 mm inner diameter). The solvents used were A: 0.5 M ammonium acetate in methanol and water (85:15, v:v), B: acetonitrile and water (90:10, v:v), and C: 100 % ethyl acetate. The solvent gradient followed the Brotas & Plante-Cuny method (2003), with a flow rate of 0.5 $mL.min^{-1}$. Identification and calibration of the HPLC peaks were performed with chlorophyll *a*, ββ-carotene, chlorophyll *c2*, diatoxanthin, diadinoxanthin and fucoxanthin standards. All peaks detected were identified by their absorption spectra and relative retention times using the Open Lab CDS software (ChemStation Edition for LC/MS Systems, Agilent Technologies). Quantification was performed by repeated injections of standards over a range of dilutions to establish a standard curve of concentrations. The relative abundance of each pigment (%) was calculated from their respective concentrations ($µg.cm^{-2}$).

2.3. Extraction of Polymeric substances

Since our samples were frozen before extraction, this could have broken the cell wall, and some cell content would have been released and mixed with extracellular polymeric substances (EPS). Thus, although this input of intracellular material is probably negligible, our chemical analyses may reflect the total polymeric substances (PS).

All samples (i.e. Ds, Cg and Cw cobblestones) were mixed with 2 mL of artificial seawater and 2 g of cation exchange resin (Dowex® Marathon™ C sodium form previously activated in PBS) for 1.5 h with a tube roller (Denley Instruments). Samples were then centrifuged (6030 ×

g, 10 min) and the supernatants containing the polymers (exo- and intra-) were retrieved (PS fraction: intracellular material with colloid and bond substances from extracellular material). Previous studies showed that the cation exchange resin method is more efficient than other extraction methods (e.g. with EDTA or NaOH), leading to high PS yields with no apparent cell lysis and no impact on subsequent biochemical analysis (Jachlewski et al. 2015)

2.4. Quantification of carbohydrate concentration by colorimetric assay

Carbohydrate analyses were performed following the phenol assay protocol (Dubois et al. 1956). Briefly, 200 µl of the PS fraction were mixed with 200 µl phenol (5 %) and 1 mL sulphuric acid (98 %). Mixtures were then incubated for 35 min at 30 °C and the carbohydrate concentration was measured with a spectrophotometer at 488 nm (Milton Roy Spectronic Genesys 2). A calibration curve was prepared using glucose as standard.

Protein analyses were performed following the modified LOWRY assay protocol (Raunkjær et al. 1994, Frølund et al. 1996), using five reagents as described in Table II-1.

Table II-1:Composition of the solutions used in the modified LOWRY assay protocol

Solutions	Composition
1	143 mM NaOH with 270 mM Na_2CO_3
2	57 mM $CuSO_4$
3	124 mM Na-tatrate
4	mix of solution 1, 2 and 3 solutions with fraction 100 : 1 : 1 (v : v : v).
5	Folin with distilled water 5 : 6 (v : v)

250 µl of the PS fraction were mixed with 250 µl of SDS (2 %) and 700 µl of solution 4, and mixtures were then incubated for 15 min at 30°C. 100µl of solution 5 were added to each tube and vortexed immediately. Mixtures were then incubated for 30 min at 30 °C. The protein concentration was measured with a spectrophotometer at 750 nm (Milton Roy Spectronic Genesys 2). A calibration curve was prepared using bovine serum albumine (BSA) as standard.

2.5. Amino acid composition of polymers by HPLC

Amino acids of the PS fraction were identified and quantified by HPLC. PS fractions were dialysed against distilled water (cut-off 12-14 kDa) and freeze-dried. 10 mg were then mixed with 200 µl of HCl (6N). The acid mixture was carefully degassed to reduce the level of oxidative destruction and proteins were then hydrolysed (24 h at 110°C) in vacuum using a sealed glass ampule. Ampules were then dried using a speedvac after hydrolysis. The resulting amino acids were then reconditioned in Pickering diluent prior to injection in the HPLC system. Amino acids were separated by ion-exchange HPLC using a high-efficiency sodium column (4 × 150 mm; Pickering Lab, LCTech, Dorfen, Germany) with a Waters 2695 separation module (Waters). The elution buffers and gradient conditions were those recommended by the manufacturer (Table II-2).

Table II-2: HPLC solvents for amino acid detection

Buffer	Composition
Pickering diluent NA220	Water (97.9%), sodium citrate (2%), Pro Clean 400 (<0.1%)
A: Buffer Na pH 3.14 Sodium eluant 1700-0112	Water (93%), Sulfolane (5%), Hydrogen Chloride (0.6%), Sodium acetate (1.8%), Phenol (<0.1%, pH 3.15)
B: Buffer Na pH 7 Sodium eluant N740	Water (94%), Sodium chloride (5%), sodium acetate (1.4%), phenol (<0.1%, pH 7.40)
C: NaOH Sodium regenerant RG011	Water (99%), Sodium hydroxyde (0.6%), Sodium chloride (0.4%, pH 13)

Separating amino acids were first subjected to post-column derivatization with Ninhydrin (Pickering Lab.) by using a PCX 5200 derivatizer (Pickering Lab.) and later detected on a Waters 2996 Photodiode as a UV module detector at 570 nm for all the amino acids containing a primary amine, and at 440 nm for the Proline which holds a secondary amine. Quantification was performed by repeated injections of standards over a range of dilutions to determine the relationship between peak area and standard concentrations. The relative abundance of each amino acid (%) was calculated from their respective concentration (µg.cm^{-2}), and protein concentration was calculated from the total amino acid concentration.

2.6. Data analysis

All statistical tests have been done with the open source software R (3.4.1), using "FactoMineR" (Husson et al. 2016), "vegan" (Oksanen et al. 2017) and "agricolae" (De Mendiburu 2016) packages. Differences in time and between substrates of the total concentration of pigment, sugar and proteins were tested using the univariate non-parametric Van-der-Warden test. Permutational Multivariate Analysis of variance (PERMANOVA) was performed using a Bray-Curtis dissimilarity index calculated with pigment percentages. The multivariate homogeneity of group dispersion (PERMDISP2 procedure; Anderson 2001) was verified before applying a PERMANOVA. Post-hoc pairwise PERMANOVA tests were performed to identify significant differences between modalities of factors (Anderson 2001). A Principal Component Analysis (PCA) was applied on pigment concentrations and supplementary variables (sugar and protein concentrations).

3. Results

3.1. Pigment analysis

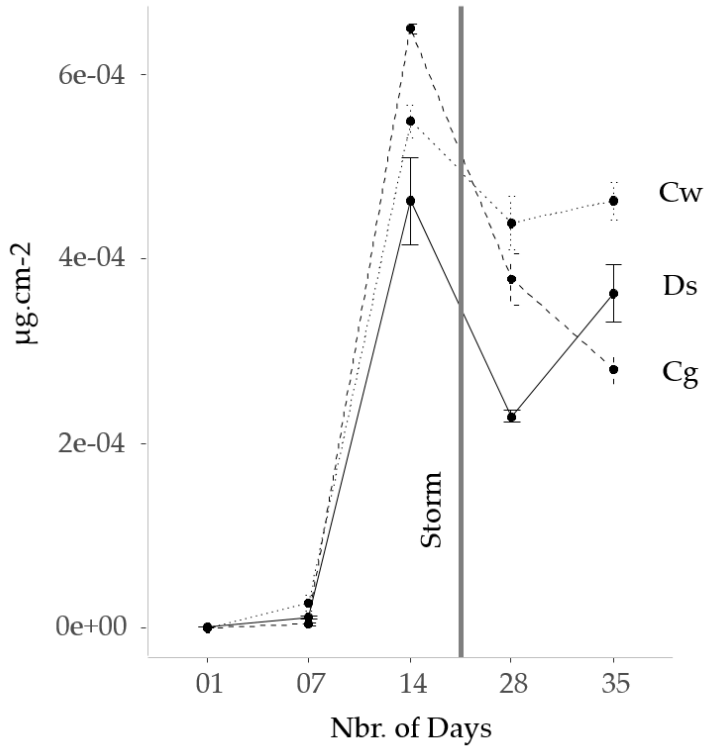

Figure II-1: Variation of pigment concentration over time on the different substrates (dashed line: grey concrete Cg, solid line: dolomite Sorel cement Ds, dotted line: white concrete Cw). (Van-der-Waerden test on substrates: p= 0.867)

Pigment concentrations varied between 0.006 µg·cm^{-2} and 6.647 µg·cm^{-2}, taking all substrates and times together (Figure II-1). On all substrate samples, it increased drastically after two weeks of immersion (Figure II-1). At this time, maximum average concentration was measured on grey concrete (Cg: 6.503 ± 0.054 µg·cm^{-2}; Cw: 5.494 ± 0.181 µg.cm^{-2}; Ds: 4.630 ± 0.465 µg.cm^{-2}). It then remained stable until the end of monitoring for white concrete despite a slight decrease after the storm. However, it decreased dramatically on grey concrete and dolomite Sorel cement after the storm event. In addition, dolomite Sorel cement had a lower concentration than grey and white concrete after the storm event (day 28: Cg: 17.801 ± 1.672 µg.mm-², Ds: 6.333 ± 0.190 µg.mm-², Cw: 15.537 ± 1.479 µg.mm-²). At the end of the monitoring period, concentrations remained constant on grey and white concrete and increased again on dolomite Sorel cement up to a level comparable to the two other substrates.

On average, chlorophyll *a,* fucoxanthin and chlorophyll *c* were the major pigments detected (Table II-3). The results of the PERMANOVA revealed significant differences for each factor (time and substrate) and their interaction (2-way PERMANOVA: time: $p = 0.001$, substrate: $p = 0.035$, interaction: $p = 0.001$; Permutation test for homogeneity of multivariate dispersions: $p = 0.067$). However, pairwise post-hoc test revealed significant differences only between sampling times except between d01 and d07 (Post-hoc pairwise PERMANOVA between sampling time with Bonferroni correction: d01-d07: $p = 1$, d07-d14, d14-d28: $p = 0.01$, d28-d35: $p = 0.02$). During the first week, we only detected fucoxanthin and chlorophyll *a* on all substrates (Table II-3). After two weeks of immersion, the proportion of chlorophyll *a* and fucoxanthin decreased due to the detection of chlorophyll *c*, pheopigments, prasinoxanthin, diadinoxanthin, and a small proportion (<1%) of carotene, hex-fucoxanthin, diatoxanthin, antheraxanthin, zeaxanthin and chlorophyll *b*. After the storm event (between day 14 and day 28), carotene and chlorophyll *b* could not be detected anymore, whereas chlorophyll *c* and prasinoxanthin increased. During the last week of monitoring, chlorophyll *b* and carotenes were detected anew and chlorophyll *c* and prasinoxanthin decreased (Table II-3).

Table II-3: Mean proportion of pigments over time on each substrate (Cg: grey concrete, Ds: dolomite Sorel cement, Cw: white concrete)

	Day 01			Day 07			Day 14			Day 28			Day 35			Global
	Cg	**Ds**	**Cw**	**Cg**	**Ds**	**Cw**	**Cg**	**Ds**	**Cw**	**Cg**	**Ds**	**Cw**	**Cg**	**Ds**	**Cw**	**Mean**
Chlorophyll *a*																
mean	62.34	71.78	59.71	63.1	68.63	61.28	51.48	52.74	49.8	40.43	45.3	40.42	45.3	42.17	45.01	53.09
se	*0.98*	*0.62*	*0.86*	*0.46*	*0.61*	*0.73*	*0.18*	*0.4*	*0.23*	*0.37*	*1.1*	*0.29*	*0.29*	*1.58*	*1.18*	*0.24*
Chlorophyll *b*																
mean	0	0	0	0	0	0	0.09	0.08	0.08	0	0	0	0.12	0.06	0.07	0.03
se	*0*	*0*	*0*	*0*	*0*	*0*	*0*	*0.01*	*0.01*	*0*	*0*	*0*	*0.01*	*0*	*0*	0.00
Chlorophyll *c*																
mean	0	0	0	0	0	0	16.17	14.52	16.18	22.65	19.49	24.88	17.74	15.48	15.08	11.06
se	*0*	*0*	*0*	*0*	*0*	*0*	*0.18*	*0.89*	*0.18*	*0.6*	*1.35*	*0.49*	*0.73*	*0.84*	*0.16*	0.21
Pheopigments																
mean	0	0	0	0	0	0	4.63	6.11	5.08	6.31	7.45	4.45	7.68	6.75	10.35	4.01
se	*0*	*0*	*0*	*0*	*0*	*0*	*0.19*	*0.32*	*0.41*	*0.85*	*0.58*	*0.39*	*0.32*	*0.47*	*1.13*	0.08
Caroten																
mean	0	0	0	0	0	0	0.85	0.85	0.79	0	0	0	0.74	0.57	0.55	0.30
se	*0*	*0*	*0*	*0*	*0*	*0*	*0.02*	*0.01*	*0.04*	*0*	*0*	*0*	*0.02*	*0.07*	*0.16*	0.01
Antheraxanthin																
mean	0	0	0	0	0	0	0.19	0.22	0.24	0.26	0.26	0.24	0.14	0.31	0.28	0.15
se	*0*	*0*	*0*	*0*	*0*	*0*	*0.01*	*0.01*	*0.01*	*0.01*	*0.02*	*0.01*	*0.04*	*0.02*	*0.01*	0.00
Diadinoxanthin																
mean	0	0	0	0	0	0	0.79	0.89	0.81	1	0.95	0.93	1.19	1.47	1.18	0.63
se	*0*	*0*	*0*	*0*	*0*	*0*	*0.01*	*0.02*	*0.01*	*0.01*	*0.03*	*0.03*	*0.05*	*0.04*	*0*	0.01
Diatoxanthin																
mean	0	0	0	0	0	0	0.28	0.14	0.31	0.03	0.04	0.05	0.14	0.11	0.11	0.08
se	*0*	*0*	*0*	*0*	*0*	*0*	*0*	*0.02*	*0.01*	*0*	*0.01*	*0.01*	*0.01*	*0.01*	*0.01*	0.00
Fucoxanthin																
mean	37.66	28.22	40.29	36.9	31.37	38.72	23.03	22.29	24.31	25.48	22.7	25.14	25.19	30.73	25.22	28.96
se	*0.98*	*0.62*	*0.86*	*0.46*	*0.61*	*0.73*	*0.06*	*0.43*	*0.3*	*0.1*	*0.65*	*0.11*	*0.71*	*1.22*	*0.16*	0.14
Hex-fucoxanthin																
mean	0	0	0	0	0	0	0.09	0.16	0.13	0.22	0.18	0.19	0.27	0.21	0.32	0.12
se	*0*	*0*	*0*	*0*	*0*	*0*	*0.01*	*0.03*	*0.02*	*0.01*	*0.01*	*0.02*	*0.02*	*0.01*	*0.06*	0.00
Prasinoxanthin																
mean	0	0	0	0	0	0	2.27	1.83	2.1	3.63	3.63	3.71	1.33	2.02	1.73	1.52
se	*0*	*0*	*0*	*0*	*0*	*0*	*0.05*	*0.16*	*0.06*	*0.05*	*0.16*	*0.03*	*0.08*	*0.14*	*0.16*	0.03
Zeaxanthin																
mean	0	0	0	0	0	0	0.14	0.16	0.16	0	0	0	0.16	0.11	0.09	0.06
se	*0*	*0*	*0*	*0*	*0*	*0*	*0.01*	*0.01*	*0.01*	*0*	*0*	*0*	*0.01*	*0.01*	*0.01*	0.00

3.2. Sugar and protein concentration dynamics on the different substrates

Sugar concentrations ranged between 0.674 and 14.628 µg·cm^{-2} (Figure II-2) and were significantly different between dolomite Sorel cement and the two types of concrete (Van-der-Waerden: p = 0.0315, post hoc test: Cg-Ds: p = 0.049; Cg-Cw: p = 0.537; Ds-Cw: p = 0.0104). They increased gradually over the monitoring period on grey and white concretes samples to reach on average 7.904 ± 2.472 µg·cm^{-2} and 10.546 ± 1.295 µg·cm^{-2}, respectively, at the end of monitoring. The concentration of sugars in dolomite Sorel cement samples increased slightly, with a maximum mean concentration of 2.733 ± 0.240 µg·cm^{-2} at the end of monitoring. Protein concentrations ranged between 0.208 and 1.552 µg·cm^{-2} (Figure II-2) and followed approximately the same pattern as the sugar concentration over time. However, the concentrations did not differ between substrates (Van-der-Waerden: p = 0.322).

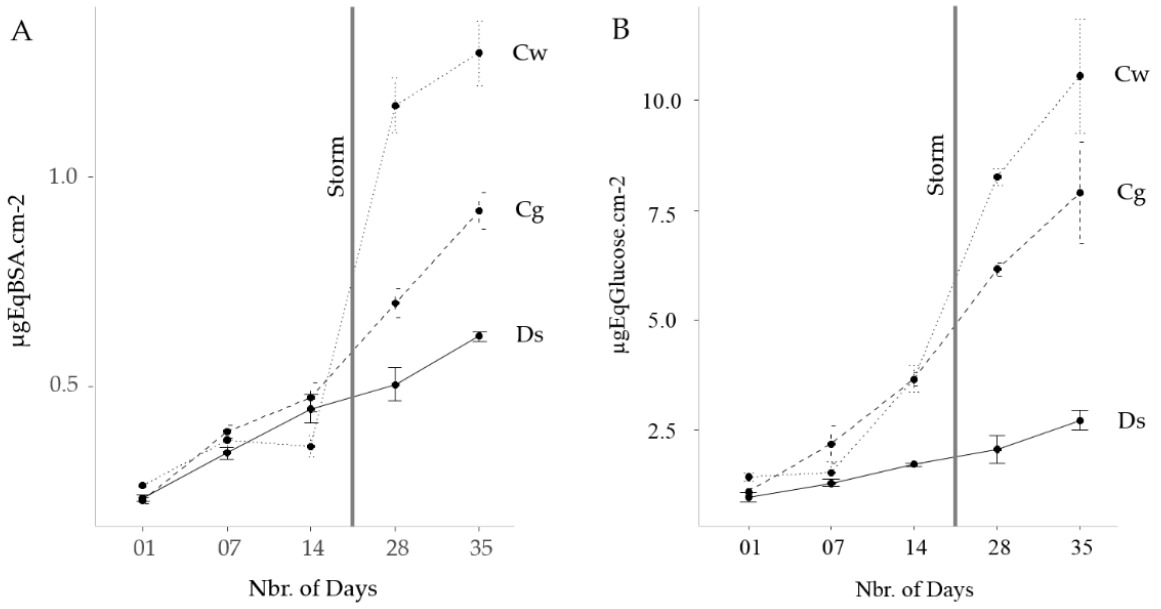

Figure II-2: Variation of (A) sugar concentration (equivalent glucose) and of (B) protein concentration (equivalent BSA) over time on the different substrates (dashed line: grey concrete Cg, solid line: dolomite Sorel cement Ds, dotted line: white concrete Cw). (Van-der-Waerden test on substrates: sugar: p = 0.0315; proteins: p = 0.322)

The ratio of sugar to protein was equivalent between substrates for the two first sampling times (mean of the ratio for the 3 substrates at d01: 4.84 ± 0.13, at d07: 4.68 ± 0.29). It remained the same on dolomite Sorel cement till the end of the monitoring, while it increased drastically on the two other substrates from the second week of monitoring and then remained

stable at high values till the end of the monitoring (Table II-4). Overall, it showed significant differences between dolomite Sorel cement and other substrates (Van-der-Waerden: p = 0.0042, post hoc test: Cg-Ds: p = 0.0022; Cg-Cw: p = 0.9472; Ds-Cw: p = 0.0026)

Table II-4: Means of sugar to protein ratio over time on each substrate (Cg: grey concrete, Ds: dolomite Sorel cement, Cw: white concrete)

Ratio	Day 1			Day 7			Day 14			Day 28			Day 35		
sugar:protein	Cg	Ds	Cw	Cg	Ds	Cw	Cg	Ds	Cw	Cg	Ds	Cw	Cg	Ds	Cw
mean	4.79	4.26	5.46	5.80	3.90	4.34	7.98	3.99	10.37	8.90	4.17	7.18	8.26	4.38	7.96
se	*0.15*	*0.56*	*0.39*	*1.36*	*0.37*	*0.89*	*0.65*	*0.32*	*0.79*	*0.36*	*0.72*	*0.43*	*0.88*	*0.32*	*0.53*

3.3. Amino acid composition

Proportions of amino acids showed significant differences over time but not between substrates (2-way PERMANOVA: time: p = 0.001, substrate: p = 0.078, interaction: p = 0.918; Permutation test for homogeneity of multivariate dispersions: p = 0.716). Post hoc analyses revealed significant differences before and after the storm event (between d14 and d28, Post-hoc pairwise PERMANOVA, Bonferroni correction: p = 0.01). On average, the PS fraction contained amino acids mainly composed of glutamic acid (20.83 ± 0.14 %), aspartic acid (10.25 ± 0.08 %), glycine (11.80 ± 0.09 %), alanine (8.23 ± 0.4 %), proline (7.70 ± 0.21 %) and serine (9.31 ± 0.12 %), 26.18 ± 1.12 % were essential amino acids (Table II-5). Even if no significant differences were detected between substrates, dolomite Sorel Cement showed a lower proportion of essential amino acids than on the two types of concrete at d14 (Cg: 27.78 ± 2.31; Ds: 18.94 ± 0.91; Cw: 28.04 ± 1.77) and d35 (Cg: 32.25 ± 1.57; Ds: 24.78 ± 0.27; 27.70 ± 1.10).

Table II-5: Mean proportion of amino acids over time on each substrate (Cg: grey concrete, Ds: dolomite Sorel cement, Cw: white concrete)

	Day 1			Day 7			Day 14			Day 28			Day 35			Global
	Cg	Ds	Cw	Cg	Ds	Cw	Cg	Ds	Cw	Cg	Ds	Cw	Cg	Ds	Cw	Mean
Essential amino acids																
Isoleucine																
mean	13.88	2.22	3.47	3.09	4.09	3.58	3.78	2.74	4.18	3.55	3.91	4.66	4.61	3.34	4.57	**4.15**
se	*8.29*	*0.11*	*0.37*	*0.5*	*0.37*	*0.48*	*0.42*	*0.13*	*0.28*	*0.83*	*0.06*	*0.38*	*0.96*	*0.06*	*0.43*	***0.08***
Leucine																
mean	2.65	4.58	5.88	4.07	6.9	6.11	5.45	4.4	6.39	5.75	5.65	6.76	6.6	4.74	5.43	**5.46**
se	*0.97*	*0.19*	*0.51*	*0.73*	*0.66*	*0.63*	*0.79*	*0.18*	*0.33*	*1.12*	*0.09*	*0.47*	*1.05*	*0.03*	*0.04*	***0.04***
Lysine																
mean	2.34	1.42	3.49	5.34	3.17	3.74	4.15	1.62	2.69	2.63	3.33	3.48	3.24	3.1	4.02	**3.20**
se	*0.48*	*0.23*	*0.3*	*0.79*	*0.55*	*0.46*	*0.53*	*0.33*	*0.64*	*0.41*	*0.45*	*0.56*	*0.82*	*0.68*	*0.94*	**0.04**
Methionine																
mean	1.63	0.32	0	0.4	0	0.42	1.04	0.59	1.02	1.58	1.4	1.81	0.81	1	0.88	**0.84**
se	*1.15*	*0.13*	*0*	*0.13*	*0*	*0.13*	*0.05*	*0.02*	*0.01*	*0.48*	*0.04*	*0.24*	*0.28*	*0.07*	*0.25*	**0.02**
Phenylalanine																
mean	3.51	1.43	2.45	1.71	1.43	3.39	2.99	2.01	3.09	3.12	2.54	3.66	3.57	2.36	3.36	**2.67**
se	*1.18*	*0.16*	*0.29*	*0.84*	*0.41*	*0.3*	*0.43*	*0.1*	*0.24*	*0.75*	*0.11*	*0.4*	*0.46*	*0.12*	*0.52*	**0.03**
Threonine																
mean	2.3	4.27	3.74	2.94	3.77	4.66	4.11	2	4.1	4.61	4.86	4.68	4.08	4.49	4.32	**3.96**
se	*0.11*	*0.68*	*0.06*	*0.85*	*0.3*	*0.5*	*0.2*	*0.5*	*0.21*	*0.53*	*0.09*	*0.19*	*0.13*	*0.15*	*0.26*	**0.03**
Valine																
mean	3.83	3.88	4.33	5.6	5.66	4.58	5.39	3.52	5.63	6.84	5.5	6.26	6.19	4.82	3.57	**5.04**
se	*0.9*	*0.41*	*0.36*	*1.31*	*0.44*	*0.27*	*0.3*	*0.19*	*0.32*	*0.87*	*0.05*	*0.42*	*1.42*	*0.13*	*0.89*	**0.04**
TOTAL																
mean	20.21	19.07	25.80	25.30	25.37	27.32	27.79	18.94	28.04	29.01	28.45	32.61	32.25	24.78	27.70	**26.18**
se	*0.25*	*0.41*	*0.96*	*0.56*	*1.39*	*1.48*	*2.31*	*0.81*	*1.77*	*2.26*	*0.67*	*2.31*	*1.57*	*0.27*	*1.10*	***1.12***
Non essential amino acids																
Alanine																
mean	6.45	8.29	7.47	7.03	9.45	8.55	8.9	6.75	8.78	9.22	8.46	9.14	8.33	8.03	8.1	**8.23**
se	*1.26*	*0.34*	*0.53*	*1.82*	*0.33*	*0.57*	*0.2*	*0.3*	*0.31*	*0.97*	*0.17*	*0.21*	*1.51*	*0.21*	*0.31*	***0.04***
Arginine																
mean	0.67	2.21	1.32	7.94	1.7	1.58	2.16	5.53	3.51	2.43	3.04	3.46	4.22	2.65	3.13	**3.06**
se	*0.47*	*0.44*	*0.1*	*3.54*	*0.47*	*0.46*	*0.05*	*0.68*	*0.13*	*0.86*	*0.12*	*0.56*	*0.21*	*0.16*	*0.78*	***0.07***
Aspartic Acid																
mean	7.4	14.28	9	7.95	10.99	10.91	10.23	8.76	10.75	12.28	9.42	10.99	9.86	9.6	10.17	**10.25**
se	*0.66*	*3.42*	*0.57*	*2.04*	*0.55*	*0.12*	*0.02*	*0.38*	*0.47*	*0.92*	*0.29*	*0.13*	*1.16*	*0.3*	*0.61*	***0.08***
Cysteine																
mean	0	0.63	0.03	0.43	0.11	0.8	0.64	0.3	0.53	0.34	0.37	0.4	0.13	0.25	0.14	**0.35**
se	*0*	*0.1*	*0.02*	*0.17*	*0.06*	*0.34*	*0.07*	*0.09*	*0.05*	*0.1*	*0.04*	*0.02*	*0.05*	*0.06*	*0.03*	***0.01***
Glutamic Acid																
mean	15.76	18.19	21.62	17.41	24.47	19.15	25.53	28.58	20.78	15.85	20.59	17.66	18.8	25.59	20.11	**20.83**
se	*2.9*	*1.29*	*2.62*	*4.1*	*1.52*	*2.17*	*2.57*	*1.47*	*1.16*	*1*	*0.74*	*1.28*	*1.15*	*1.18*	*1.06*	***0.14***
Glycine																
mean	15.39	16.42	16.07	9.75	14.81	12.16	11.97	12.57	10.84	8.21	8.79	8.09	7.17	12.77	11.7	**11.80**
se	*3.54*	*0.81*	*0.94*	*2.48*	*0.43*	*0.22*	*0.04*	*0.76*	*1.09*	*0.3*	*0.27*	*0.51*	*0.17*	*0.59*	*0.54*	***0.09***
Histidine																
mean	1.59	0.95	2.43	2.13	0.36	0.84	0.88	2.06	0.93	0.92	1.24	1.3	3.15	0.93	1.55	**1.37**
se	*0.76*	*0.31*	*1.31*	*0.91*	*0.11*	*0.33*	*0.08*	*0.43*	*0.04*	*0.27*	*0.06*	*0.08*	*1.22*	*0.1*	*0.19*	***0.03***
Proline																
mean	2.72	0	1.17	15.79	0.71	8.36	3.19	4.36	6.64	15.24	13.43	10.45	12.68	8.7	12.07	**7.70**
se	*1.37*	*0*	*0.36*	*9.12*	*0.41*	*3.24*	*0.52*	*1.36*	*1.48*	*2.78*	*0.34*	*1.36*	*4.87*	*1.41*	*1.42*	**0.21**
Serine																
mean	15.36	19.52	15.88	7	11.55	9.48	8.47	12.56	8.02	5.61	5.87	5.05	4.77	6.2	4.8	**9.31**
se	*1.89*	*1.88*	*0.93*	*2.02*	*1.05*	*0.31*	*0.52*	*1.14*	*0.86*	*0.68*	*0.25*	*0.3*	*0.09*	*0.21*	*0.36*	**0.12**
Tyrosine																
mean	4.52	1.38	1.64	1.41	0.84	1.69	1.11	1.64	2.1	1.82	1.57	2.17	1.78	1.45	2.08	**1.75**
se	*2.22*	*0.08*	*0.37*	*0.41*	*0.24*	*0.49*	*0.32*	*0.08*	*0.17*	*0.52*	*0.05*	*0.22*	*0.11*	*0.11*	*0.38*	**0.03**
TOTAL																
mean	68.27	80.93	74.20	74.70	74.63	72.68	72.21	81.06	71.96	70.99	71.55	67.38	67.75	75.22	72.30	**73.06**
se	*3.59*	*0.41*	*0.96*	*0.55*	*1.39*	*1.48*	*2.31*	*0.81*	*1.77*	*2.26*	*0.67*	*2.31*	*1.57*	*0.27*	*1.10*	***0.13***

3.4. Principal Component Analysis

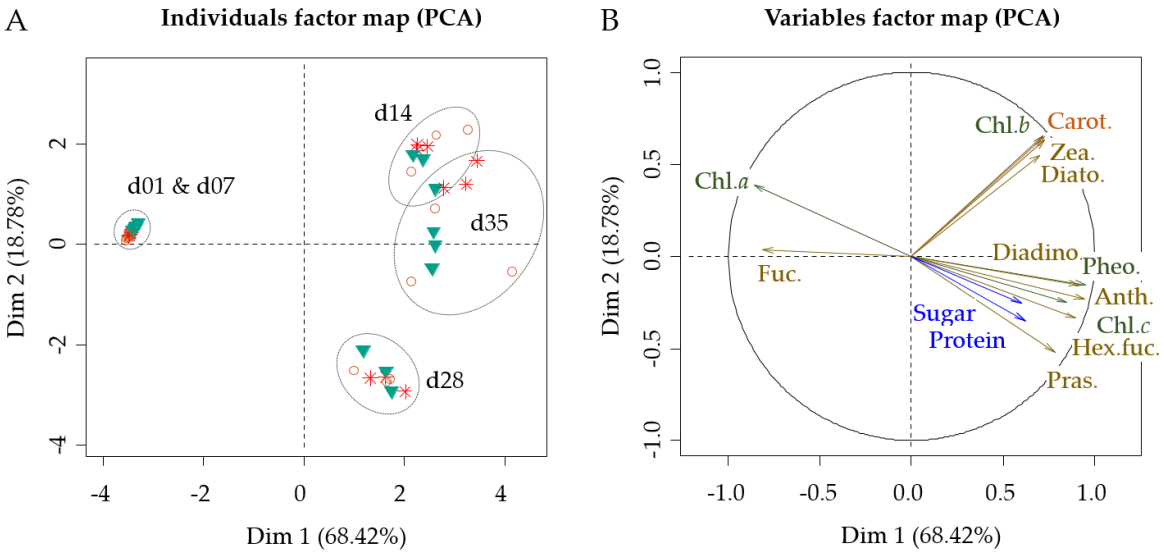

Figure II-3: Principal component analysis: A) Ordination of the samples according to sampling time (d01: first day, d07: 1 week, d14: 2 weeks, d28: 4 weeks, d35: 5 weeks) and substrates (red star: grey concrete, green triangle: dolomite Sorel cement, brown circle: white concrete). B) Correlation circle of the pigments variables (Carotens: Carot., Chl.a: Chlorophyll a, Chl.b: Chlorophyll b, Chl.c: Chlorophyll c, Pheo.: Pheopigments, Anth.: Antheraxanthin, Diadino.: Diadinoxanthin, Diato.: Diatoxanthin, Fuc.: Fucoxanthin, Hex.fuc.: Hex-fucoxanthin, Pras.: Prasinophyte, Zea.: Zeaxanthin) and supplementary variables (sugar and protein concentrations).

The PCA was performed on pigment variables (12 pigments) and supplementary variables (sugar and protein concentrations) have been computed to verify potential correlations. The samples were collected according to substrates (Ds, Cg and Cw for dolomite Sorel cement, grey concrete and white concrete, respectively) and sampling dates (from d01 to d35; Figure II-3). The first axis, which represented 67.03 % of total inertia, mainly structured the samples. The second axis also explained a large part of the total inertia (19.23 %), while the third axis (5.4 % of the total inertia, <mean threshold 1/12 = 8.33 %) was not retained in the analysis. The first two dimensions showed a good projection of the data, as all variables were close to the correlation circle, except the supplementary variables, and individuals had cumulative squared cosinus above 0.7 on these two dimensions (except the first and third replicates from Cw at d35). Chlorophyll *a*, fucoxanthin, pheopigments, diadinoxanthin, antheraxanthin, hex-fucoxanthin and chlorophyll *c* concentrations from d01 and d7 samples, and the Ds and Cw samples from d35 mainly contributed to the construction of the first dimension. Chlorophyll *b*, diatoxanthin, zeaxanthin, and prasinoxanthin concentrations

measured in the d14 and d28 samples and the grey concrete sample at d35 mainly contributed to building the second dimension. On one hand, chlorophyll *a* and fucoxanthin concentrations from samples of the first week were negatively correlated with the first dimension, while pheopigments, diadinoxanthin, antheraxanthin, hex-fucoxanthin and chlorophyll *c* concentrations of the Ds and Cw samples at d35 were positively correlated with the first dimension. On the other hand, chlorophyll *b*, diatoxanthin, zeaxanthin within d14 samples and grey concrete samples at d35 were positively correlated with the second dimension, whereas prasinoxanthin and d28 samples were negatively correlated with this dimension (Figure II-3). Supplementary variables did not show significant correlations with the first two dimensions.

4. Discussion

The assessment of the quality of total polymeric substances (PS) in conjunction with photosynthetic communities of biofilm on different types of substrates enabled a better understanding of the first step of colonisation of AR, and established the first basis for a protocol to assess the ecological quality of different AR materials. We hypothesised that the substrate type is likely to induce differences (i) in microbial diversity during the colonisation process, and (ii) in the composition of biofilm secretions. The influence of substrate on biofilm attachment and diversity has been extensively investigated and most of the studies revealed significant differences (Dexter et al. 1975, Dexter 1979, Fletchert & Loeb 1979, Fletcher & Pringle 1985, Pringle & Fletcher 1986, Fletcher & Callow 1992, Cooksey & Wigglesworth-Cooksey 1995, Finlay et al. 2002, D'Souza et al. 2005, Patil & Anil 2005, Jones et al. 2007, Sweet et al. 2011, Lakshmi et al. 2012, Ozkan & Berberoglu 2013, Tan et al. 2015). In this study, diversity, abundance and secretion were significantly different according to sampling time, but only sugar secretion showed significant differences between substrates.

The biofilm on each substrate became mature after two weeks of monitoring, as shown by the high concentration and diversity of pigments, and the sugar to protein ratio that reached a stable value. Previous studies showed that the maturity of biofilm influences the settlement of various larvae of *Mytillus galloprovencialis* (Bao et al. 2007), *Hydroides elegans* (Huang & Hadfield 2003, Chung et al. 2010), *Enteromorpha* sp. (Dillon et al. 1989), *Balanus amphirite* (Faimali et al. 2004) and *Bugula neritina* (Dahms et al. 2004) according to diversity, density and secretion of PS.

The overall pattern of changes of the communities is well illustrated by the two first axes of the PCA performed on pigment variables. The first axis represented the diversity of these biofilm communities over time, where communities of the first week (d01 and d07) were related to chlorophyll *a* and fucoxanthin, and the other sampling times to chlorophyll *c* and all the minor pigments and supplementary variables (sugar and protein concentrations). The second axis represented the split due to the storm event that eroded the biofilm, with samples at d14 characterised by the presence of the less abundant pigments (chlorophyll *b*, diatoxanthin, zeaxanthin and carotene), contrasting with samples at d28 characterised by the loss of rare pigments and the increase of prasinoxanthin, antheraxanthin, chlorophyll *c*, hex-fucoxanthin and diadinoxanthin. At the end of monitoring, the communities are more scattered

and recovered slowly to reach the initial state (d14). The loss of zeaxanthin, carotene and chlorophyll *b* might be due to the limitations of HPLC detection. The concentrations of these pigments were very low before the storm and could be undetectable after it. Thus, this loss is not to be considered as a variation in terms of diversity of the pigment composition of communities, but rather as a variation in terms of proportion of the different pigments.

Consistent with the presence of the three types of chlorophyll (*a*, *b* and *c*), the communities were composed of green and brown algae, and perhaps of photosynthetic bacteria (cyanobacteria including prochlorophytes, Jeffrey et al. 2011). According to the proportions of fucoxanthin, chlorophyll *c*, diadinoxanthin and diatoxanthin, brown algae were dominant. Diatoms should be the main taxon represented, since fucoxanthin can represent up to 60% of their pigment content (Strain et al. 1944). It is known that Raphids diatoms generally represent the main taxa of marine biofilm (78%; Wahl 1989; Callow & Callow 2006; Salta et al. 2013). The presence of hex-fucoxanthin may reveal the specific presence of benthic haptophytes of the Coccolithophyceae class (Jeffrey et al. 2011), although this was not documented in the biofilm community. The association of antheraxanthin and prasinoxanthin may reveal the presence of prasinophytes among the green algae (Egeland et al. 1995, Jeffrey et al. 2011). Finally, endosymbiotic dinoflagellates with pigments of haptophyte, diatoms and prasinophytes origin, can also occur (Jeffrey et al. 2011). Dinoflagellates and green flagellates (like prasinophytes) are known to each represent 1% of the biofilm communities (Wahl 1989, Callow & Callow 2006, Salta et al. 2013). The increase of diadinoxanthin, hex-fucoxanthin and prasinoxanthin after the storm might reveal a shift in the community toward the increase of flagellate organisms (dinoflagellates, coccolithophores and prasinophytes), perhaps coming from the water column after the storm, since those flagellate organisms are planktonic (Jeffrey et al. 2011). Besides, the increase of sugar concentrations on grey concrete and white concrete might also reveal the increasing activity of diatoms. Diatoms, previously identified as the main taxa of the community, secrete a mucilage rich in polysaccharides to adhere to substrates (Hecky et al. 1973, Myklestad et al. 1989, Hoaglang et al. 1993, Underwood & Paterson 2003, Stal & Défarge 2005, Bruckner et al. 2008). Pigment concentrations, mainly related to fucoxanthin produced by diatoms, strongly increased on all substrates from d14, thus the dynamic of sugar secretions appeared not to be synchronous with their settlement on these different substrates. Previous culture studies have shown that benthic diatom cells produce

higher concentrations and greater proportions of extracellular carbohydrates when cells enter the transition from exponential growth to stationary phase (Sutherland et al. 1998, Underwood & Smith 1998, Staats et al. 1999, Underwood & Paterson 2003). It might be possible that diatoms settled on grey concrete and white concrete start their stationary phase after the 14th day of monitoring, whereas they continue to grow on dolomite Sorel cement. These differences in secretion of PS between substrates might also be due to differences in diatom species composition. Culture studies showed that species composition can affect the amount of PS secreted, some species having significantly higher rates of PS production than others under the same conditions (Smith & Underwood 2000, De Brouwer et al. 2002, Underwood & Paterson 2003). Although HPLC detection of pigments could not identify differences in terms of diatoms diversity, our results are consistent with previous studies that showed that substratum type can influence the diversity of the diatom community and of their PS secretion (Cooksey & Wigglesworth-Cooksey 1995, Finlay et al. 2002, Patil & Anil 2005, Chung et al. 2010, Ozkan & Berberoglu 2013). Diatoms represent a large part of the feeding resources and they are often associated with the post-larval dietary requirement for suspension feeders (Lam et al. 2003) or grazing juvenile invertebrates, such as gastropods (Slattery 1992, Bryan & Qian 1998, Siqueiros-Beltrones & Voltolina 2000, Dahms et al. 2004, Siqueiros Beltrones & Valenzuela Romero 2004), sea urchins (Rahim et al. 2004) and sea cucumbers (Ito & Kitamura 1997). Thereby, the significant differences in sugar concentration on dolomite Sorel Cement compared to the other substrates might have a negative impact on the feeding resources of suspension feeders and grazing invertebrates.

To the best of our knowledge, analyses of global amino acids in *in situ* biofilm development are rare. Bhosle et al. (1997; 2005) monitored the amino acid composition of biofilms on aluminium panels in an Indian tropical bay, focusing on the contribution of the major sources of organic matter in the biofilm chemical composition. They observed that the distribution of individual amino acids did not vary in time, and was very similar to that observed in the two main sources of organic matter, and was dominated by aspartic acid, glycine, alanine, serine, leucine, lysine and glutamic acid. In our study, the amino acid composition of the biofilms was dominated by glutamic acid, glycine, aspartic acid, proline, alanine and serine. This composition could stem from the sinking organic matter of marine snow and/or from the microbial community itself that produces protein. But it is generally difficult to distinguish

differences between proteins produced by different taxa on the basis of their amino acid composition. The amino acid composition of the proteins is highly conserved among different species, even those performing specific functions. For instance, it has been shown that 16 microalgae species exhibited minor differences in the amino acid composition of their hydrolysates (Brown 1991). Aspartic acid and glutamic acid are generally found at the highest concentrations, while cysteine, methionine, tryptophan, histidine and proline are found at the lowest concentrations. Therefore, it would be spurious to estimate biofilm diversity on the basis of their amino acid composition. However, the high degree of conservation in amino acid composition among species exudates makes it an interesting biomarker to monitor changes in biofilm functioning. Amino acids can indeed play a key role in the settlement of the macrofouling, Trapido-Rosenthal & Morse (1985) showed that the presence of lysine at a micromolar concentration facilitates the induction of larval settlement and the metamorphosis of *Haliotis rufescens*. In addition, the proportion of essential amino acids in the biofilm is a useful proxy of biofilm nutritional quality for higher trophic levels. The slight differences detected between the dolomite Sorel cement and the other substrates at d14 and d35 could potentially imply a lower nutritional quality on the dolomite Sorel cement.

Taken together, these results suggest that the use of different substrates for ARs may lead to differences in the biofilm composition and secretions, and thus biofilm characterization in this context proves to be a good tool. Through the characterization of the PS composition secreted by the biofilm communities, we have been able to highlight significant differences in sugar concentration of the biofilm between the dolomite Sorel cement and the two types of concrete. This could potentially have an impact on organisms that settle and/or feed on this biofilm. Thus, it is essential to understand these mechanisms in the context of ARs, in order to enhance the colonisation. Otherwise, the two concrete substrates did not show significant differences in the parameters surveyed in this study, while white concrete contains less metallic oxide than grey concrete (Telford 1999, BETOCIB 2000). Further analyses are thus needed to determine whether or not those two substrates present equivalent substrate quality for AR communities. Further research is also needed to understand the mechanisms involved in the adaptation of communities to substrates and to determine whether those differences might imply differences in the settlement of sessile macro-organism larvae and propagules at higher

trophic levels. We need to determine whether the physical or chemical properties or both are involved in these mechanisms.

Conclusions

We identified a photosynthetic biofilm community mainly composed of diatoms, prasinophytes, coccolithophores and dinoflagellates on each substrate. We also identified differences between communities on the dolomite Sorel cement and those of white and grey concrete. The lower sugar to protein ratio on the dolomite Sorel cement community might be the result of differences in biofilm community composition and activity and is potentially determinant in the recruitment of various larvae and with regard to the diet of grazing invertebrates. We showed that biofilms are useful bio-indicators in that they develop quickly and give a rapid estimation of the quality of AR substrates.

III. CHAPTER 2: COLONISATION OF ARTIFICIAL REEF SUBSTRATES: "THE HABIT DOES NOT MAKE THE MONK."

To be submitted

Authors: Riera E., Francour P., Hurel C., Lamy D. & Hubas C.

Résumé

Le premier matériau à base de ciment Sorel n'ayant pas eu une stabilité suffisante dans le milieu marin, un nouveau matériau a été développé à base de ciment blanc, de sable des Dolomites et de cendre volcanique. La composition de ce matériau limite la présence de métaux lourds, d'adjuvants chimiques et a un pH neutre dans le milieu marin. Poursuivant les travaux décrits dans le chapitre 1, la présente étude évalue l'influence de différents matériaux (le béton, le nouveau matériau utilisé pour l'impression des récifs 3D et la roche naturelle) sur les communautés de biofilm et de macrofouling. Le suivi s'est effectué au cours d'une année, dans deux aires marines protégées : la réserve du Larvotto de Monaco en zone hyper-urbanisée et la réserve de Roquebrune Cap Martin en zone urbanisée.

Nous supposons que le matériau est susceptible d'influencer la qualité du biofilm jusqu'au recrutement des macro-organismes aussi bien au niveau de leur structure, de leur sécrétion et de leur capacité à accumuler les métaux lourds présents dans l'environnement ou dans les matériaux eux-mêmes. Nous supposons également que l'ensemble de ces variables seront susceptibles d'être influencées par le site d'échantillonnage.

La structure des communautés du biofilm a été identifiée à l'aide de biomarqueurs pigmentaires extraits par HPLC et par méthode de métabarcoding sur le 16S des procaryotes. La matrice extracellulaire du biofilm a été analysée en termes de concentrations totales en sucres et en protéines par colorimétrie. La structure des communautés de macrofouling a été analysée par identification taxonomique visuelle. Enfin le contenu en métaux lourds au sein du biofilm, du macrofouling, des matériaux et de la matière organique particulaire a été déterminé par ICP-OES.

Nous avons pu démontrer que la nature du matériau a peu d'influence sur la structure des communautés (biofilm & macrofouling). Cependant, sur les échantillons de béton, la sécrétion du biofilm ainsi que la séquestration de métaux lourds présents dans l'environnement est plus importante que sur les autres matériaux. Cette réponse est davantage significative au sein des communautés échantillonnées dans la réserve de Monaco.

Les différences observées entre les matériaux sont probablement liées aux caractéristiques du pH et de la microrugosité. Celles-ci impliquent des sécrétions plus abondantes des communautés de biofilm, ce qui a pour conséquence d'augmenter leur capacité d'absorption des métaux lourds. Cette capacité d'absorption semble s'observer également au sein du macrofouling dans une moindre mesure. La différence entre les deux sites est probablement liée au niveau d'urbanisation de la côte favorisant le lessivage des métaux lourds qui se retrouvent ainsi dans le milieu marin.

Abstract

In order to meet some of the prerogatives of the UNEP guidelines for artificial reefs, it seems worthwhile to be concerned about the quality of the substrates used for the construction of artificial reefs. Little comparative monitoring exists to date and does not allow to determine if pollutants are trapped within the communities that develop on these substrates. The present study evaluates the quality of different substrates (concrete, dolomite and rock) over a one-year monitoring from the biofilm communities to the succession of the macrofouling communities in two marine protected area (Larvotto reserve of Monaco and Roquebrune Cap Martin). We have been able to demonstrate that the nature of the substrate has little influence on the structure of communities (biofilm & macrofouling), however it significantly influences the secretion of biofilm as well as the sequestration of heavy metals present in the environment.

Key words : artificial reef substrates, artificial reef colonisation, biofilm community, photosynthetic pigments, metagenomic on prokaryote, biofilm matrix, extracellular polymeric substances, macrofouling community, heavy metal contamination, bio-indicator

1. Introduction

Since ages, in the marine environment, Man has immersed artificial structures in order to create dedicated habitats to attract species of interest. These structures have been immersed, these last decades, only according to judgment expert and rarely based on scientific criteria. Once the artificial reef has been immersed, the material used to build it constitutes the first element in contact with the marine environment. Its colonization follows a well-known basic pattern named “fouling sequence model”. Firstly, the surface is covered by a conditioning film formed by the surrounding water, this film can sometimes mask the physicochemical characteristics of the material. Following this film, the first microorganisms colonize the reef allowing the formation of a biofilm at the surface. The matrix extracellular substances produced by this biofilm can in turn positively or negatively influence the colonization of larvae of multicellular organisms constituting the reef macrofouling (Wahl 1989, Svane & Petersen 2001).

The term biofilm refers to a microbial community that binds to a biological or non-biological submerged surface as well as the diversity of molecules produced by the microbes outside the cells membrane (Costerton et al. 1994, Hall-stoodley et al. 2004). In the photic marine environment, it is mainly composed of diatoms and cyanobacteria (Wahl, 1989; Callow and Callow, 2006; Salta et al., 2013). The adhesion of these microorganisms is mediated by the secretion of these external compounds named extracellular polymeric substances (EPS) composed of macromolecules such as polysaccharides, proteins, nucleic acids, lipids and other polymeric substances (Flemming & Wingender 2010). The composition of these EPS can vary according to the environmental conditions to which the microorganisms are subjected. The expression of particular phenotypes confers them a better access to nutrients, a better colonization capacity and a better resistance to environmental pressures (Salta et al. 2013). The subsequent colonisation by macrofouling is determined by the local biological environment, but the substrate can also have a preponderant influence on it (Bohnsack & Sutherland 1985, Bohnsack 1991, Svane & Petersen 2001). In Mediterranean Sea, Ardizzone et al. (2000) determined a global model of colonisation with early benthic colonization by diatoms, hydroids, serpulid polychaetes, barnacles and molluscs. Then, the equilibrium of the community is an interactive and dynamic process driven by environmental conditions and interspecific competition of the assemblage (Svane & Petersen 2001). The success of artificial reefs

according to the use of different material used has been rarely investigated (Brown 2005, Riera et al. 2018), and these studies focus mainly on biofilm and macrofouling community structure and EPS secretion of biofilm. However, it is important to determine if the material itself is a source of pollution to the marine environment and/or the reef food web.. Biofilm and biofouling are known to highly bioaccumulate heavy metals, and could be the first step in the contamination of the entire food web (Kratochvil & Volesky 1998, Bhaskar & Bhosle 2006, Romera et al. 2007, Das et al. 2008, Pal & Paul 2008, Dash et al. 2013, Decho & Gutierrez 2017)

This study aims to study the evolution of epibenthic communities developing on different substrates used for the construction of artificial reefs. In addition, this study makes it possible to determine whether certain substrates promote the phenomena of bioaccumulation of heavy metals. This monitoring has been carried out from the first stages of colonization of the biofilm until the establishment of macrofouling communities. We hypothesized (i) that the nature of the substrate used to build artificial reefs could affect the structure of the biofilm microbial community and its EPS secretion, and (ii) that substrates and biofilm could influence the colonisation by macrofouling. Finally, we hypothesized that these differences between substrates could affect the sequestration by biofilms and/or macrofouling of heavy metals present in the environment and/or in the substrates used for this monitoring. To test these hypotheses, we first monitored the colonisation of biofilm microbial communities on different artificial reef substrates by metagenomic sequencing on prokaryotic 16S rDNA genes (bacteria and archaea) and by HPLC to identify photosynthetic communities. Colorimetric analyses on sugar and proteins were performed to characterize the content of the EPS of the biofilm matrix. Secondly, we monitored macrofouling communities over a period of one year by taxonomic identification. Both monitorings were completed by an analysis of heavy metals content in biofilm and macrofouling, compared to the heavy metals contained in the virgin substrates and in sinking and suspended particulate organic matter (POM) collected by sediment traps.

2. Materials & methods

2.1. Substrates

Three different substrates used for artificial reefs have been tested: the rock, mainly used for dikes and rockfills, the concrete, mainly used to build classical module of artificial reefs nowadays, and a substrate based on dolomite sand and white cement made by the Boskalis industry and used to build artificial reef using giant 3D printers (D-Shape). This substrate will be named thereafter "dolomite". The samples were cut in different shapes according to the monitoring type. For the biofilm monitoring, each cobblestone sized 1.5x2x5 cm in order to fit in a 50 ml Falcon tube. For the macrofouling monitoring, each plate sized 25*25*5 cm, and mimics a quadrat used for the determination of benthos on the rocky reefs. In total 330 samples for the biofilm monitoring and 96 samples for the macrofouling monitoring have been immersed.

2.2. Monitoring and sampling

The monitoring took place during one year on two different sites: in the coastal waters of the Marine Protected Area (MPA) of Larvotto (Monaco) (7.440066°E, 43.74633°N), managed by the AMPN (*Association Monaco pour la Protection de la Nature*); and in the MPA of Roquebrune Cap Martin (7.449783°E, 43.75158°N) managed by "le Service de l'eau, des déchets et des énergies de la Direction de l'Environnement et de la Gestion des Risques du Département des Alpes Maritimes". These two MPA have been chosen to see whether highly artificial coast in the Monaco Larvotto reserve would show differences with the protected and natural coast of the MPA of Roquebrune (Figure III-1).

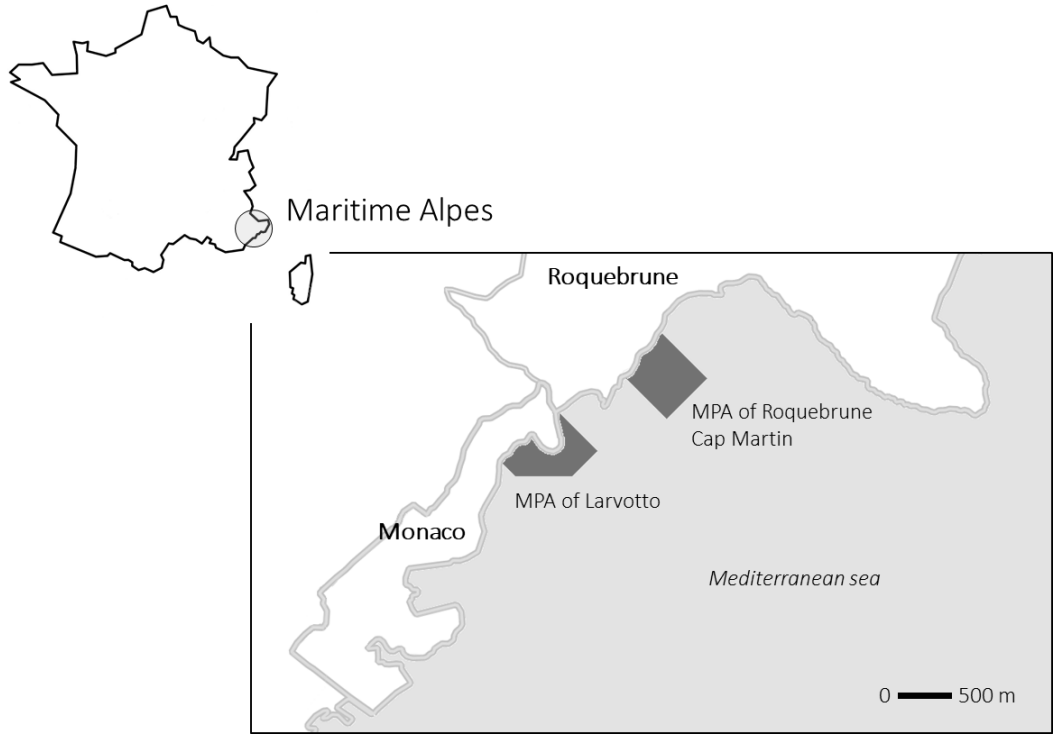

Figure III-1: Map of the two Marine Protected Areas (MPA) selected for the sampling design: The Larvotto reserve (Monaco) with a highly artificialized coast and Roquebrune Cap Martin (France) with a natural coast

The biofilm monitoring was done within a month in May 2017, in order to get a mature biofilm. The samples were retrieved every week to follow this maturation of the biofilm communities. The sampling took place 7, 14, 21, and 28 days after immersion. The samples were immersed at 25 m depth, 2 meters above artificial reefs of the two different MPAs. They were fixed on 5 different 1m² plastic frames (1 frame for each sampling date), suspended from a 10 litres buoy and anchored to the artificial reefs. The immersion, the installation and the sampling follow the same methods as Riera et al. 2018 (Chap. 1, p.55).

The macrofouling monitoring was done over a year, the samples were retrieved every season to monitor the macrofouling communities. The plates have been immersed in May 2017. The sampling took place in August 2017 (Aug. 2017), October 2017 (Oct. 2017), February 2018 (Feb. 2018), and April 2018 (Apr. 2018). The samples were placed on the artificial reefs of the two different MPAs. Immersion, installation and sampling were done by scuba divers. Before the retrieval of each plate, it was wrapped in plastic film and placed in a plastic bag in order to prevent any detachment of the organisms. It was then placed in a solid plastic box and elevated to the surface by diving parachute of 50 litters.

We immersed replicates of the 3 substrates for each sampling period at each site and for every kind of analysis, our replicates are then not paired between analyses. In total 330 samples for the biofilm monitoring and 96 samples for macrofouling monitoring have been immersed. In addition, two sediment traps have been placed in both selected sites with three temperature loggers. They were retrieved and replaced at the end of the biofilm monitoring (May 2017) and at each sampling date of macrofouling (Figure III-2)

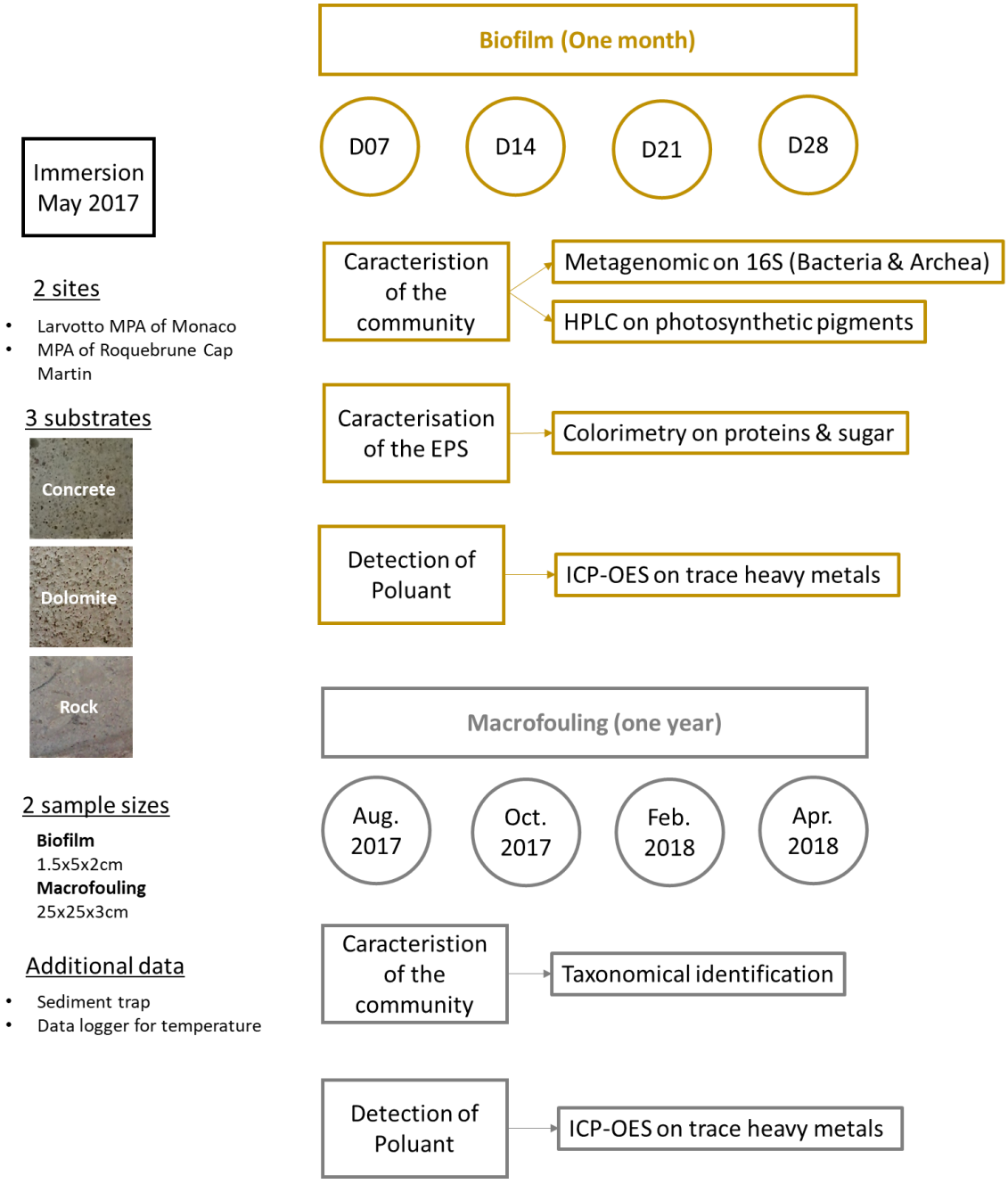

Figure III-2: Sampling design for the monitoring of the biofilm and macrofouling on 3 different substrates (Concrete, Dolomite, Rock) in two different Marine Protected Area (Larvotto MPA of Monaco, and MPA of Roquebrune Cap Martin), and analyses related to both monitoring

2.3. Biofilm analysis

Each cobblestone was directly stored in a sterile 50 mL Falcon tube after each sampling occasion. Except for the samples used for extracellular polymeric substances (EPS) analyses, all samples were immersed in liquid nitrogen to stop any activity and deterioration of the community. To prevent the samples dedicated to EPS analyses from freezing (and therein to prevent cell lysis and release of internal sugar and proteins), they were stored in a cooler at 4°C during the way back from the fieldwork to the laboratory, where it was immediately processed.

The extraction of EPS and subsequent colorimetry analyses as well as pigment analyses by High Performance Liquid Chromatography (HPLC) were done according to the same methodologies described in Riera et al. (2018) (Chap.1, p.56-57).

2.3.1. Prokaryotic communities: DNA extraction, sequencing and data analysis

Biofilm was scratched from the substrate using a scalpel and fibber glass filter (GF/F). The DNA was extracted from biofilm with the "DNeasy PowerBiofilm" Kit (Qiagen). 20 µl of extracted DNA (min: 3.5 $ng.\mu l^{-1}$, max: 13.91 $ng.\mu l^{-1}$, spectrophotometrically measured with Nanodrop) was sent to the Laboratory MR DNA (MR DNA, Shallowater, TX, USA) a full-service next generation sequencing service provider, that processed the amplification and sequencing of the samples. The V4-V5 region of the 16S rDNA gene was amplified with the primer sets 515f-Y (GTGYCAGCMGCCGCGGTAA) and 926r (CCGYCAATTYMTTTRAGTTT; (Parada et al. 2016)) with barcode on the forward primer. A PCR of 30 cycles with the HotStartTaq Plus mixing kit (Qiagen, Valencia, CA) was performed under the following conditions: 94 °C for 3 minutes, followed by 28 cycles at 94 °C for 30 seconds; 53 °C for 40 seconds and 72 °C for 1 minute, then a final elongation step at 72 °C for 5 minutes. After amplification, the PCR products of the different samples were monitored in a 2 % agarose gel to determine the success of the amplification and the relative intensity of the bands. Multiple samples were mixed in equal proportions based on their molecular weight and DNA concentrations, and then purified with calibrated Ampure XP beads. These pooled and purified products were used to prepare a DNA library following Illumina TruSeq DNA library. After the amplification and denaturation steps, the libraries were grouped and sequenced. 50 ng of DNA from each sample was used to prepare

the libraries using the Nextera DNA Sample Preparation Kit (Illumina). The size of the library insert was determined by the Experion Automated Electrophoresis Station (Bio-Rad). The size of library inserts ranged from 300 to 850 bp (average 500 bp). The pooled library (12 pM) was loaded into a reagent cartridge 600 Cycles v3 (Illumina) and Sequencing was performed on a MiSeq according to the manufacturer's instructions. Mock community DNA (ZymoBIOMICS, Ozyme) was used as a standard for subsequent analyses. The sequences data were processed using MR DNA analysis pipeline (www.mrdnalab.com, MR DNA). In short, sequences were joined and the barcodes and primers sequences were trimmed. Short sequences < 150 pb, the sequences with ambiguous base calls were deleted. The remaining sequences were denoised and clustered at 97 % sequence similarity to define Operational taxonomic units (OTUs). Singletons and chimeras were removed from analyses. Final OTUs were taxonomically classified using BLASTn against a database organized from GreenGenes, RDPII and NCBI (www.ncbi.nlm.nih.gov, DeSantis et al., 2006, http: // rdp.cme.msu.edu).

2.4. Macrofouling identification

The plates were unwrapped and gently placed in a plastic tray. With the help of a guillotine blade, all the organisms were detached from the substrate and gathered in the plastic tray. Each sample was then passed under a 100 µm sieve to get rid of the fine sediments, then placed in a container with artificial seawater (30 g. L^{-1} of salt, equivalent to the salinity of the study site), and stored at 4 °C before sorting organisms at the lab. No preservatives were added because all samples were pre-sorted within two days after the sampling. Sorting was carried out using different sieves inferior to 400 µm as recommended in Ganbi and Dappiano (2004) for macrofouling identification. A pre-identification step was done with a binocular Nikon SMZ -10. The different species (higher taxa) were then kept in adequately sized containers and frozen until final identification using a Stereomicroscopes LEICA M80, connected to a Qimaging RoHS camera and a lamp LEICA CLS 150 XE. Pictures of samples were done for post-verification, using the Image Pro plus 7.0 software. Depending on the individual development and their state after being detached from the plates, some of them could be identified up to the species. The identification has been done with the help of referenced manuals (Giulia & Stefano 1991, Riedl 1991, Pansini et al. 2011, Rodriguez-Prieto et al. 2015). The database

Worms (http://www.marinespecies.org/) and Algae Base (http://www.algaebase.org/) were used to verify the species terminologies according to their phylogeny. After the last identification, samples have been dried in an oven at 70°C and weighed to the nearest milligram with a balance (Denver instrument company TR-64) to obtain the total macrofouling dry weight (expressed in mg cm^{-2}).

2.5. Heavy metals analyses

The heavy metals concentration (As, Cd, Cr, Cu, Ni, Pb, Zn) was measured in the biofilm, the macrofouling, the 3 substrates and in the sinking and suspended marine particulate organic matter (POM) collected in the sediment trap (Figure III-2) to assess the contamination level in all the compartments of this study.

Samples preparation - To gently detach the biofilm from the substrate, 5 ml of ultra-pure water was added to the sample before agitation with optoelectronic speed control (VXR basic Vibrax ®) at 2.2 rpm for 30 seconds. The substrate was then removed and the biofilm retrieved in the tube was frozen and lyophilized. The macrofouling was retrieved with a plastic ruler previously cleaned with alcohol and ultra-pure water, placed in petri glasses and dried in an oven at 110 °C. Three virgin samples of the different substrates that were not immersed were crushed with a plastic harmer. The sediment was recovered from the two sediment traps after 24h of sedimentation after sampling and dried in an oven at 110 °C. After being weighted separately to assess the sedimentation rate (in g m^{-2} day^{-1}), the marine POM coming from two different sediment traps was pooled. All the different sample types (biofilm, macrofouling, marine POM and substrate) have been then reduced in powder with a ceramic pestle.

Heavy metals quantification - 3 aliquots of each sample type were weighed in an Erlenmeyer flask before the addition of 5 ml ofpure HNO_3 (> 65%; puriss. p.a.) was added for the first digestion step. The sample was then heated on a hotplate at 90° C and 3. 30ml of aqua regia (1/3 HNO_3 + 2/3 HCl (37%, Fisher Chemical) . was progressively added. Once this second digestion step was complete, 5ml of H_2O_2 (30% (v/v) EPR) was added to end the sample digestion, and the sample was reduced to the maximum, without however drying it. After this last digestion step, in order to reduce the acidity, the digestion products were diluted and

reduced three times with 100 ml of ultra-pure water. The rinsed and diluted sample was resuspended in ultrapure water up to 40 ml. After centrifugation at 4 000 rpm for 10 min, the supernatant containing the heavy metals in suspension was recovered in a beaker and reduced again on a hotplate at 90 °C. The pellet, containing the sediment was resuspended in ultrapure water up to 15 ml and centrifuged again at 4000 rpm for 10 min. The supernatant was then added to the previous one, and reduced again on a hotplate at 90 °C. Then, the sample was 1/10 or 1/2 diluted with Ultra-pure water, depending on the concentration of the sample. The pellet was dried in an oven at 110 °C and weighted in order to determine the quantity of undigested material to be deduced from the mass of the studied samples. The quantities of heavy metals were then expressed in ppm ($mg.kg^{-1}$) of samples. The detection of the elements was carried out on an Optima™ 8000 DV ICP-OES, using corresponding wave length of the targeted elements (As: 193.696 nm, Cd: 228.802 nm, Cr: 267.716 nm, Cu: 324.752 nm, Ni: 231.604 nm, Pb: 220.353 nm, Zn: 206.200 nm). A standard from 0.02 to 10 ppm of the targeted heavy metals was carried out for quantification. Quantification allowed us to raise a comparative study of heavy metals repartition in biofilm and macrofouling depending on their growth on the different substrates. Heavy metals concentrations were compared to data from Seytre et al. (2012), relative to the quality of the water column in Monaco and Roquebrune Cap Martin areas.

2.6. Statistical analyses

All statistical tests and illustrations have been done with the open source software R (3.4.1), using “FactoMineR” (Husson et al. 2016), “vegan” (Oksanen et al. 2017), ade4 (Dray et al. 2018), ggplot2 (Wickham & Winston 2019) and “agricolae” (De Mendiburu 2016) packages.

Univariate data:

- Colorimetry analyses: concentration of sugar and proteins within biofilm EPS
- Macrofouling identification: the total dry weight of macrofouling;
- Heavy metals analyses: total concentration of heavy metals contained in biofilm, macrofouling, sediment trap and virgin substrates

We used the univariate non-parametric Van-der-Warden test to determine differences in time, sites and between substrates on the different univariate data. The illustration related

to these results have been proceeded with the ggplot2 package, we used the non-parametric LOcally weighted Scatterplot Smoother (LOESS) regression method to calculate the best fit (average +- confidence interval) .

Multivariate data:

- Metagenomic analyses: relative abundance of bacteria identification at classes level for each sample
- HPLC analyses: percentage of pigments for each sample
- macrofouling identification: percentage of the total dry weight of macrofouling identification at the highest taxonomical level for each sample

To test differences between sites, sampling and substrates, we used the non-parametric statistical test of the analysis of similarities (ANOSIM) using a Bray-Curtis dissimilarity index.

To illustrate the dissimilarities between samples, we followed the different step described below:

1. A Bray-Curtis dissimilarity matrix has been calculated on each set of multivariate data (vegan package)
2. A hierarchical classification has been processed on the Bray-Curtis matrix using the Ward agglomeration method (Murtagh & Legendre 2014) to identify the distance between each cluster (R base)
3. The best partition of the dataset was performed by k-means partitioning using a range of values of k clusters. Function cascadeKM (package vegan) creates several partitions forming a cascade from a small to a large number of clusters (i.e. from 2 to 24 in the present sutdy). The “Calinski-Harabasz” criterion has been used to select the best partition (Calinski-Harabasz 1974).

A Principal Coordinates Analysis (PCoA), has been performed on the Bray-Curtis dissimilarity matrix of the data using ade4 package.On the ordination plot, scores were then grouped according to the hierarchical classification and the best partition previously evidenced (steps 2 and 3)

Heavy metals analyses

The percentage of the heavy metals has been processed for each sample of biofilm at D28 and for each sample of macrofouling at Apr. 2018, and where compared to the mean percentage of the marine POM in sediment traps for each biofilm and macrofouling monitoring, and to the mean percentage of each virgin substrates.

Two Principal Component Analysis (PCA) were applied to the percentage of heavy metals results, one for each monitoring. Total heavy metals concentration for both monitorings was added as supplementary variable to identify potential correlation, but did not influence the ordination of the PCA: The samples were collected according to partition determined by Hierarchical Clustering On Principle Components (HCPC) function corresponding to the higher relative loss of inertia.

3. Results

3.1. Temperature and sedimentation rates during the monitoring

The temperature was similar between sites during the biofilm monitoring (16.9 ± 0.4 C° at Monaco and 16.8 ± 0.4 C° at Roquebrune. During the macrofouling monitoring, the temperature was higher at Monaco than at Roquebrune in summer (2017_08) and autumn (2017_10) season (Student test $p<0.01$). Then, the temperature was similar between sites for winter (2018_02) and spring (2018_04) season (Figure III-3: A) Average temperature of the sea, B) average sedimentation rate during biofilm and macrofouling monitoring at Monaco and Roquebrune.. During the monitoring of macrofouling, the sedimentation rate was greater in Monaco than in Roquebrune (Figure III-3: A) Average temperature of the sea, B) average sedimentation rate during biofilm and macrofouling monitoring at Monaco and Roquebrune.). On both sites, the sedimentation rate increased drastically after six months of monitoring, especially at Monaco (Monaco: from 8.02 ± 0.06xxx g.m-².day-1 to 52.34 ± 1.02 g.m-².day^{-1}, Roquebrune: from 4.84 ± 0.25 g.m-².day-1 to 15.14 ± 2.07 g.m-².day^{-1}), peaked during the winter season (Monaco: 161.73 ± 0.04 g.m-².day-1, Roquebrune: 98.33 ± 6.94 g.m-².day-1) and then decreased at the end of the monitoring (Monaco: 91.55 ± 0.86 g.m-².day-1, Roquebrune: 54.22 ±0.12 g.m-².day-1) (Figure III-3: A) Average temperature of the sea, B) average sedimentation rate during biofilm and macrofouling monitoring at Monaco and Roquebrune.).

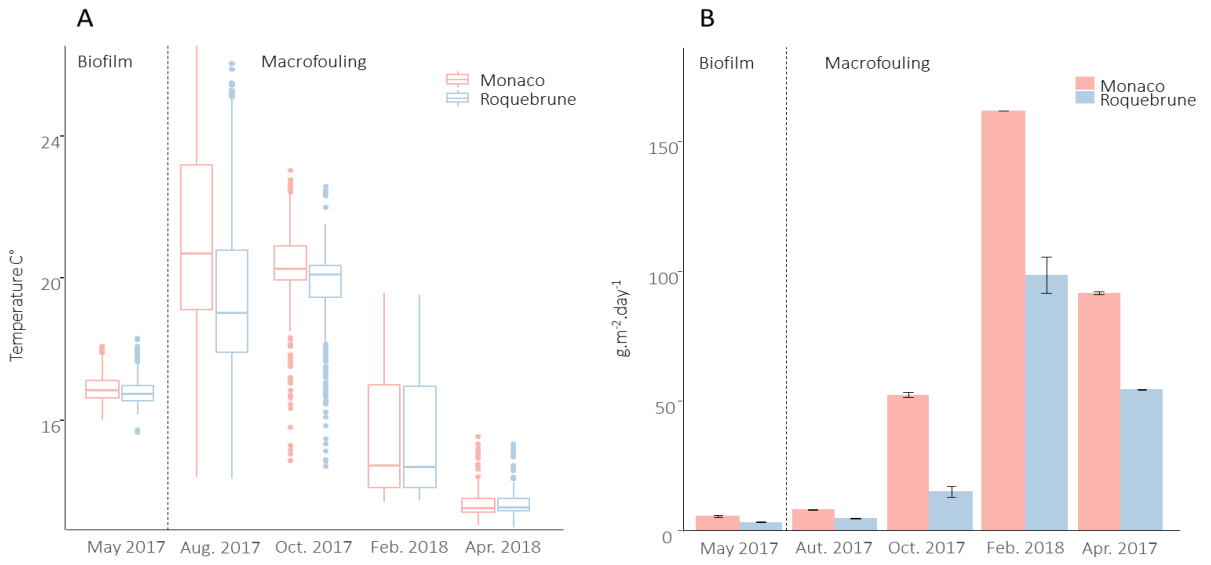

Figure III-3: A) Average temperature of the sea, B) average sedimentation rate during biofilm and macrofouling monitoring at Monaco and Roquebrune.

3.2. Structure of the biofilm microbial communities

3.2.1. Prokaryotic community

10 643 different OTUs have been sequenced, more than 99% of them were related to bacteria, only 76 different OTUs were related to archaea. The archaea were mainly represented by *Nitrosopumilus spp.* and *Candidatus nitrosoarchaeum* (respectively: relative abundance of archaea: 53.62% and 23,82%). No differences in archaeal community have been identified between substrates, time or sites. (Permutation test for homogeneity of multivariate dispersions: $p < 0.05$).

Among the 10 567 different OTUs related to bacteria globally sequenced, the first one thousand represented 82% were identified . Among these OTUs, the most abundant phylum were the Proteobacteria (relative abundance of bacteria: 40.75 ± 4.63%), Bacteroidetes (34.83 ± 9.23%) and Cyanobacteria (11.67 ± 7.60%), followed by Verrucomicrobia (4.43 ± 1.44%), Planctomycetes (4.11 ± 1.16%), Firmicutes (1.29 ± 1.59%) and Actinobacteria (1.24 ± 2.5). Among the Proteobacteria, the Alphaproteobacteria and the Gammaproteobacteria were the most abundant classes, accounting for 24.74 ± 4.32 % and 13.12 ± 3.48 % of the relative abundance of bacteria, respectively. Cyanobacteria were mainly represented by the Oscillatoriophycideae class (10.01 ± 7.24%). Bacteroidetes were mainly represented by the Flavobacteriia class (22.36 ± 5.82%). The most abundant species identified were *Cyanobacterium spp.* (relative abundance of bacteria: 9.99% ± 7.24) and *Flavobacterium spp.* (7.41% ± 2.54). On average, no significant differences between substrates have been identified from the finest to the widest identification (ANOSIM Bray Curtis dissimilarity: on highest taxonomical identification: R:0.386, p=0.047; Phylum identification: R:0.00249, p=0.389). The main differences of bacterial communities were explained by sampling time, while the sites explained a slight part of the community's dissimilarities (ANOSIM Bray Curtis dissimilarity: Sampling: R: 0.6658, p=0.001; Site: R: 0.118, p=0.002, Substrate: R: 0.04201, p=0.056).

The PCoA has been computed on the bacterial classes that represent more than 1% of the total relative abundance (Figure III-4). The two first axes explained 43.68 % of the total inertia of the data and have been retained to illustrate the Bray-Curtis dissimilarity between samples. We used the second best Calinski-Harabasz (CH) criterion that identified 5 different

clusters (CH Criterion 84.20, see: 4.23), the first one determining only two groups was too wide to explain differences between data (CH Criterion 86.92, see: 11.58) (Figure III-4). The species that explained the main differences between clusters were Oscillatoriophycideae, Flavobacteriia, Alphaproteobacteria, Gammaproteobacteria, Sphingobacteriia, Cytophagia, Verrucomicrobiae, Clostridia and Cyanobacteria. The first cluster gathered the D14 samples from Roquebrune, characterised by the high relative abundance of Cyanophyceae (17.97 ± 0.61%). The concrete and rock samples at D14 from Monaco and D21 from Roquebrune were grouped in the second cluster and were characterised by the highest relative abundance of Alphaproteobacteria (30.50 ± 0.67%). The third cluster grouped the dolomite samples at D21 from Roquebrune, and all the D28 samples except concrete samples from Monaco. This group showed the highest relative abundance of Clostridia (2.45 ± 0.41%) and Verrucomicrobiae (5.10 ± 0.21%). The fourth cluster gathered the dolomite samples at D14 from both sites, all the D21 samples from Monaco, and the concrete samples at D28 from Monaco. This cluster corresponded to the highest relative abundance of Flavobacteria (29.29 ± 0.83%), Sphingobacteriia (9.93 ± 0.44%), and Cytophagia (8.09 ± 0.30%), and the lowest relative abundance of Gammaproteobacteria (9.53 ± 0.21%). The fifth cluster gathered all the D07 samples, and was characterised by the highest relative abundance of Gammaproteobacteria (16.77 ± 0.84%) and Cyanophyceae (22.63 ± 0.78%) (Figure III-4).

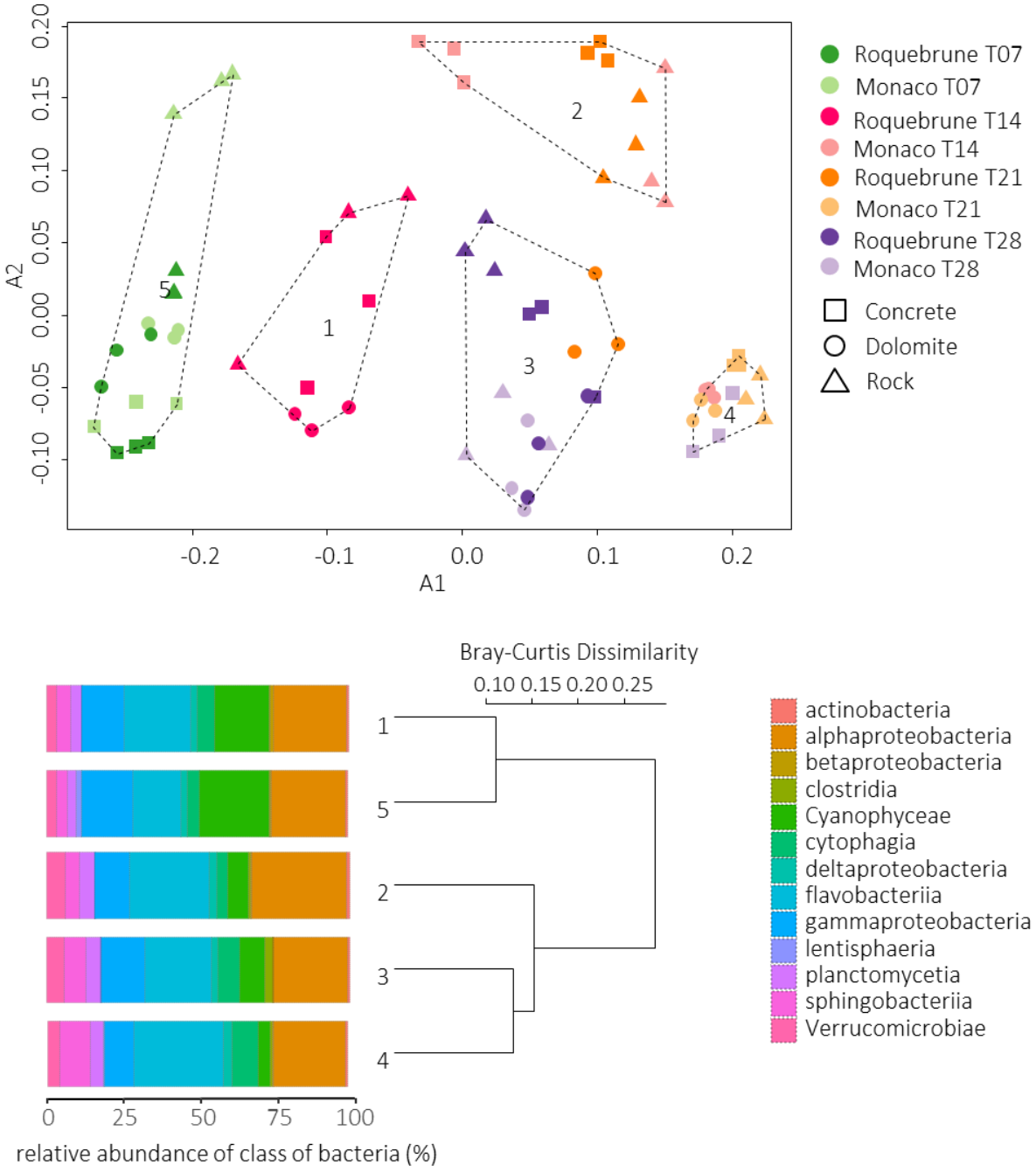

Figure III-4: A) PcoA computed on the Bray Curtis dissimilarity matrix of the relative abundance of the bacterial classes ≥ 1 % sequencing in the biofilm over the monitoring period (D07, D14, D21, D28), at both sites (Monaco and Roquebrune), and on each substrate (concrete, dolomite, rock). Samples are ordinated according to clusters determined by cascade Kmean (5 clusters: Calinski Criterion 84.20, SSE: 4.23). B) The relative abundance of bacterial classes ≥ 1% of each cluster and its hierarchical classification

3.2.2. Photosynthetic community

The main pigments secreted by the photosynthetic communities of the biofilm growing on the different substrates were chlorophyll *a* (56.89 ± 0.45%), fucoxanthin (28.71 ± 0.40%), chlorophyll *c* (7.01 ± 0.23%), and pheopigments (3.98 ± 0.23%). The other minor pigments secreted were diatoxanthin (0.55 ± 0.03%), diadinoxanthin (1.72 ± 0.06%), zeaxanthin (0.43 ± 0.04%), chlorophyll *b* (0.17 ± 0.03%) and *β* carotene (0.54 ± 0.06%). As for prokaryotic communities, differences between photosynthetic communities were due to sampling times and sites (ANOSIM Bray Curtis dissimilarity: Sampling: 0.4729, p=0.001; Site: R: 0.1982, p=0.001), and not to the different substrates (Substrate: R: 0.008118, p = 0.201).

A PCoA has been performed on all the different pigments (Figure III-5). The first two axes explain 30.07 % of the total inertia of the data (Figure III-5) and have been retained to illustrate the dissimilarity between samples. Our clusters have been determined by the best Calinski-Harabasz criterion (CH Criterion 89.1, see: 6.09) (Figure III-5). The pigments that explained the main differences between clusters were chlorophyll *a* and *c*, fucoxanthin and pheopigments (Figure III-5.B). The first cluster gathered the rock and concrete samples at D07 from both sites and one dolomite sample at D07 from Roquebrune, and was characterised by the highest percentage of chlorophyll *a* (63.09 ± 0.55%), chlorophyll *c* (8.60 ± 0.39%), and the lowest percentage of all the other pigments (fucoxanthin (23.10 ± 0.32%), diadinoxanthin (0.97 ± 0.04%), diatoxanthin (0.28 ± 0.04%), zeaxanthin (0.15 ± 0.06%), chlorophyll *b* (0.01 ± 0.01%), and absence of *β* carotene). The second cluster grouped all the Roquebrune samples at D28, except one rock sample. It was characterised by the highest percentages of pheopigments (8.51 ± 0.47%), diadinoxanthin (2.10 ± 0.09%), zeaxanthin (1.07 ± 0.12%), Chlorophyll *b* (0.92 ± 0.15%), and *β* carotene (0.87 ± 0.10%), and the lowest percentage of chlorophyll *c* (3.04 ± 0.15%). The third cluster grouped all the Monaco samples at D21 and D28, except one dolomite sample at D21, that showed the highest percentages of fucoxanthin (35. ± 0.44%), and diatoxanthin (0.89 ± 0.08%), and the lowest percentage of chlorophyll *a* (50.79 ± 0.52%), pheopigments (2.93 ± 0.32%), and *β* carotene (0.15 ± 0.02%), and the absence of chlorophyll *b*. The fourth cluster gathers all the D14 samples from both sites, the D21 samples from Roquebrune and one dolomite sample at T21 from Monaco, and all the samples of dolomite at D07 except one sample from Roquebrune. This cluster showed percentage of pigments very closed to the global average, determined by 57.86% (± 0.21%) of chlorophyll *a*,

28.08 % (± 0.33%) of fucoxanthin, 6.98 % (± 0.30%) of chlorophyll *c* and 3.75 % (± 0.26%) of pheopigments (Figure III-5).

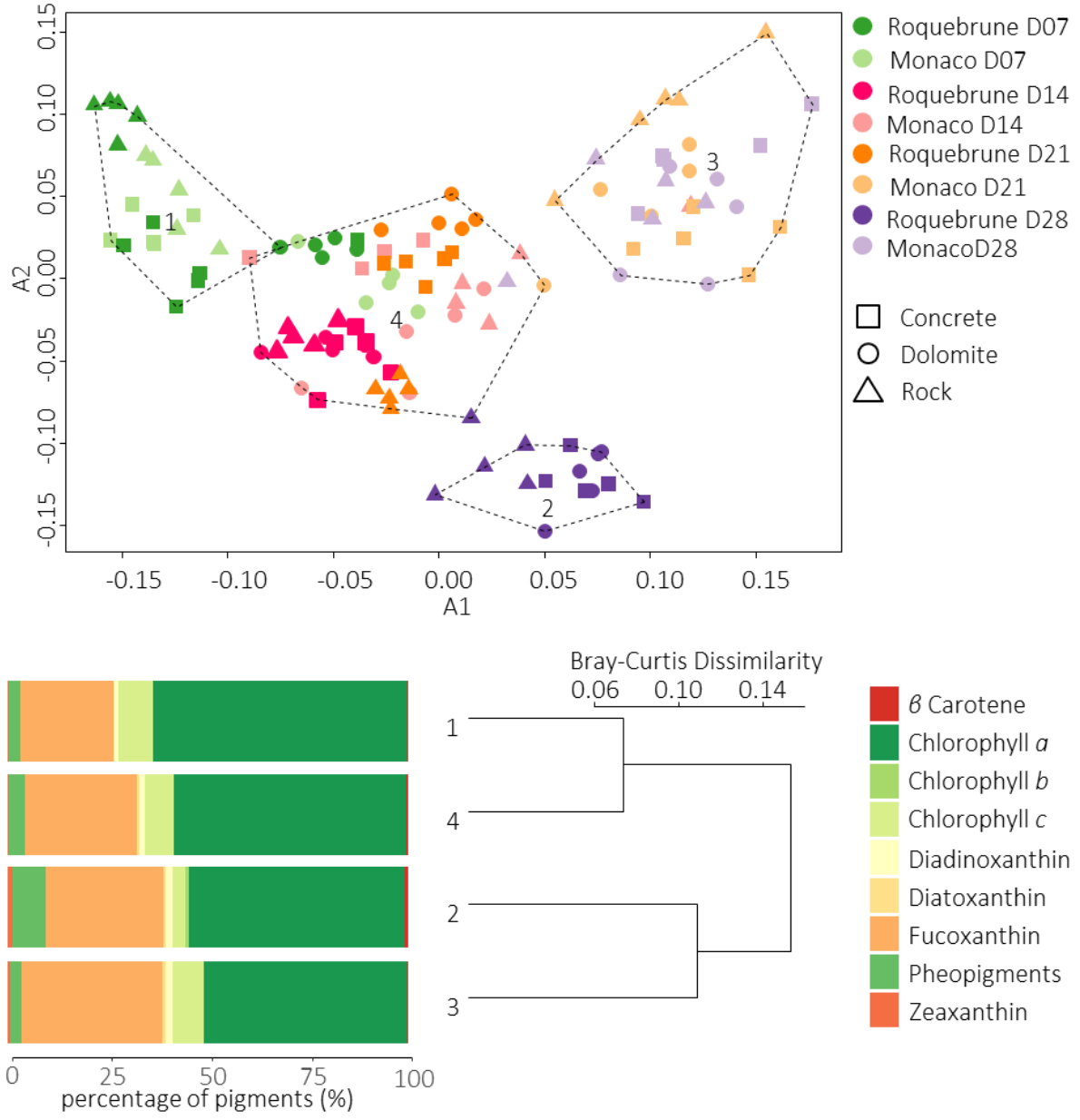

Figure III-5: A) PcoA computed on the Bray Curtis dissimilarity matrix of the relative abundance of pigments detected by HPLC in the biofilm over the monitoring period (D07, D14, D21, D28), at both sites (Monaco & Roquebrune), and on each substrate (concrete, dolomite, rock). Samples were ordinated according to clusters determined by cascade Kmean (4 clusters: Calinski Criterion 89.1, SEE: 6.09), B) Relative abundance of the type of pigments of each cluster and its hierarchical classification

3.3. Sugars and proteins content in the Extracellular Polymeric Substances (EPS) of the biofilm

The sugars concentration ranged between 5.04 and 57.34 µg.cm^{-2} at Monaco, and between 4.23 and 24.15 µg.cm^{-2} at Roquebrune. At Monaco, it increased on each substrate over the sampling period and picked after 21 days of monitoring. At the end of the monitoring, it decreased drastically except on rock where it increased slightly (Figure III-6). In average, the concentration was found higher on the concrete than on the other substrates (Van der Waerden test: p= 0.03; post-hoc test: C – D: p= 0.01, C – R: p=0.03, D – R: p=0.78). At Roquebrune, it followed to a lesser extent the same trend (Figure III-6), and was lower on the dolomite than on the other substrates during the last two weeks of monitoring (Van der Waerden test: p= 0.002; post-hoc test: C – D: p=0.0006, C – R: p=0.9674, D – R: p=0.0006).

Proteins concentration ranged between 7.30 and 25.47 µg.cm^{-2} at Monaco, and between 5.45 and 27.53 µg.cm^{-2} at Roquebrune. At Monaco, it increased on each substrate from the beginning to pick after 21 days of monitoring. Then, at the end of the monitoring, it decreased slightly, except on the dolomite where it decreased more intensely (Figure III-6). As for sugars, the protein concentration was found higher on the concrete than on the other substrates (Van der Waerden test: p= 0.001; post-hoc test: C – D: p= 0.0004, C – R: p=0.0019, D – R: p=0.5961). At Roquebrune, it followed the same trend except on the rock, were it increased drastically after 21 days (Figure III-6), but no significance difference was found between substrates.

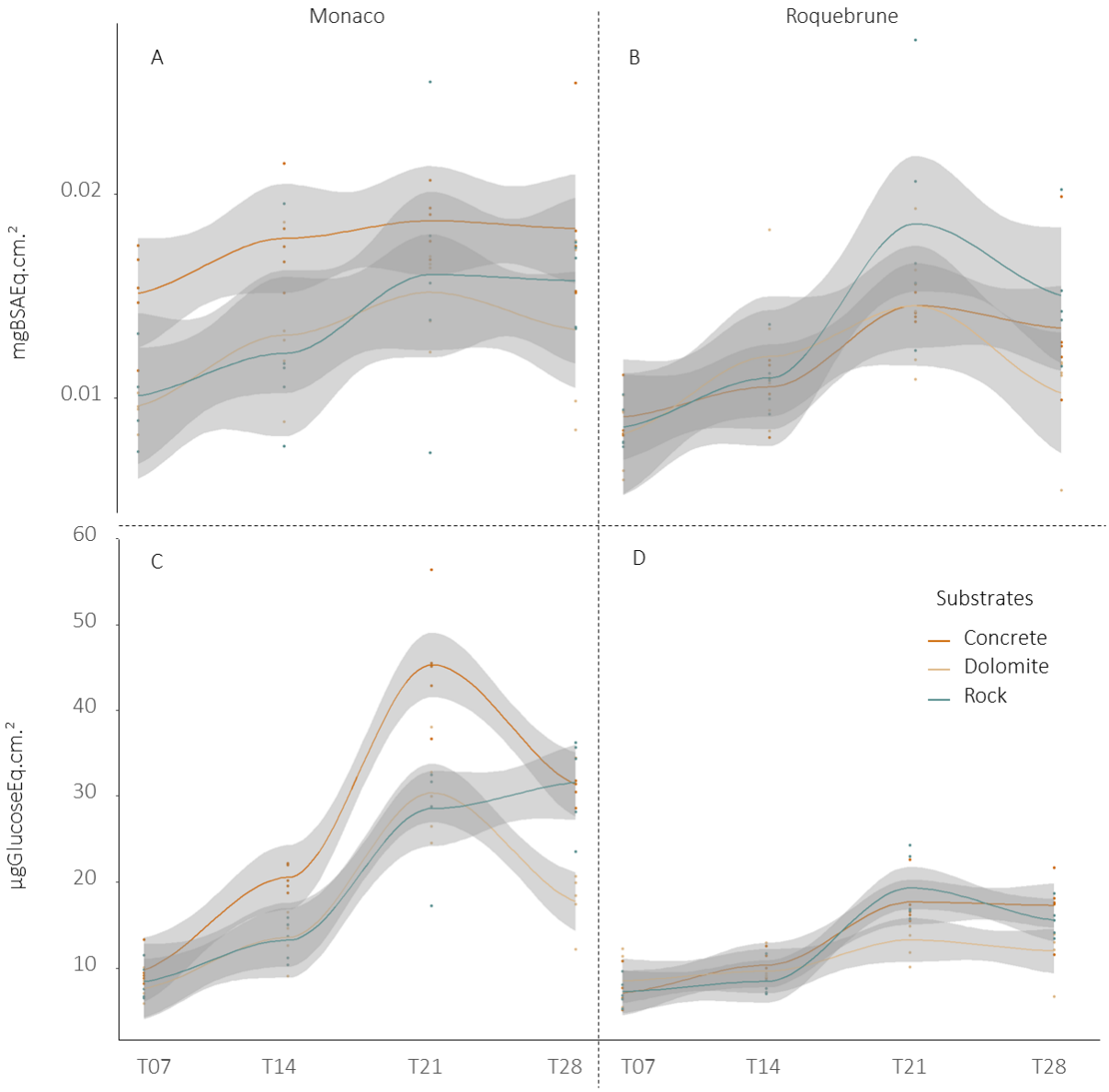

Figure III-6: Mean concentration of sugars (glucose equivalence) and proteins (BSA equivalence) detected by colorimetry at each sampling period (T07, T14, T21, T28), at both sites (Monaco and Roquebrune) and on each substrate (concrete, dolomite, rock). Grey zone corresponds to the confidence interval

3.4. Macrofouling communities

For the first two sampling dates, both sites showed the same seasonal dynamic of colonisation, with increasing macrofouling dry weight from summer (Aug. 2017) to autumn (Oct. 2017). Then, during winter season (Feb. 2018), the community at Monaco diminished 10 times more than at Roquebrune (Monaco: 1.88 ± 0.26 mg.cm^{-2}; Roquebrune 10.23 ± 1.67 mg.cm^{-2}) and the recovering of the community in spring (Apr. 2018) was slighter at Monaco than at Roquebrune (Monaco: 7.81 ± 1.30 mg.cm^{-2}; Roquebrune: 50.82 ± 7.59 mg.cm^{-2}) (Figure III-7). On average, Roquebrune supported a higher amount of macrofouling than Monaco (Monaco: 16.42 ± 3.88 mg.cm^{-2}; Roquebrune: 32.43 ± 4.38 mg.cm^{-2}, Van der Waerden test: p=0.0007). The dolomite and rock supported higher colonisation than concrete during autumn at Monaco (test). At the end of the monitoring, the macrofouling colonisation was similar on the different substrates at Monaco but was significantly higher on the rock at Roquebrune (Van der Waerden test: p= 1.102759e-10; post-hoc test: C – D: p= 0.2517, C – R: p < 0.0001, D – R: p<0.0001) (Figure III-7).

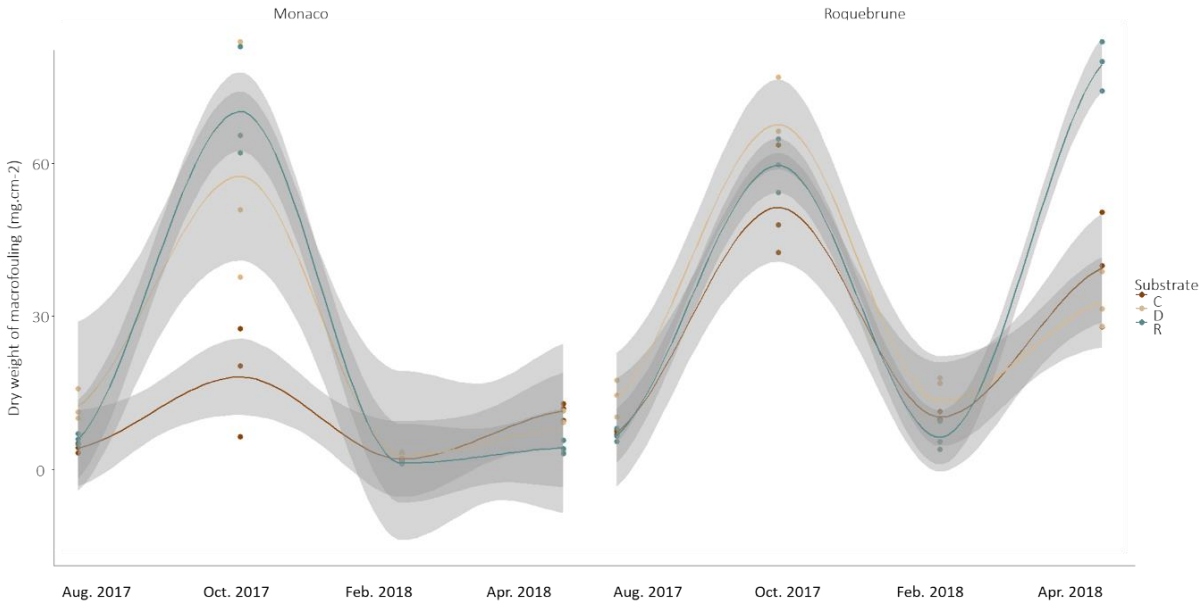

Figure III-7: Mean total macrofouling dry weight (mg.cm^{-2}) over time, on both sites and on the three different substrates. Grey zone corresponds to smoothed conditional means

A large part of the macrofouling was composed of algal turf (56.90 ± 3.74 %). A total of 58 different taxa have been identified along the monitoring period of the macrofouling. *Dictyota sp.* (13.53 ± 2.34 %) and *Bitium reticulatum* (10.70 ± 2.20 %) were the most abundant species. The number of taxa identified was higher at Roquebrune than at Monaco. Indeed, 24 taxa were found only at Roquebrune while 14 were found only at Monaco, and 33 taxa were common to both sites. Regarding the sampling periods, 8 taxa were specific to the summer season, 5 to autumn season, 5 to winter season, and 8 to spring (Figure III-8). Regarding the substrates, 29 taxa were common to all of them, 7 taxa were found only on the concrete (*Aphrodita sp., Cerastoderma sp., Limaria hians, Patella pellucida, Alvania sp., Setia ambigua, Jujubinus sp.*), 8 only on the dolomite (*Arca tetragona*, Dentaliidae, *Tritia reticulata, Oncaea sp., Clanculus corallinus, Flabellia sp.*) and 4 only on the rock (*Chama asperalla, Cythara sp., Womersleyella sp., Rissoa sp.*). The macrofouling growing on the dolomite samples shared 8 taxa with the one growing on concrete and ten others with the one growing on the rock (D-C: *Crisia sp., Dexamine sp., Fusinus pulchellus, Galathea nexa,* Veneridae*, Watersipora subtorquata;* D-R: *Calliostoma sp., Clathrina sp.*, Fasciolariidae, Lichenoporidae, Muricidae, *Peyssonnelia sp.*, *Nereis sp.*, *Folinella excavata*, Sycettidae). Finally, the macrofouling growing on the concrete and the rock shared 5 different taxa (*Amphipoda, Peltidium purpureum, Triphora sp., Truncatella hamersmithi, Valonia sp.*). Overall, over the entire monitoring period and at both sites, the macrofouling growing on the dolomite showed the highest gamma diversity, while the macrofouling growing on the concrete showed the lowest gamma diversity (Figure III-8).

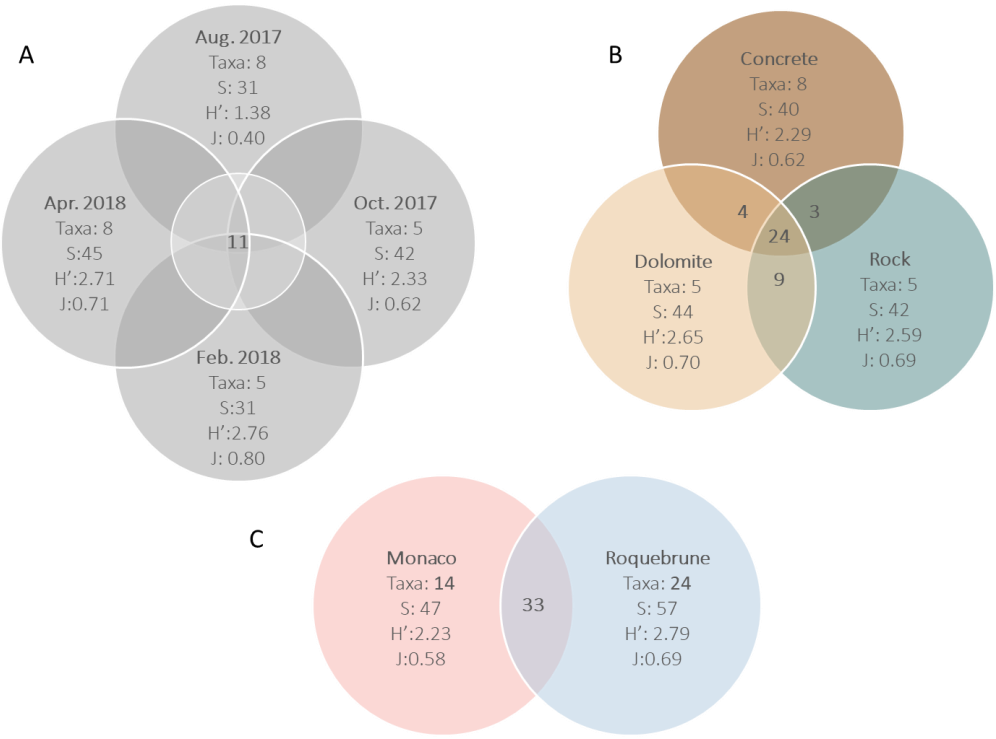

Figure III-8: A) Venn diagrams representing the taxa for each season: B) substrates, C) and sites. Gamma diversity computed with specific richness, Shannon index and Pielou index of equitability for each season, site, and substrate

Dissimilarities between communities at the family rank were mainly explained by the seasonal sampling and the sites (ANOSIM : Season:Site:Substrate: R: 0.74, p=0.001; Season: R: 0.52 p=0.001; Site: R: 0.23, p=0.001; Substrate: R: -0.02, p=0.83). A PCoA has been performed for each site on the percentage of the family rank of the dry weight of macrofouling growing on the different substrates over the monitoring period (Figure III-9). At Monaco, the two first axes explained 36.35 % of the total inertia of the data. Only two clusters have been determined by the best Calinski-Harabasz (CH) criterion (CH Criterion: 30.60, see: 29.52) (Figure III-9). The first cluster gathered the samples of Summer and Autumn seasons 2017 and was characterised by the presence of Dyctyoceae (54,05 ± 6.39%), Rhodomelaceae (7.87.09 ± 2.60%) Arthrocladiaceae (5.38 ± 2.28%). Whereas the second cluster grouped Winter and Spring season 2018 and was characterized by Serpulidae (12.52 ± 5.25%), Cerithiidae (55.98 ± 8.65%), and Textulariidae (2: 1.41 ± 0.59%) (Figure III-9). At Roquebrune, the first two axes explained 35.95 % of the total inertia of the data We identified 5 different clusters (CH Criterion 84.20, see: 4.23) (Figure III-9.B). The first cluster gathered the samples of Oct 2017 and one dolomite sample of Aug. 2017, and was characterised by the highest percentage of Peyssonneliaceae (13.00 ± 5.30%) and high percentage of Dictyotaceae (53.36 ± 4.82%). The second cluster

grouped two outliers: one dolomite sample from Apr. 2018 and one rock sample from Feb. 2018, where the assemblage showing a slight percentage or even no Dictyotaceae compared to all samples, and were dominated for the dolomite sample by Serpulidae (61.46%) and by Triphoridae on the rock sample (45.50%) The third cluster grouped all the samples of Feb. 2018 except one rock sample, and showed higher percentage of Rhodomelaceae (23.23 ± 3.88%), Serpulidae (16.31 ± 6.39%) and Textulariidae (12.05 ± 2.58%), and lower percentage of Dictyotaceae (14.07 ± 3.70%). The fourth cluster gathered the samples of Aug. 2017, with higher percentage of Dictyotaceae (77.42 ± 6.32%). The fifth cluster gathered the samples of Apr. 2018, determined by higher percentage of Arthrocladiaceae (11.39 ± 3.36%), Cerithiidae (10.43 ± 4.49%), Costellariidae (5.02 ± 2.61%), Fasciolariidae (9.19 ± 5.07%), Lithodermataceae (7.81 ± 1.79%), high percentage of Rhodomelaceae (22.53 ± 3.38%), and low percentage of Dictyotaceae (13.96 ±1.91%) and Textulariidae (0.18 ± 0.11%) (Figure III-9).

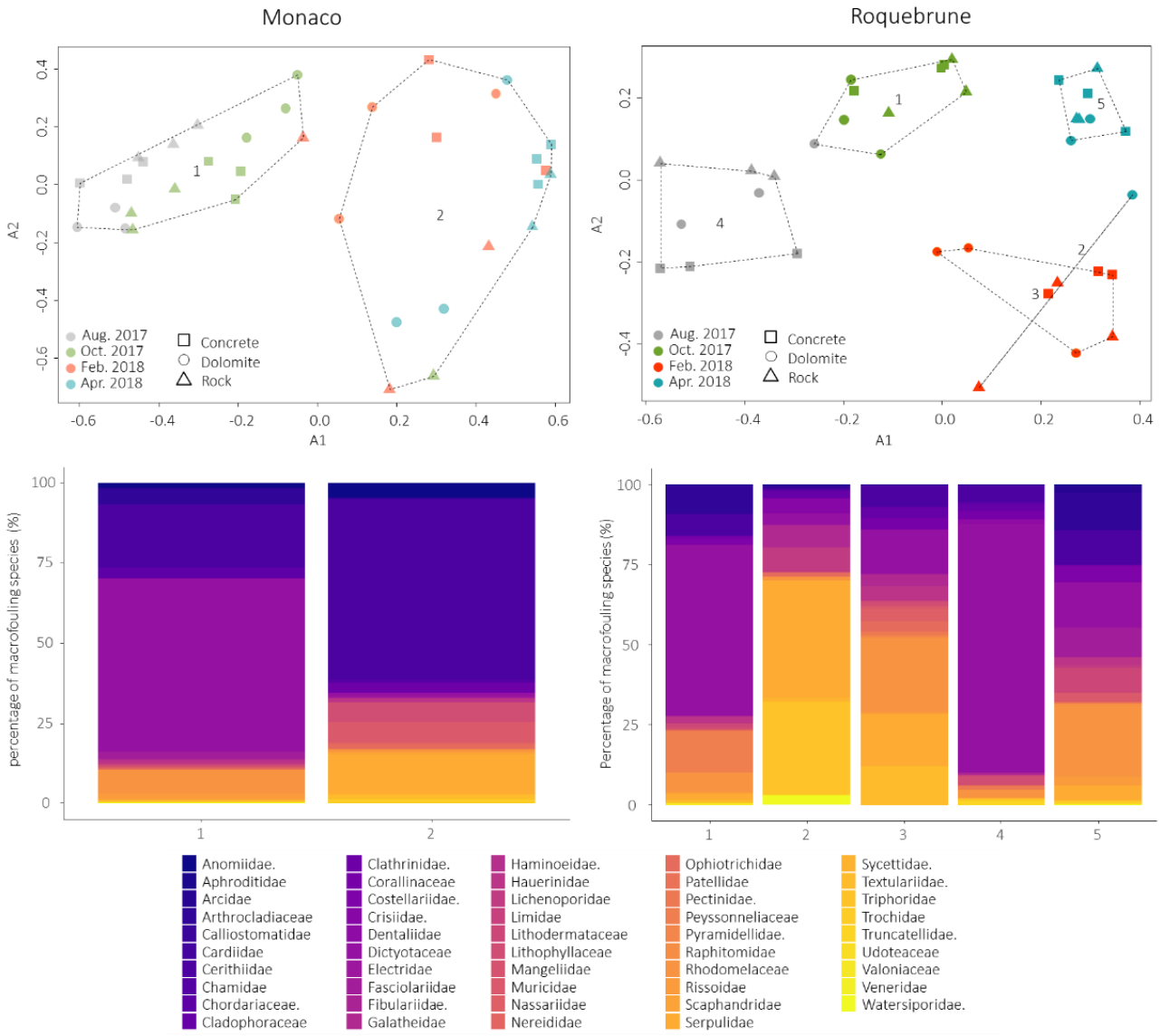

Figure III-9: PcoA computed on the Bray Curtis dissimilarity matrix of the relative abundance of the dry weight of macrofouling taxa family from Aug. 2017 to Apr. 2018, on each substrate (concrete, dolomite, rock): A) Monaco community, B) Roquebrune community. Samples are ordinated according to clusters determined by cascade Kmean (Monaco: 2 clusters: Calinski Criterion: 30.60, SEE: 29.52; Roquebrune: Calinski Criterion 84.20, SSE: 4.23), C) Relative abundance of Families of each cluster

3.5. Heavy metals in sinking and suspended POM and virgin substrates

The concrete is the substrate that contained the highest heavy metals concentration (Van der Waerden test: p=0.031, post-hoc test: C-D: p=0.0198; C-R: p=0.0007; D-R: p=0.0198) (Figure III-10). The heavy metals concentration appeared higher during biofilm monitoring than macrofouling monitoring. On both sites, the concentrations of total heavy metals contained in the biofilm and macrofouling were lower than the one contained in the sinking and suspended material collected from the sediment trap. However, the concentrations were higher in biofilm and macrofouling than in the substrates used for the monitoring. The heavy metals concentration was lower in biofilm and in macrofouling growing on the dolomite than on the other substrates (Van der Waerden test: Biofilm monitoring: p=0.003, post-hoc test: C-D: p<0.001; C-R: p=0.099; D-R: p=0.0013; Macrofouling monitoring: p=0.002, post-hoc test: C-D: p= 0.001; C-R: p= 0.074; D-R: p<0.001.) (Figure III-10).

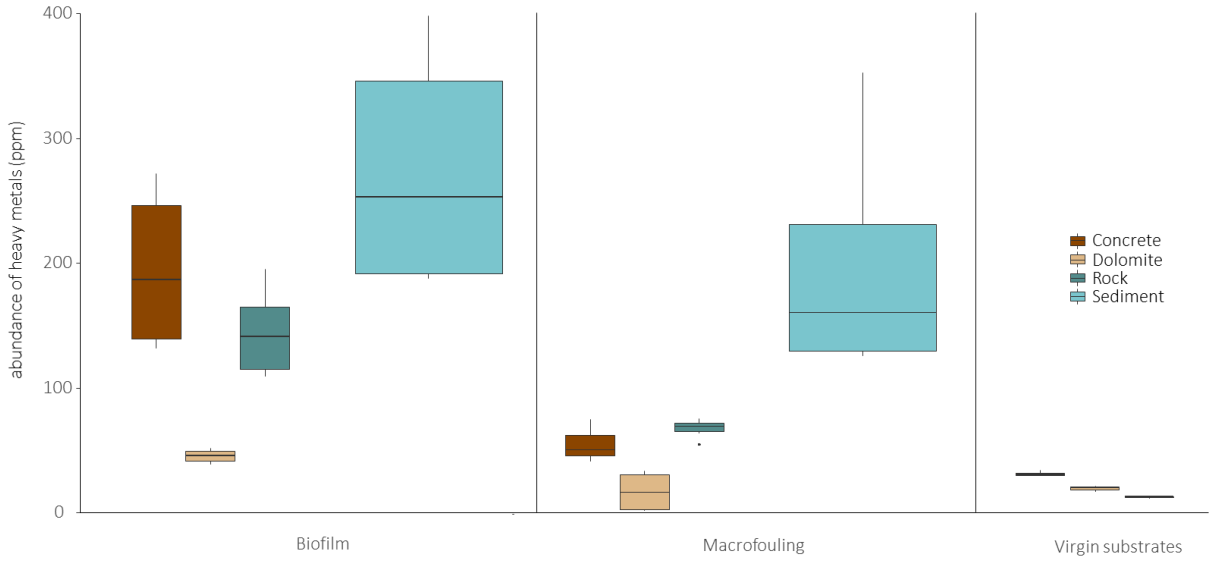

Figure III-10: Heavy metals concentration (ppm) in the biofilm, the macrofouling, the 3 virgin substrates and suspended material in sinking during biofilm and macrofouling monitoring

3.5.1. Biofilm

A PCA was performed on the percentage of heavy metals present in the biofilm after one month of monitoring (D28), in the virgin substrates and in the sinking and suspended POM collected from sediment traps (

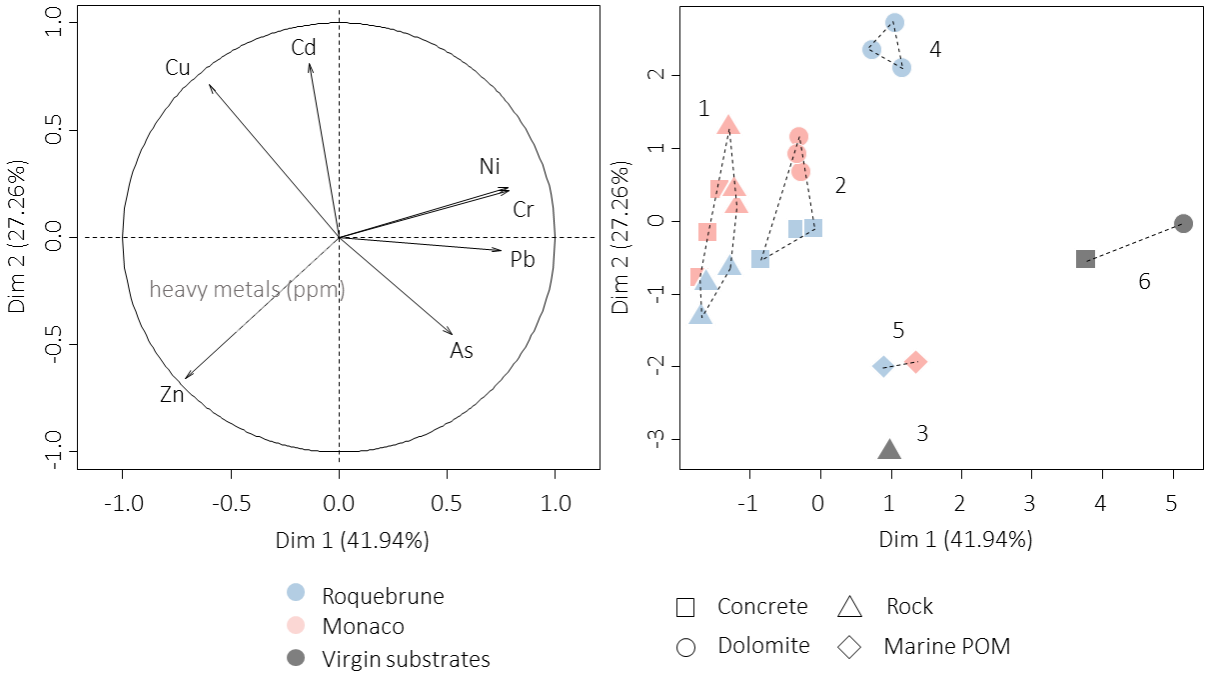

Figure III-11). The first two dimensions explained more than 69 % of the inertia, it showed a good projection of the data, as all variables were close to the correlation circle. The first dimension is mainly built by chromium, nickel, lead and zinc percentage; it opposed the first and second to the fifth clusters. The second dimension is mainly built by cadmium, copper, and zinc; it opposed the third and sixth to fourth clusters. The other variables are better explained in the other dimension. The first cluster grouped the samples of biofilm growing on rock at both sites and concrete at Monaco, described positively by total concentration of heavy metals and percentage of zinc but negatively by nickel, lead, and chromium. The second cluster gathered the biofilm samples on dolomite at Monaco and concrete at Roquebrune, positively described by the percentage of copper. The third cluster grouped the virgin rock samples positively described by the percentage of arsenic. The fourth cluster gathered the biofilm samples on dolomite at Monaco and concrete at Roquebrune described positively by the percentage of cadmium and chromium and negatively by the percentage of zinc. The fifth cluster grouped the samples from sediment traps at both sites, described by total concentration of heavy and the percentages of lead, but negatively by the percentage of

copper. Finally, the sixth cluster grouped the virgin substrates of concrete and dolomite, described positively by the percentage of nickel, chromium, lead, and negatively by the percentage of copper and zinc.

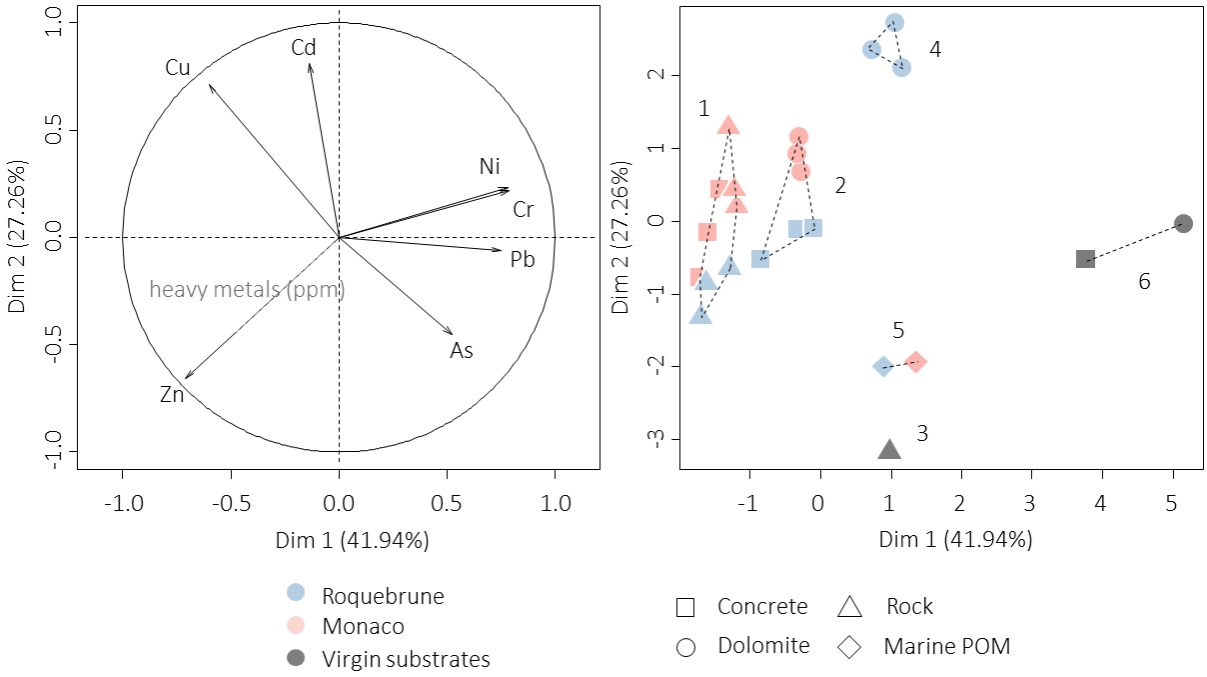

Figure III-11: Principal component analysis on the percentage of heavy metals within the biofilm, the sinking material and the virgin substrates used for the biofilm monitoring at D28 on both sites (Monaco and Roquebrune): A) Correlation circle of the variables, B) and ordination of the samples on the first two dimensions

3.5.2. Macrofouling

A PCA was performed on the percentage of heavy metals contained in the macrofouling after one year of monitoring (Apr. 2018), in the virgin substrates and in the marine POM (Figure III-12). The first two dimensions explained more than 60 % of the inertia, it showed a good projection of the data, as variables were close to the correlation circle, except arsenic and nickel that were better represented on the third dimension. The first dimension was mainly built by chrome and zinc, whereas the second dimension was equally built by the other heavy metals except for arsenic and nickel. The first dimension opposed the first to the sixth clusters, whereas the second dimension opposed the second and fourth clusters with the fifth. The third cluster is distributed close to origin of the 1:2 plan. The first cluster grouped the samples of macrofouling growing on dolomite at Monaco. It is positively described by its percentage of

cadmium and lead and negatively by its content of total heavy metals. The second cluster gathered the samples of macrofouling growing on Rock at Monaco, positively described by their percentage of copper. The third cluster grouped all the samples of macrofouling growing on all substrates at Roquebrune, described positively by its percentage of nickel and negatively by its percentage of arsenic. The fourth cluster grouped the samples from the sediment traps at both sites and the samples of macrofouling growing on concrete, described positively by its content of total heavy metals, its percentage of zinc, and negatively by its percentage of lead. The last two clusters corresponded to the virgin concrete and dolomite (cluster 5) and the virgin rock (cluster 6) samples, and their heavy metals composition was previously described (see previous paragraph, p.103).

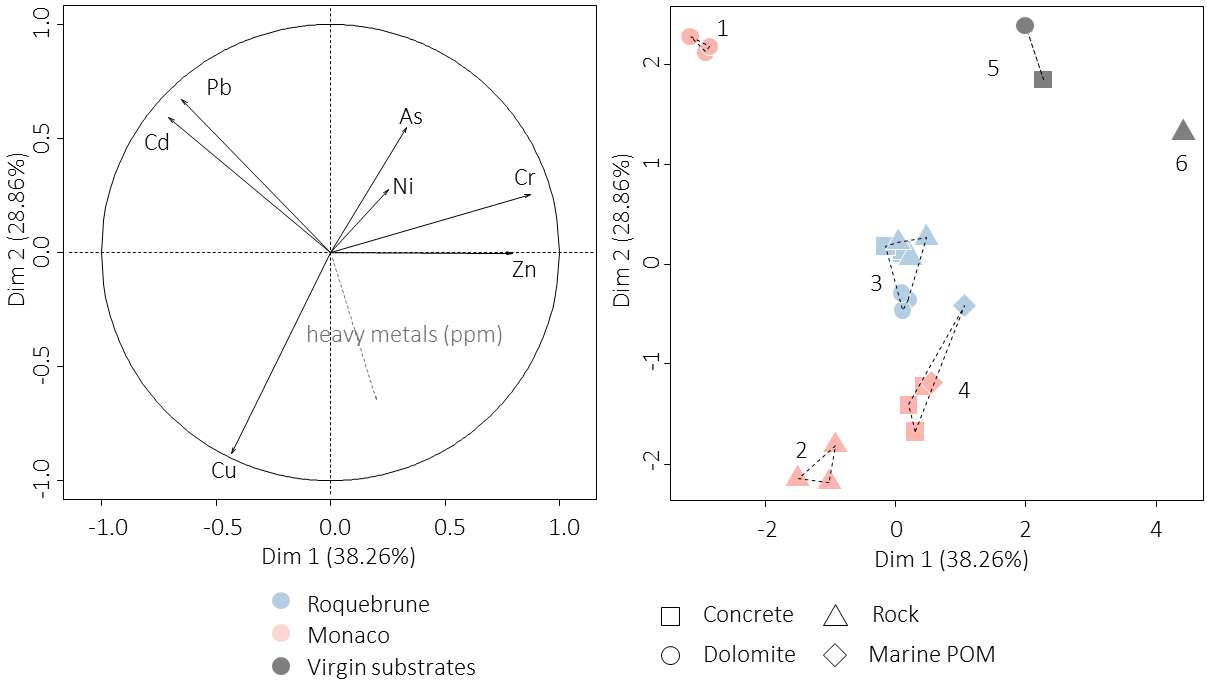

Figure III-12: Principal component analysis on the percentage of heavy metals within the macrofouling, the marine POMl and the virgin substrates in April 2018 on both sites (Monaco and Roquebrune): A) Correlation circle of the variables, B) and ordination of the samples on the first two dimensions

4. Discussion

Cyanobacterial growth potentially influences biofilm development and explains differences between sites:

In a previous study on biofilm monitoring on Sorel cement (made with dolomite sand for artificial reefs 3D print design) and different types of concrete (white and grey), we already highlighted significant differences between materials in biofilm secretion of sugars, but this study did not show difference in photosynthetic communities (Riera et al. 2018). In the present study, the analyses of the biofilm microbial communities (total prokaryotes and photosynthetic prokaryotes and eukaryotes) did not highlight significant differences between substrates either. According to metagenomic identification, the prokaryotic community was composed of few archaea, mainly represented by species of *Nitrosopumilus spp.* and *Candidatus nitrosoarchaeum* from the oxidize ammonia aerobicall phylum Thaumarchaeota, that prove to be highly represented in a wide variety of ecosystems (Pester et al. 2011, Brochier-Armanet et al. 2012), including marine environments (Parada et al. 2016). To the best of our knowledge, no previous study investigates archaea community within a marine biofilm, our results suggest that the archaea do not structure the prokaryote community within time, sites or substrates. The prokaryotic communities were mainly dominated by Alphaproteobacteria and Flavobacteria all along the monitoring. These results are consistent with various studies of biofilm in Mediterranean costal seas (Brian-Jaisson et al. 2014, Briand et al. 2017, Pollet et al. 2018). These bacterial classes seem ubiquitous in marine biofilm growing on hard substrates, as they are often the most abundant in most case studies (Chung et al., 2010; Dang et al., 2008; Dang and Lovell, 2002, 2000; Huang and Hadfield, 2003; Huggett et al., 2009; Jones et al., 2007; Webster and Negri, 2006). The dynamic of the other taxa may change according to environmental condition and depth of the study, in shallow water cyanobacteria prove to increase with time in Mediterranean sea (Briand et al. 2017), in Baltic sea (Sanli et al. 2015) and or even in Oman sea (Muthukrishnan et al. 2014, Abed et al. 2019) whereas in our study it decreased with time, suggesting they represent primary colonizers at 30 meters depth, followed by secondary colonizers, such as Gammaproteobacteria, Sphingobacteriia, Cytophagia, Verrucomicrobiae and Clostridia in the present study. According to pigments analyses, the presence of fucoxanthin, chlorophyll *c*, diadinoxanthin, and diatoxanthin might reveal the presence of brown algae from Bacillariophyceae class (i.e. diatoms). The presence of

β carotene and chlorophyll *b* might reveal the presence of green algae, and the zeaxanthin might reveal more precisely the presence of Cyanophyceae which is coherent with the metagenomic identification and with the literature. Indeed, in microphytobenthos biofilms growing on hard substrates, diatoms and cyanobacteria are often the most abundant phylum (Cooksey & Wigglesworth-Cooksey 1995, Lam et al. 2003, Briand et al. 2012, Salta et al. 2013). Globally the photosynthetic communities became mature rapidly, from the first week on the dolomite samples, and from the second week on the other substrates with the presence of all pigments represented by cluster 4. These results are consistent with our previous study, where biofilm became mature after two weeks (Riera et al. 2018). At the end of the monitoring, photosynthetic communities were significantly different between sites, Roquebrune showed a community with more diverse photosynthetic communities with the settlement of green algae related to the presence of chlorophyll *b*, whereas Monaco was still dominated by brown algae according to fucoxanthin and chlorophyll *c* percentage. The presence of green algae at Roquebrune could be linked to the recruitment of sporophytes of green macroalgae. Indeed, a previous study showed that the rate of settlement of the green algae *Enteromorpha intestinalis* (*Ulva intestinalis*) prove to be more effective when surface was colonized by mixed bacterial biofilm close to the one of our case study without cyanobacteria (Dillon et al. 1989, Patel et al. 2003). In the present study, we did not identify green algae of this family, indeed the depth at which the samples were placed does not match the distribution of Ulva spp. that lives in the supralittoral. However, the Roquebrune site was characterised by a higher diversity of seaweed than at Monaco. The only difference that could explain this better settlement of green algae at Roquebrune is the decline of cyanobacteria demonstrated by the decrease of zeaxanthin, and Cyanophyceae sequences in the bacterial community.

The material does not influence the diversity and composition of microbial communities:

No significant differences in microbial communities between substrates have been detected, which is in contradiction with many studies (e.g: Cooksey and Wigglesworth-Cooksey, 1995; Dexter, 1979; Fletchert and Loeb, 1979; Jones et al., 2007; Ozkan and Berberoglu, 2013; Patil and Anil, 2005; Pringle and Fletcher, 1986) However, Dang and Lovell, (2016), highlighted that the nutritional conditions and physicochemical properties of primary film can have a “mask effect” by wiping off the hydrophobicity or roughness of a given surface. Tan et al., (2015) also

suggested that changes in bacterial communities might be related to habitat characteristics such as orientation or complexity of the substrate. Nevertheless, the biofilm matrix revealed differences over time, between sites and substrates. On the concrete the higher amount of EPS secretion could be explained by the pH of the substrate that is known to be alkaline (close to 13 pH). Dogsa and colleagues (2005) showed that low pH favour larger EPS structures dense and homogeneous. At both sites, the proteins and sugars contained in EPS increased at D21 and globally decreased at the end of the monitoring except on rock in Monaco where their concentration slightly increased. This trend was also observed by Riera et al., (2018) in the winter season, and has been associated with a disturbance in biofilm growth due to a storm. In the present study, the biofilm followed the same pattern yet in spring, without any apparent influence of the weather conditions. The shift of the global structure of the community, from second to third sampling dates, could explain the decrease of the EPS production. Indeed, Cyanobacteria are known to produce high amount of EPS during biofilm growth (Rossi & De Philippis 2015).

EPS production does affect heavy metals sequestration in artificial reefs biofilms

Differences between sites have also been revealed in terms of EPS secretion, as the EPS were more abundant at Monaco than at Roquebrune. Location have been proved to influence the EPS secretion rate and, alternatively the same structure of communities is also known to show differences in secretion under specific environmental conditions (Ortega-Morales et al. 2010, Underwood 2010, Underwood et al. 2010, Fang et al. 2014, Decho & Gutierrez 2017), or substrate type (Chung et al. 2010, Riera et al. 2018). Over all the monitoring, on both sites, biofilms growing on concrete and rock showed higher heavy metals concentrations than on dolomite and rock. The higher amount of EPS within biofilm growing on concrete and rock might explain the higher amount of heavy metals on these two substrates. Indeed, EPS are known to contribute to trophic-transfer of environmental contaminants (Bhaskar & Bhosle 2006, Leguay et al. 2016, Decho & Gutierrez 2017) and are even used in bioremediation (Pal & Paul 2008, Dash et al. 2013), the dead biomass of biofilm and their EPS constitute a biosorption site for heavy metals (Kratochvil & Volesky 1998, Romera et al. 2007, Das et al. 2008). The main heavy metals contained in the biofilm were copper and zinc. The high amount of zinc could be explained by the high abundance of this metal within the marine particulate organic matter (POM) , but the presence of copper can't be explained neither by marine POM nor by virgin

substrates used for the monitoring because it was not present it these two compartments or at a concentrations below the detection limit. Copper is however present in the water column of the western Mediterranean Sea at very low concentration of 90 ng.l^{-1} on average (Laumond et al., 1984; Seritti et al., 1990). It is therefore very likely that the bioaccumulation of copper in the biofilm is related to the presence of this element dissolved in the marine POM. In a previous study Muhamed and Saly (2011), monitored biofilm during different seasons in Cochin estuary, South India, during 24 hours and 72 hours. They showed that zinc was the most abundant heavy metals sequestered by the biofilm, copper was also very high even if it was expected to be at a minimum. Even if copper is an essential trace element for different biological reactions, it is toxic to microorganisms even at very low concentrations (Gadd & Griffiths 1977, Ochoa-Herrera et al. 2011).

EPS sequestration determines the fate of heavy metals in artificial reefs food web

The macrofouling analyses, following the analyses of biofilm, allowed to identify seasonal changes. The macrofouling dry weight increased between summer and autumn, then diminished during the winter season and increased anew in spring. Roquebrune supported a higher amount of macrofouling than Monaco, mainly due to a very slight recovering of the community after winter at Monaco, which could be explained by the important sedimentation rate that might have impacted the global evolution of the assemblage. Slight differences between substrates have been highlighted and were site dependant, the dolomite and rock supported higher colonization than concrete during autumn at Monaco, and the community was significantly more abundant on the rock at Roquebrune.. The global colonization observed on the plates was close to the artificial reefs colonization model in Mediterranean sea determined by Ardizzone et al. (2000), with an early benthic colonization by diatoms, hydroids (*Obelia dichotoma, Bouganvillia ramosa*), serpulid polychaetes (*Pomatoceros triqueter, Pomatoceros lamarckii, Hydroides pseudouncinata*), barnacles (*Balanus eburneus, Balanus peiforatus*), and molluscs (*Anomia ephippium, Mytilus galloprovincialis*). To the best of our knowledge, no study in the Mediterranean Sea conducts comparative analyses on different substrates and their epibiotic colonization. In Loch Linnhe artificial reef, the choice of construction material had little effect on the long-term epifaunal community structure (Brown 2005); equivalent results were found in Dubai, United Arab Emirates, in the south-eastern basin of the Persian Gulf, where differences in recruitment patterns were more site dependant than

substrate material dependant in determining early benthic community structure and coral recruitment (Burt et al. 2009). It is known that EPS plays a key role in the settlement and stabilization of macrfouling larvae (Huang & Hadfield 2003, Shikuma & Hadfield 2006). However, in our study this parameter did not significantly influence the colonization of the substrates, as the lesser amount of EPS on the dolomite did not impact the biofilm and macrofouling settlement. Chung et al. (2010) showed that finally, the chemical composition of the substrate had no effect on the recruitment of *Hydroides spp.*, and Huggett et al. (2009), assumed that after 10 days, the same species is recruited whatever the substrate used. Conclusively, the colonization would depend principally on the neighbouring natural habitat and on the larvae and spores that the current can bring to the structure (Svane & Petersen 2001).

Nevertheless, the analyses of heavy metals content in biofilm and macrofouling brought interesting results. Like biofouling (biofilms & macrofouling) communities growing on dolomite accumulate fewer heavy metals than those growing on the other substrates. furthermore, macrofouling growing on concrete at Monaco showed the same signature as the marine POM whit a high amount of zinc. Thus, the substrate seems to play a preponderant role in the fate of heavy metals in the food web of an artificial reef. This role is rather indirect and the present study demonstrated that the type of material (especially concrete) used to build artificial reef influences biofilm EPS production which in turn favour the sequestration of heavy metals from marine POM and their fate in the food web. The presence of heavy metals, from the first stage of colonization, are likely transferred to the macrofouling and to the mobile fauna feeding on the reefs which may cause bioaccumulation in the food web (Bhaskar & Bhosle 2006). Given that many artificial reefs are designed in concrete and that their main role is to help artisanal fisheries, it is of utmost importance to better understand the relationships between EPS quantity and quality and heavy metals (or other organic and inorganic pollutants) sequestration and bioaccumulation in the food web of artificial reefs according to the type of substrate.

Conclusion

This study revealed for the first time that the monitoring of the structure and diversity of the communities is probably not the best way to infer about the quality of a given material to build an artificial reef. Most of the time, microbial and macrofouling assemblages are similar whatever the material used. However, we highlighted that substrates influence significantly the amount (and very likely also the quality) of EPS secretion in the biofilm matrix, which has strong incidence in terms of heavy metals sequestration and bioaccumulation in biofouling (biofilm & macrofouling). These differences between substrates were stronger at Monaco, a site highly impacted by its artificial coast and permanent building work occurring there.

IV. CHAPTER 3: STUDY THE COMPLEXITY OF ARTIFICIAL REEFS FROM THE MICRO TO THE MACRO SCALE

Part 1: Toward a purposeful design of artificial reefs: A first method to assess their structural complexity and heterogeneity

To be submitted in Ecological Engineering

Authors: Riera E., Mauroy B., Barthélémy J., Hubas C. & Francour P.

Résumé

Les récifs artificiels (RA) sont souvent considérés comme des outils d'ingénierie écologique favorisant la mise en place de mesures de restauration et de conservation. Outre la qualité et l'innocuité des matériaux utilisés pour leur construction, notions discutées dans les deux premiers chapitres, l'agencement tridimensionnel des récifs artificiels est déterminant pour l'établissement de communautés riches et fonctionnelles. A l'heure actuelle les structures des RA sont conçues et arrangées selon des dires d'expert, aucune méthode quantitative ne permet d'en évaluer la complexité et l'hétérogénéité.

Nous supposons que l'élaboration d'une méthode permettant d'évaluer la complexité et l'hétérogénéité permettrait d'offrir une classification des différents types de récifs artificiels.

Dans cette étude, la complexité de modules de RA a été déterminée à l'aide de modèles numériques 3D à partir de quatre variables normalisées entre 0 et 1: la rugosité (Topo), la porosité (Poro), la dimension fractale (Dn) et la déviation standard des normales sur le plan vertical (SDnz). Par la suite, l'hétérogénéité des différentes combinaisons possibles de modules (agrégat, village, champs) a été déterminée selon l'indice de Shannon (H') pondéré par le volume des modules déployés.

Cette étude démontre que notre méthode est fiable pour évaluer la structure de tous types de récifs artificiels, d'un module donné à des combinaisons plus complexes. La classification proposée par la méthode regroupe des typologies de récifs selon leurs usages et les communautés qu'ils recrutent.

Cette première étude de la structure des récifs artificiels est prometteuse et permettra d'offrir un outil efficace pour jouer sur les paramètres de complexité et d'hétérogénéité lors de l'élaboration de nouveaux designs de récifs artificiels. Il est cependant nécessaire d'effectuer une vérification sur le terrain de l'influence de ces paramètres sur les communautés afin de mieux définir des designs spécifiques selon des espèces cibles.

Abstract

Artificial reefs (AR) are often considered as a true ecological engineering solution for restoration and conservation issues. In order to become a real Nature Based Solution, it is necessary to focus on their intrinsic characteristics such as the material used to design them or even their three-dimensional arrangement as relevant characteristics for the settlement of specific communities. In this study, the structural complexity of common single AR modules has been computed using 3D computer aided design (CAD) models. Their structural complexity has been determined by calculating four different variables normalised between 0 and 1: roughness (Topo), porosity (Poro), fractal dimension (Dn) and the standardised deviation of the normal on the vertical plane (Sdnz). Then, the heterogeneity of different kinds of combinations of AR modules (set, group, complex) has been computed with the Shannon index (H') weighted by the volumes of the deployed unit reefs. This study demonstrates that our method is reliable to evaluate the structure of virtually all kinds of artificial reefs, from a given module to any kind of combination.

Keywords: Artificial reef, Complexity structure, 3D CAD model, method

1. Introduction

The artificial reefs (AR) are "submerged structures placed on the seabed deliberately to mimic some characteristics of natural habitats" (Pickering et al. 1998). In France, it represents a volume of nearly 90 000 m^3 mainly to promote fisheries (Tessier et al. 2015). Facing the artificialization of coastal areas, that can reach up to 90% of the coast line, the artificial reefs must be considered as a true ecological engineering solution for the restoration and conservation issues (UNEP 2009).

These objectives imply to improve their efficiency by focusing on the intrinsic characteristics of an AR which are linked to the material used to design it and its three-dimensional structure. Some studies already investigate the effect of different substrates on the primary communities that settle on the artificial reefs (Salamone et al. 2016, Liu et al. 2017, Riera et al. 2018). But regarding their three-dimensional structure, artificial reefs are currently mainly designed empirically according to expert judgment, but never according to scientific criteria (Turner et al. 1969, Bohnsack & Sutherland 1985, Pickering & Whitmarsh 1997, Barnabé et al. 2000, Jeansen et al. 2000, Svane & Petersen 2001, Williams 2006, Shokry & Ammar 2009, Tessier et al. 2015). Few studies have used numerical methods to determine structure complexity of artificial reefs. Most of them focused on surface rugosity (or roughness) (Ferreira, Gonçalves and Coutinho, 2001; Wilding, Rose and Downie, 2007), or the fractal dimension (Caddy and Stamatopoulos, 1990). More recently Loke and colleagues (2014, 2015;2016) proposed a way to improve surface structure by increasing heterogeneity, in order to increase epibiotic settlement. Lan and colleagues (2008), proposed a method for the arrangement in space of the artificial reefs based on fractal design, but it did not concern the design of the structure itself. One study followed the recommendation of Bohnsack (1991) by counting the number of space, voids and crevices to determine the preference of fish according to shelter types (Hackradt et al. 2011). However, no universal method exists to evaluate their structure complexity, in order to know whether they can mimic the spatial heterogeneity and high three-dimensional complexity of natural habitat. For now, only comparative studies between communities of artificial and natural habitats could give us a first answer (e.i.: Bohnsack, 1989; Caddy and Stamatopoulos, 1990; Pickering and Whitmarsh, 1997; Barnabé *et al.*, 2000; Jeansen, Collins and Lockwood, 2000; Hunter and Sayer, 2009; Aguilera, Broitman and Thiel, 2014; Tessier *et al.*, 2015). Since the early '90s most of the structure modules used are simple

shapes and are gathered in aggregates without offering a high heterogeneity. It has been quite common to practice post complexification of ARs to enhance their efficiency (Charbonnel et al., 2001, 2002; Bodilis et al., 2008, 2011; Cépralmar, 2015; Tessier et al., 2015). Recently, giant three dimensional (3D) print gives rise to a new generation of artificial reefs (Rageh et al. 2009, Erioli Alessandro & Zomparelli Alessio 2012, Frau et al. 2016, Mohammed 2016, Riera et al. 2018). For now, 3D printing remains expensive, but increasing the use of printed artificial reefs could reduce their price, making possible to build artificial structures whose properties are closer to the more complex structure of natural habitats, at a cost-efficient price.

In the natural environment, complexity and heterogeneity of the habitat strongly influence the diversity and abundance of species that settle (MacArthur & MacArthur 1961, MacArthur et al. 1962, McCoy & Bell 1991, Beck 2000, Tews et al. 2004, Tagliapietra & Sigovini 2010, Kovalenko et al. 2012, Tokeshi & Arakaki 2012, Musard et al. 2014, Loke et al. 2015). The term complexity is closely related to the shape of the structures which is itself linked to the variation of its physical features in space, whereas heterogeneity defines the abundance and diversity of the elements that compose the habitat (McCoy and Bell, 1991;[2] Tews et al., 2004, beck 1998, 2000). Different variables are used to determine the complexity of habitat, the most common in marine environment is the roughness assessed by the chain and tape method (e.i.: Luckhurst and Luckhurst, 1978; Beck, 1998, 2000; Friedlander and Parrish, 1998; Willis, Winemiller and Lopez-Fernandez, 2005; Pais *et al.*, 2013; Sánchez-Caballero *et al.*, 2017; Young *et al.*, 2017); but the roughness can be defined with more accurate variables such as area ratio (Jenness 2004, Friedman et al. 2012, Bryson et al. 2017), vector dispersion (orientation), standard deviation of the elevation Z value (Carleton & Sammarco 1987, Beck 1998, 2000, Grohmann et al. 2009, Kovalenko et al. 2012, Young et al. 2017). All these variables are coming from the study of the surface topography, some of them can be adapted to the artificial reef structure to determine the variability of their surface orientation and the roughness aspect of their structure. The fractal dimension (D) is also often used. It translates the way an object fills the space, at all scales (e.g.: Mark and Aronson, 1984; Frontier, 1987; Beck, 1998, 2000; Schmid, 1999; Johnson M. P. *et al.*, 2003; Halley *et al.*, 2004; Frost *et al.*, 2005; Kostylev *et al.*, 2005; Warfe, Barmuta and Wotherspoon, 2008; Wilding, Palmer and Polunin, 2010; Tokeshi and Arakaki, 2012; Young *et al.*, 2017). Tews et al. (2004) summarise four methods to assess heterogeneity ; two are based on discrete variables: the structural richness based on species

richness and the structural diversity based on Shannon index ; the two others are based on continuous variable: the structural extent based on structural qualities such as percentage coverage, and structural gradient based on gradient length of Euclidian distance measured on differences between the structural elements. The most common variable used is the Shannon index computed on the different elements that compose the habitat (e.g.: MacArthur and MacArthur, 1961; MacArthur, MacArthur and Preer, 1962; Roberts and Ormond, 1987; García-Charton *et al.*, 2004; Tews *et al.*, 2004; Gratwicke and Speight, 2005; Pittman and Brown, 2011; Kovalenko, Thomaz and Warfe, 2012). Regarding ARs, it is important to consider the different scales of their combination. Indeed, artificial reefs are first designed as a unitary module. These unit modules can be immersed in aggregate, and several aggregates can form a village (Charbonnel et al., 2011; Cépralmar, 2015; Tessier et al., 2015). When combined together, modules offer a heterogeneity of structure of different complexity.

Based on the specific combinations of the artificial reefs and inspired by different indexes of complexity used on the natural environment, we propose a method to evaluate the theoretical structure of artificial reefs from the modules to any kind of combination of modules. We hypothesised that (i) the index of complexity proposed will increase according to the different variables chosen, (ii) and could help to categorise and classify the reefs with a standardized numerical method.

2. Material & method

2.1. The numerical object of artificial reefs and fictive objects

To test the influence of the structural parameters on the indexes, we created 7 different fictive 3D computer aided design (CAD) models. From one simple cube of 1 m^3, we increased the surface complexity using a three steps iterative process. Then, we added successively circular cavities of different size three times (Figure IV-1). Those fictive 3D CAD models have been created on the online free access software Tinkercad for 3D computer aided design (CAD). An STL file, that describes the surface geometry of a 3-dimensional object, was generated and exported.

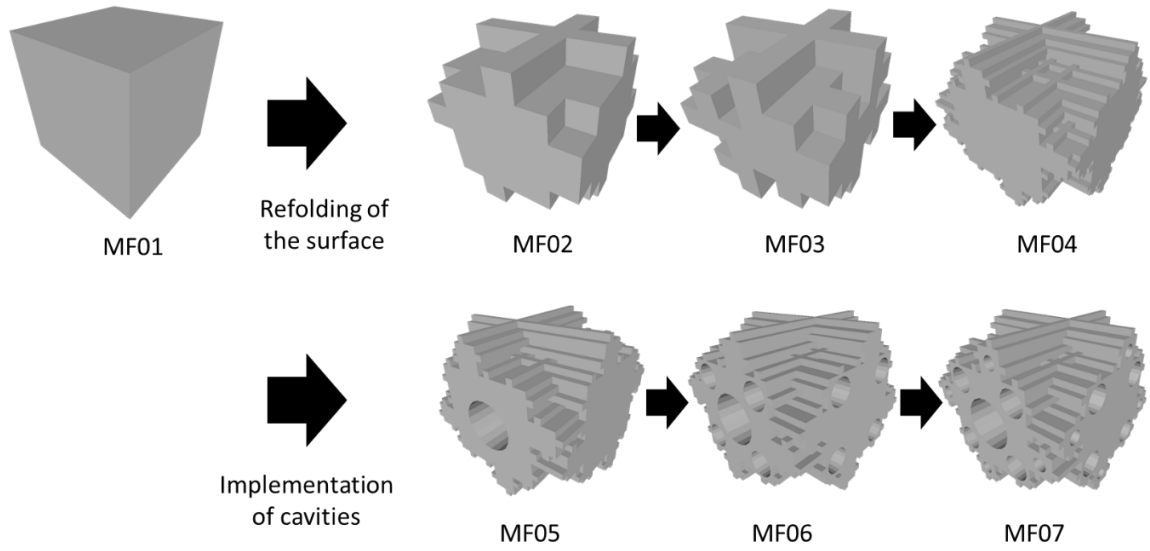

Figure IV-1: Fictive 3D CAD models generated on Tinkercad. The surface of a simple cube has been refolded three times, and tree different cavities have been added

In order to evaluate the structural parameters on ARs modules, we also sampled 16 different artificial reefs used in France. The dimensions and shapes have been collected in the literature (Tessier et al. 2015). Most of the 3D CAD models have been produced thanks to the online free access software Tinkercad. More complex structures such as the one developed by Boskalis© were directly provided by the company (Figure IV-2). Dimensions, shapes, origin, and references are available in supplementary materials (Annexe 4).

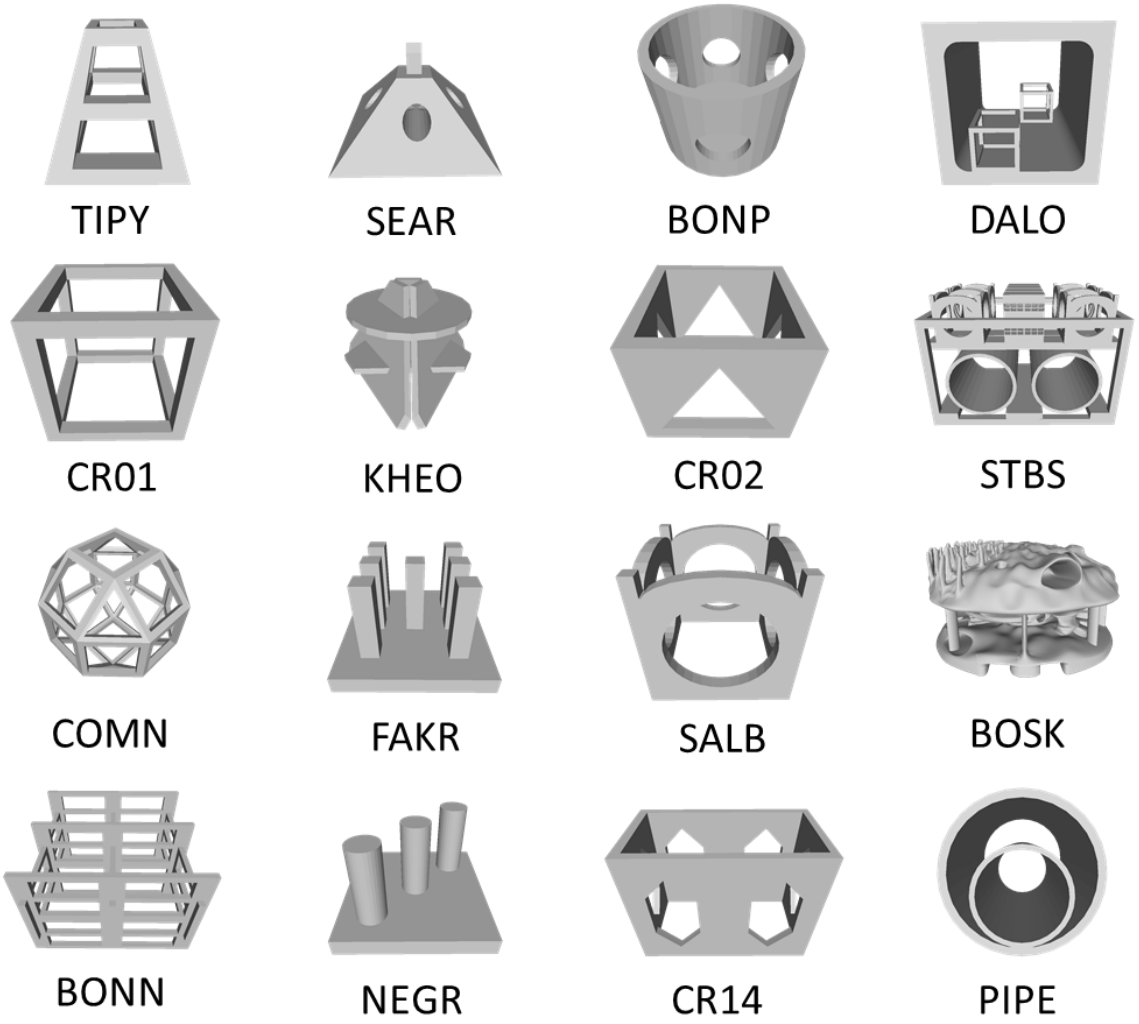

Figure IV-2: Samples of Artificial reef modules from Tessier et al.2015 generated on Tinkercad and model from Boskalis (scales are not respected)

2.2. Normalization of the 3D CAD models and process of the input.

2.2.1. Surface & Volume of the 3D CAD models

All fictive 3D CAD models have been processed on MeshLab, an open-source software for processing and editing 3D triangular meshes. It provides a set of tools for editing, cleaning, healing, inspecting, rendering, texturing and converting meshes. We used the "compute geometric measures" tool of MeshLab to compute surface area, volume of the 3D CAD models, and size of the bounding box in which the model fit (Figure IV-3). See the method in supplementary materials (Annexe 1 & Annexe 2). From these measures we exported:

From the bounding box

Vo: width*length*high

Sg: width*length

From the 3D CAD models:

St: total surface area

Vr: total volume

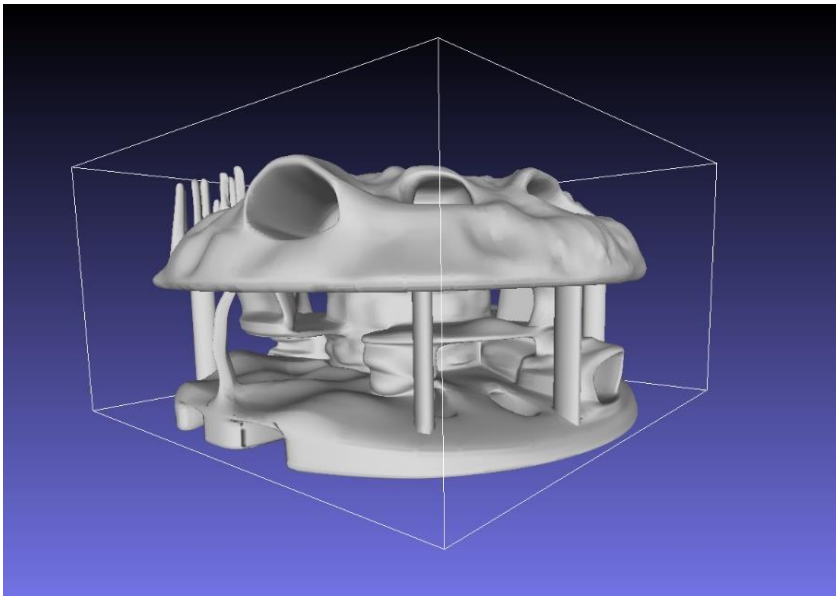

Figure IV-3: representation on MeshLab of the 3D CAD model of the module designed by Boskalis. The box surrounding it it the its bounding box that correspond to the volume occupied by the module. The dimension of the bounding box is used to compute the parameters Topo and Poro.

2.3. Point clouds and normals

The mesh 3D CAD models have been exported to Cloud Compare in order to get similar points resolutions for each 3D CAD models. Cloud Compare is a 3D points cloud (and triangular mesh) processing software, including many advanced algorithms (registration, resampling, colour/normal/scalar fields handling, statistics computation, sensor management, interactive or automatic segmentation, display enhancement, etc.). The surface meshes have been transformed in points cloud with coordinates X Y Z. Three different densities of points by square unit have been exported for the fictive 3D CAD models (density per square unit: 1, 5 and 10) to determine the variability of the indexes according to the density. For each point (or vertex), a normal has also been exported (Figure IV-4). The normals are the directional cosines (cosx, cosy, cosz) of the normal vector of each point with respect to the orthogonal plane of the 3D CAD models, each directional cosines varies between -1 and 1. In three dimensions, a normal vector to a surface at point P is a vector perpendicular to the tangent plane of the surface at P, it gives the orientation of each vertex that composed the 3D CAD model.

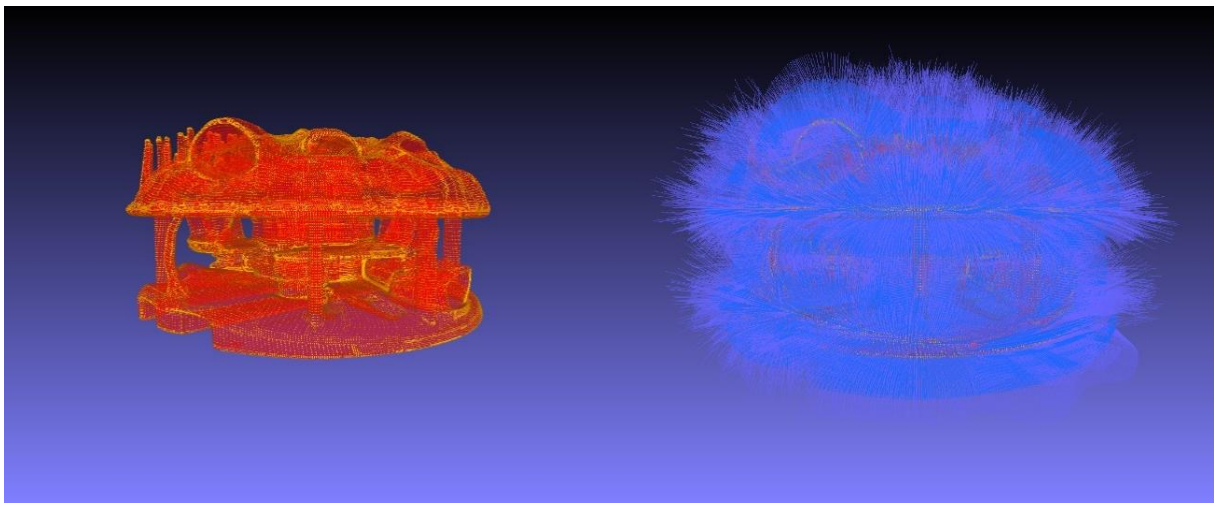

Figure IV-4: representation on MeshLab of the 3D CAD model of the module designed by Boskalis. on the left: the 3D CAD model with vertices (points) highlighted in yellow, on right: the 3D CAD model with the normal computed in blue. The points and normals are used to compute the parameters SDnz and Dn.

2.4. Combination of modules

As an example, we evaluated known existing combinations of artificial reef modules. One village of the Larvotto Marine Protected Area (MPA) at Monaco, is composed of BOSK modules. One village at the MPA of Roquebrune Cap Martin, is composed of CR14 modules. Finally, one village at the MPA of Cap d'Agde, is composed of PIPE and STBS.

2.5. Evaluation of the structure

2.5.1. Module scale

Porosity, "Poro"

We proposed an Index called "Poro" that varies between 0 and 1. It is defined by the empty volume ratio (defining cavities) relative to the occupied volume (defined by the volume of the bounding box, computed on MeshLab, in which the 3D CAD model fits). It is determined by the following equation:

EQUATION 1: $Poro = (Vo - Vt)/Vo$

With:

Vt: the total volume of the 3D CAD model

Vo: volume occupied by the 3D CAD model determined by the length, width and hight of the bounding box on MeshLab

Topography, "Topo"

Based on the area ratio. We proposed a normalized Index called "Topo" that varies between 0 and 1. It is determined by the following equation:

EQUATION 2: $Topo = 1 - (So/St)$

With:

So: surface occupied by the 3D CAD model, determined by the length and width of the bounding box on MeshLab.

St: the total surface of the 3D CAD model

Fractal dimension, "Dn"

The fractal dimension has been computed thanks to the function "est.boxcount" of the package "Rdimtools" available on the open-source software R (3.4.2), the script used to

determine it is available in the supplementary material (Annexe 3). The amount of r (radius) to be tested was set to 100 and the vector of ratios for computing estimated dimension in (0,1) was set to (0.1, 0.9).

Box-counting dimension, also known as the Minkowski-Bouligand dimension, is a popular way of figuring out the fractal dimension of a set in a Euclidean space. Its idea is to measure the number of boxes required to cover the set repeatedly by decreasing the length of each side of a box. It is defined as:

EQUATION 3: $$D = \lim_{r \to \infty} \left(\frac{logN(r)}{log\left(\frac{1}{r}\right)} \right)$$

With:

$N(r)$: the number of boxes with radius r needed to cover a given set.

r: radius of boxes

The fractal dimension of an object in a 3D space ranges between 2 and 3: 2 is an object with a smooth shape and 3 an object highly folded. We normalized the results between 0 and 1 with the following equation:

EQUATION 4: $$D_n = 1 - (3 - D)$$

The standard deviation of the normal "SDnz"

Various variables derived from normals were used in benthic surface irregularity analyzes (Carleton and Sammarco, 1987; Beck, 1998, 2000; Grohmann, Smith and Riccomini, 2009; Kovalenko, Thomaz and Warfe, 2012; Young et al., 2017). These studies have their source in the method proposed by Hobson (1972) offering diverse values to identify surface topography: strength vector, vector dispersion, several standard deviations to the plane. In our case, vector strength and vector dispersion are not relevant to highlight complexity. This is explained by the fact that we study volume objects, not only surface. The orientation of the surface of a volume, even for a single cube, will always be higher than a surface, except if it is refolded and create a volume. This index remains interesting for surface studies at finer scales. We therefore used the standard deviation of the normal with respect to the Z axis. The script used on R to determine it, is available in the supplementary material (Annexe 3). It gives the variation of the orientation of the normals on the vertical plane. If the object is flat SDnz is equal to zero, and increase each time there is an elevation or a depression of the surface. This SDnz index gives a more adequate value for determining the variability of the orientation of 3D CAD

models that we are studying. It varies between 0 and 1. It is calculated with the following equation:

EQUATION 5: $$SD_{nz} = \sqrt{\frac{1}{n}\sum_{1}^{i}\left(cos_{nz_i} - cos_{nz}\right)^2}$$

With :

i: each vertex

n: number of vertices that composed the 3D CAD models

cos_{nzi}: directional cosines of the normal of each vertex with respect to the Z axis.

cos_{nz}: mean of the directional cosines of the normal of the vertex that composed the 3D CAD models with respect to the Z axis

Global index of complexity at the module scale, "C"

The score for the module is determined by the sum of the different indexes. It varies between 0 and 4, with the following equation:

EQUATION 6: $$C = Poro + Topo + Dn + SDnz$$

2.5.2. Combination of modules at different scales

The difference between scales is defined by the area occupied on the ground. If the space between unitary modules does not exceed the ground area occupied by a unitary module, it constitutes an aggregate. A village is therefore composed of several modules or aggregates whose surface which separates them is greater than the surface occupied on the ground by the modules or aggregates which compose it (Charbonnel et al., 2011; Cépralmar, 2015; Tessier et al., 2015).

We identified 2 different types of combinations: 2 types of aggregation and 2 types of the village. AG_COMN is a complex of 14 COMN modules assembled 3 by 3 in length and 2 by 2 in height & width, occupying 146 m^3 (Blouet et al. 2011). This kind of aggregate can be found at the MPA of Cap d'Agde. AG_CR14 is composed of 35 CR14 modules assembled in chaos and occupying 270 m^3, this aggregation is part of one village settled in the MPA of Roquebrune Cap Martin (Bodilis et al. 2011). VL_BOSK is composed of 6 modules BOSK that occupy 780 m^3; 2 BOSK modules are positioned at each corner of an equilateral triangular shape plane, this village is settled in the Larvotto MPA of Monaco (Monaco: 43.74582°N 7.440709°E). Finally, VL_Z3AD

is composed of 2 modules of PIPE and five modules of STBS and occupies 585 200 m^3, it is settled in the MPA of Cap d'Agde called "Zone 3" (Blouet et al. 2011).

Weight for the different scale, "W"

We added a supplementary weight called "W" depending on the combination scale: 1 for the aggregation and 2 for the village.

Weighted mean Complexity, Cw

In order to determine the complexity at the higher scales (aggregation, village, fields), we calculated the mean complexity weighted by the volume of each module. The following equation was used:

EQUATION 7: $$C_w = \frac{\sum_{i=1}^{MD}(C_i.Vt_i)}{Vt}$$

With:

MD: number of modules

i: a given module

C_i: complexity score of a given module

Vt_i: volume of the module

Vt: volume of all the modules of the combination.

Heterogeneity: Structural diversity, "H'"

We used structural diversity in order to determine the diversity of the microhabitat that composed the global habitat of the artificial reef. We computed the Shannon diversity (H') index on the volume of the different modules that compose the aggregate of the village. The Shannon index was calculated with the following equation:

EQUATION 8: $$H' = -\sum_{i=1}^{MD} p_i.log\ (p_i)$$

with:

H': Shannon diversity index

MD: number of modules

i: volume of a given module

p_i: the proportion of the volume n_i of a given module *i* relatively to the total volume of modules (N) of the structure, computed as follows: $p_i = n_i/N$

Volume occupied, "V"

To discriminate between aggregates or villages that would have the same volume occupied but with a different number of modules, we used the ratio of the total volume of modules that compose the aggregate on the volume occupied by the aggregate.

EQUATION 9: $V = (Vr/Vo)$

Vr: volume of all the modules of the combination.

Vo: volume occupied by the combination, computed as follows: $Vo = S.max(h)$

With:

S: surface at the ground

$max(h)$: maximum height reached by the artificial reefs of the village.

Combination score, "S"

The score for aggregation is determined by the sum of the different indexes of complexity with the following equation:

EQUATION 10: $S = C_w + H'$

WITH:

W: supplementary weight according to the scale

C_w: mean complexity weighted

H': heterogeneity of the combination

V: volume ratio of the combination

2.6. Data analysis

Statistical correlation tests have been done with the open-source software R (3.4.2) using the "Hmisc" package. We used the Pearson test to determine if all the variables were correlated with the increasing complexity of the fictive object. The PCA performed on the complexity variables, have been processed with the package "FactoMineR". The hierarchical clustering was done on principal components with the HCPC function of "FactoMineR". The best cut of the dendrogram has been determined by K-means cascading with the cascadeKM function of the package "vegan". It creates several partitions forming a cascade from a small to a large number of groups (2 to 8 in our case).

The Calinski-Harabasz (CH) criterion has been used to select the best partition (Calinski-Harabasz (1974). The maximum value of CH usually indicates the correct number of groups. The FunctionCatdes of the package FactoMineR was then used on the Euclidean distance matrix of the scaled complexity variables to describes the clusters.

3. Results

3.1. 3D fictive 3D CAD models

The density of the points cloud has few incidences on the computation of the variable SDnz (Figure IV-5.A). However, for the computation of the fractal dimension the density was determinant, the more the object was getting complex and the more the computation of the fractal dimension was different according to the density (Figure IV-5.B). We choose the density 10, that represents a good compromise between time processing and accuracy of the computation. The difference between the value of Dn of the most complex model, calculated with the maximum density and the density of 10 points per unit squared, is slight (FM07 density 20: Dn = 0.30, FM07 density 10: Dn = 0.32).

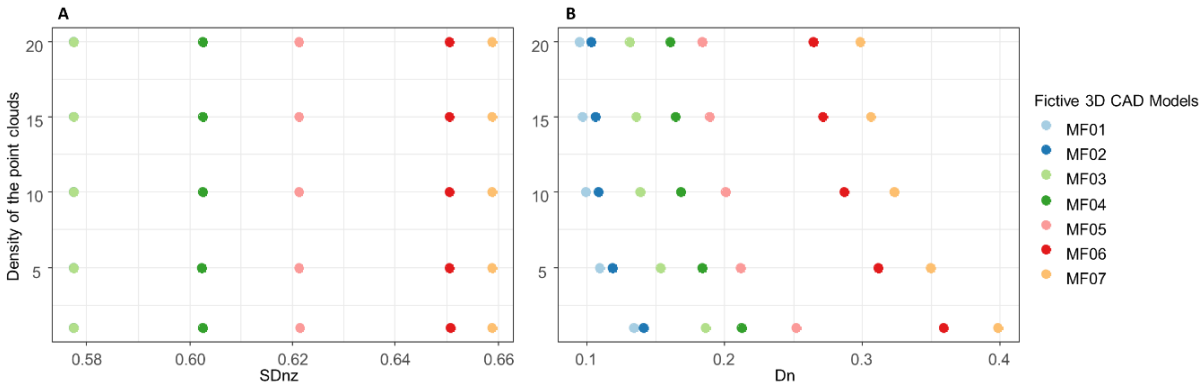

Figure IV-5: Values of SDnz (A) and Dn (B) computed on the fictive model with different density of point clouds (points per unit squared: 1, 5, 10, 15 and 20)

Table IV-1:Indexes computed on the 3D fictive 3D CAD models and evaluation of the global complexity (C)

Fictive model	Dn	SDnz	Topo	Poro	C
MF01	0.1	0.58	0.83	0	1.51
MF02	0.11	0.58	0.83	0.28	1.8
MF03	0.14	0.58	0.86	0.32	1.9
MF04	0.17	0.6	0.87	0.35	1.99
MF05	0.2	0.62	0.88	0.4	2.1
MF06	0.29	0.65	0.91	0.51	2.33
MF07	0.32	0.66	0.92	0.54	2.36

All the complexity variables computed on the fictive 3D CAD models were positively correlated to the increased complexity of these 3D CAD models (order~Topo: Rho: 0.9848992, p=5.339e-05; order~Poro: Rho: 0.9183082, p=0.003504; order~Dn: 0.969484, p=0.0003074; order~SDnz: 0.954652, p=0.0008208). The variable Dn increased at each step of complexification. The variable SDnz was not sensitive to the folded aspect of the surface, it started to increase when cavities were added. The variable Topo started to increase after the second phase of the refolding of the surface, indeed the two first 3D CAD models presented the same surface deployed. The last variable Poro had a zero value for the first model and increased continuously from the first step of refolding of the cube. The index of complexity increases all along with the 8 steps of complexification (

). For each variable, the higher gap was between MF05 and MF06, corresponding to the second step of cavities integration.

3.2. Evaluation of the structure of the AR modules

Table IV-2: Indexes computed on the artificial reef's modules and evaluation of average values for all the modules

Names	Dn	SDz	Topo	Poro	C
COMN	0.04	0.58	0.72	0.95	1.97
CR01	0.04	0.58	0.74	0.9	2.05
BONN	0.07	0.51	0.77	0.92	2.09
SALB	0.11	0.42	0.81	0.83	2.15
CR02	0.13	0.31	0.85	0.83	2.15
SEAR	0.1	0.8	0.67	0.73	2.2
TIPY	0.07	0.64	0.78	0.85	2.24
NEGR	0.1	0.76	0.71	0.74	2.27
CR14	0.16	0.42	0.85	0.78	2.29
FAKR	0.1	0.69	0.76	0.73	2.32
BONP	0.19	0.55	0.81	0.82	2.37
KHEO	0.18	0.67	0.79	0.83	2.41
DALO	0.17	0.67	0.88	0.63	2.62
PIPE	0.28	0.7	0.9	0.78	2.78
BOSK	0.3	0.75	0.85	0.74	2.78
STBS	0.3	0.7	0.94	0.82	2.88
Mean	*0.15*	*0.61*	*0.8*	*0.81*	*2.35*
sd	*0.09*	*0.14*	*0.07*	*0.08*	*0.28*

The index of complexity ranges between 2.12 for the module CR02 and 2.75 for the module STBS. According to the different variables, the modules do not show the same classification (Table IV-2). Dn ranges between 0.04 (CR01) and 0.30 (BOSK and STBS). SDnz ranges between 0.31 (CR02) and 0.80 (SEAR). Topo ranges between 0.67 (SEAR) and 0.94 (STBS). Finally, Poro ranges between 0.63 (DALO) and 0.95 (COMN). Dn shows the highest correlation with the index C (Pearson correlation : Dn~C: R: 0.8237215, p = 8.777e-05; SDnz~C: R: 0.6156684, p = 0.01112, Topo~C: R: 0.5071884, p = 0.04494, Poro~C: R: -0.1669613, p = 0.5366)

A PCA was performed on the 4 different variables that compose the index of complexity (Dn, SDnz, Topo, and Poro) of the artificial reef modules, the index of complexity C was added as a supplementary variable. The samples were collected according to optimal clustering computed with the Calinski criterion computed by cascade Kmeans (Figure IV-6).

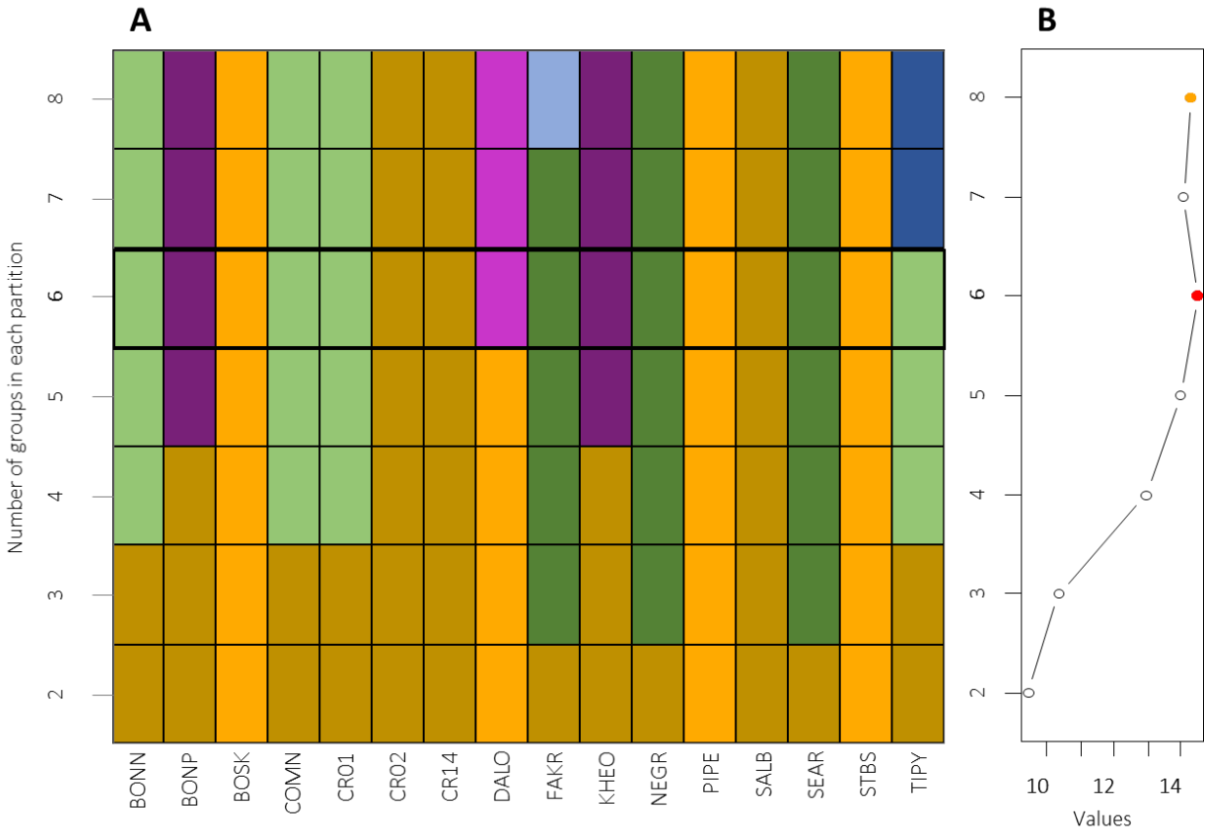

Figure IV-6: K-means cascade on the AR modules according to computed with Euclidean distance on the scaled value of the complexity variables (Dn, SDnz, Topo, and Poro), and Calinski criterion, groups ranging between 2 and 8: A)Comparison of the k-means repartitions of the AR modules according to the number of groups in each partition, B) and their value of the Calinski criterion

The first dimension, which represented 51% of total inertia, mainly structured the factor map. The second dimension also explained a large part of the total inertia (33.6%), while the third and fourth dimensions explained less than the mean threshold determined by the numbers of variables (Dim3:13.15%, Dim4:2.30%, <mean threshold 1/4 = 25%), and were not retained for the analysis. The first two dimensions showed a good projection of the data, as all variables were close to the correlation circle, and individuals had cumulative squared cosines above 0.6 on these two dimensions, except the modules KHEO (cumulative squared cosines=0.19), that was better explained by the third and fourth axis (cumulative squared cosines=0.81). Each individual contributes to less than 30% to the construction of both two first dimensions. COMN, BOSK, STBS, PIPE, DALO, CR01 and BONN mainly contributed to the construction of the first dimension. Whereas SEAR, CR02, NEGR, CR14 and FAKR mainly contributed to building the second dimension. The third and fourth dimension where mainly build by the DALO module (50%). The contribution of each variable to build the two first dimensions is well balanced (mean contribution for Dim.1 and 2: Dn: 22% SDnz: 30% Topo: 28%

Poro: 20%). Dn contributes 42% to the construction of the first dimension, and SDnz contributes to 53% to the construction of the second one. Topo and Poro contributed equally to build both dimension (Topo: Dim.1: 28%, Dim.2: 30%; Poro: Dim.1: 23%, Dim.2: 15%). On one hand, all the variables were positively correlated to the first dimension, except “Poro”. On the other hand, all the variables were positively correlated with the second dimension, except SDnz (Figure IV-7). The index of complexity as a supplementary variable shows a high correlation with the first dimension (71%).

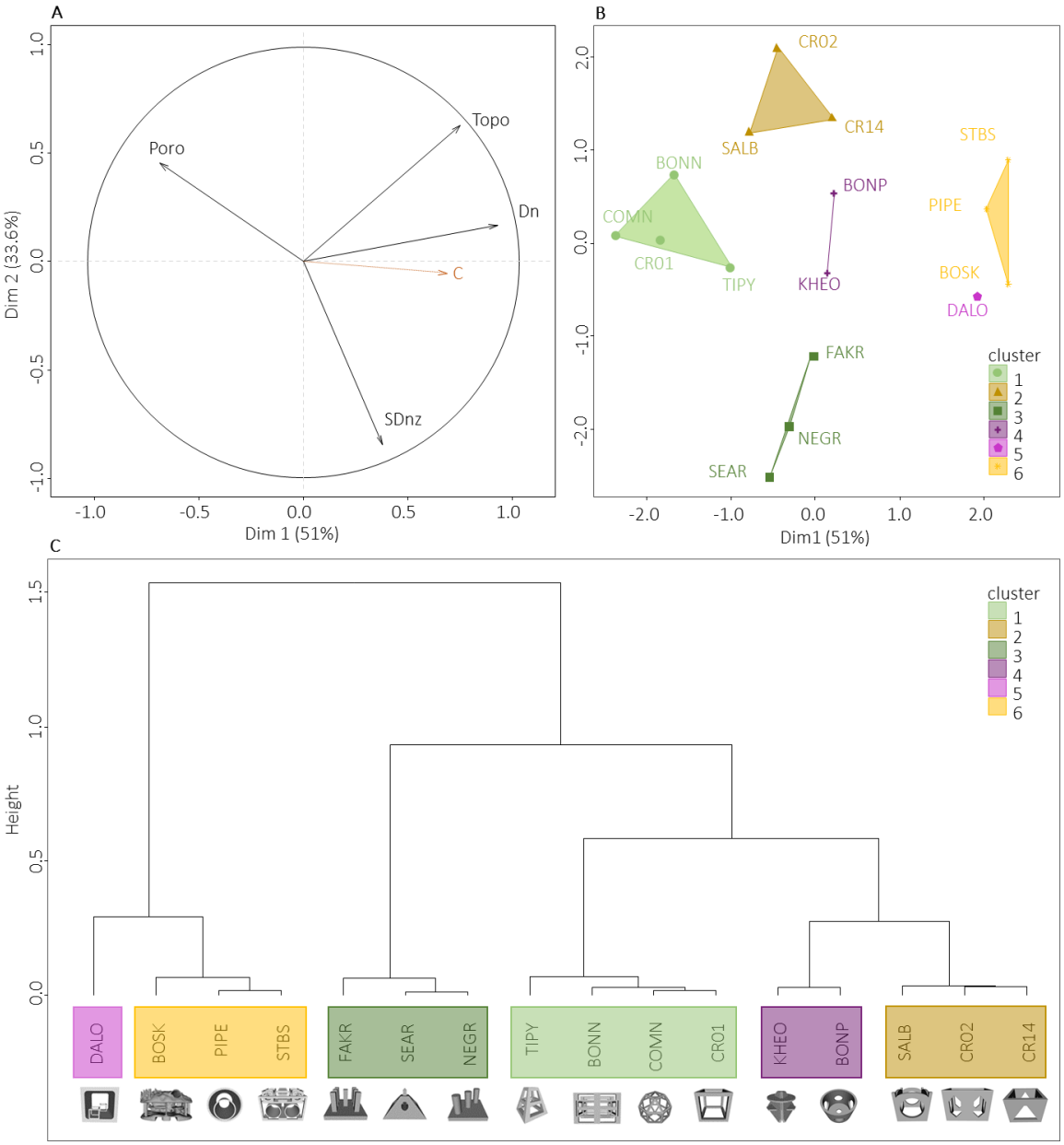

Figure IV-7:Principal component analysis: A) correlation circle of the variable of complexity (Dn, SDnz, Topo, and Poro) and supplementary quantitative variable the index of complexity "C", B) and the factor map of the artificial reef's modules, C) coloured ordination according to the optimal clustering computed by K-means cascades with Calinski criterion.

The optimal cut of the dendrogram by casacade K-means gave 6 different clusters (Figure IV-6, Figure IV-7). The first cluster (C1: BONN, COMN, CR01, and TIPY) and sixth cluster (C6: PIPE, STBS, and BOSK) were described by the dimension 1 (respectively negatively v.test: -2.727427 p= 0.006383044; and positively v.test: 2.864763 p= 0.004173218). The cluster 1 was positively described by the variable Poro (v.test: 2.856744, p= 0.004280113) and negatively by the variable Dn (v.test: -2.441173, p= 0.014639655). The cluster 6 was positively described by the variables Dn (v.test: 3.293959p= 0.000987868) and Topo (v.test: 2.432131p=

0.0150102913). The second cluster (C2: SALB, CR14, and CR02) and the third cluster (C3: SEAR, NEGR, FAKR) were described by the second dimension (respectively positively v.test: 2.466697 p= 0.01363657; and negatively v.test: -3.019897 p= 0.002528605). The cluster 2 was negatively described by the variable SDnz (v.test: -3.153912, p= 0.001610975). The cluster 3, was negatively described by the variable Topo (v.test: -2.343548 p= 0.01910133). The fourth cluster (C4: KHEO & BONP) could not be characterised by any dimension and couldn't be described by any variable in particular. The fifth cluster that counts only one module (C5: DALO), as the cluster 4, it was neither described by the two first dimension, but it was negatively described by the variable Poro (v.test: -2.2313 p= 0.02566126).

3.3. Combination of modules

Table IV-3: Index and score of the different combinations of artificial reefs

Combination	Cw	H'	V	W	S
AG_COMN	1.38	0.00	0.05	1	2.43
AG_CR14	1.65	0.00	0.04	1	2.69
VL_BOSK	2.17	0.00	0.01	2	4.18
VL_Z3AD	2.11	0.27	8.77E-05	2	4.38

The mean of the complexity index weighted by the volume stays the same for the two aggregations and the village VL_BOSK, since they are composed of one type of modules only. For the same reason, these three combinations don't show any structural diversity. The village of the MPA of Cap d'Agde shows the highest score (4.38) with a mean weighted complexity of 2.11 and a structural diversity of 0.27. The ratio of the total volume by the volume occupied has a very low value (8.77E-05). Indeed, the zone occupied by this village is very large.

4. Discussion

The development of different fictive 3D CAD models enabled us to test the best resolution to compute Dn and SDnz values. The density of 10 points per square unit was determined as a good threshold between time and efficiency of the computation. The increasing complexity of these fictive 3D CAD models was strongly correlated with all the variables (Dn, SDnz, Topo, and Poro). The fractal dimension has long been used as a variable to determine the complexity of habitats. In our case study, this is the variable that had the strongest correlation with the developed complexity index (C) for the evaluation of the artificial reefs' modules. However, it is not to be considered alone, because fractal dimension is difficult to interpret without other parameters to describe the structure (Tokeshi & Arakaki 2012). The other variables gave us more informative values to describe complexity. The SDnz was particularly sensitive to circular shapes. In fact, the refolding aspect of the surface on the fictive 3D CAD models has a stair-like aspect, and the stair orientation is the same from the cube to the highest level of refolding. This explains why SDnz increased only when cavities are added, because their circular shapes add new orientations. The same remark can be made with the variable Topo. Indeed, the two first 3D fictive 3D CAD models have the same deployed surface but with a different arrangement. However, these refolding implied differences, it brings shaded surfaces that could imply differences in settlement of epibiont and attraction for mobile species (Bohnsack 1991, Pickering & Whitmarsh 1997, Underwood & Smith 1998, Svane & Petersen 2001, Lam et al. 2003). Another variable highlighting the shaded faces should be implemented to improve the characterisation of the surface. These results again support the importance of considering several variables in order to define the complexity of an object and that none prevails to another. Indeed most of the studies used several variables to identify the complexity of the surface (e.g.: Beck, 1998, 2000; Frost *et al.*, 2005; Gratwicke and Speight, 2005; Matias *et al.*, 2010; Pittman and Brown, 2011; Bryson *et al.*, 2017; C.A. Sánchez-Caballero *et al.*, 2017; Young *et al.*, 2017). Finally, the variable Poro, as the normalised fractal dimension was the only variable that varies at each step of complexification. To the best of our knowledge variables related to porosity are rarely used in complexity studies. It is certainly due to the difficulty to evaluate it in natural environment. The index of porosity we proposed is based on the volume occupied by the bounding box. For the artificial reef modules, the modules that had a low complexity value were those with the highest porosity values. It would then be interesting

to determine a threshold of porosity according to the desired objectives. Such a threshold is difficult to determine (Sherrard, 2017). Moreover, this variable did not give us information about the quality of this porosity. Is this porosity a result of several cavities or of a single cavity. Improvements are needed to complement this information.

For now, this numerical method gave us the first opportunity to evaluate the complexity of the structure of ARs modules and to distinguish different types of artificial reefs. The principal component analysis and its clustering on the different variables computed on the 3D CAD models of ARs, gave us a good representation of the different aspects of their complexity. In fact, we distinguished 6 principal clusters. Among them we can highlight 4 principal types of artificial reefs with clusters 1, 2, 3 and 6. Cluster 1 (COMN, CR01, BONN, and TIPY) shows the highest porosity (Poro> 85%), and lowest fractal dimension (Dn<0.10). Indeed, it represents geometrically hollowed-out modules, that looks like “cage” shapes. The low value of Dn highlighted the simple geometry of their structure, basically composed of lines. This type of module is inspired by Japanese modules, preferentially used to attract pelagic fish. The BONN and TIPY can be effective as one module, but the modules COMN and CR01 need to be installed in aggregates on several floors to be effective (Bodilis et al. 2008, Cépralmar 2015, Tessier et al. 2015). However, this type of ARs cannot reconstitute a rocky habitat, their “cage” structure does not offer shelters for demersal species and surfaces to favour colonization of sessile species. Indeed, in this purpose, BONN modules have been often post-complexified in several MPA in order to increasing species richness, abundance and biomass of fish assemblages (Charbonnel et al. 2002, Bodilis et al. 2008, 2011). Cluster 2 (SALB, CR14, CR02), could be defined as the “Box” type, it shows the lowest SDnz. Indeed, it represents simple geometric shapes that look like “box” widely opened on the top and down, and showing smaller opening on the side. It has basically four different orientations of the surface. However, it presents enough surface deployed to begets settlement of sessile species, and to provide wide shelter for demersal species. As the modules BONN and CR01, these latter are most of the time installed in aggregation to increase their efficiency, and can attract pelagic species if it reached a certain height (Bodilis et al. 2008, Cépralmar 2015, Tessier et al. 2015). The Cluster 3 (SEAR, NEGR, FAKR), mainly defined by their low topography, could be defined as the ”bock” type. NEGR and FAKR are composed of a plateau on which is erected large circular or rectangular arises, whereas NEGR holds rather triangular shapes with oblique faces. All of them has no

cavities, their solid shapes can explain their low topography. These modules are used for protection against trawling (Cépralmar 2015, Tessier et al. 2015). In this context, the importance of surface deployment is not of great interest and their best asset is to be a strong enough structure to prevent trawling. Finally, cluster 6 (BOSK, PIPE, STBS) could be defined as the "nested" type, it shows the highest fractal dimension (Dn) and topography (Topo). The reefs PIPE and STBS are composed of several units nested. PIPE is composed of two single pipes, one smaller in a bigger one. STBS is composed of various other modules: a steel rectangular basket that collects 2 single pipes, 4 SALB, and 32 block works arranged on two floors. Finally, the BOSK module is the first artificial reef designed by 3D printing, it has a unique shape and much more complex than most of the modules of artificial reefs designed in a classical way, this technic allows to bring up in one single module the same complexity as the one nested. these modules give a wide surface to be colonized by benthic sessile species and nice shadow shelters and diverse surface orientation. Regarding the modules of the remaining clusters 4 and 5, BONP could be integrated with the box type. This module was immersed in aggregation like the ones of the cluster 2, however its cylinder shapes increased its surface orientation explaining why it was not gathered with the cluster 2 that shows low SDnz. The KHEO is an anti-trawling module, however its shape is not solid as the other modules that composed the cluster 3 (block type), indeed it shows a higher porosity. Finally, DALO is composed of one big cubic unit with 2 CR01 nested inside, and could be gathered in the cluster 6, but it shows a very low fractal dimension (Dn) compared to the module of this cluster that show the highest value of fractal dimension. This method seems effective in identifying different types of reefs and sufficiently sensitive to highlight the inherent variability of each module.

The index developed for other scales of the arrangement of ARs (i.e. aggregation. village. field) opens the gate to a real evaluation of the ARs according to the habitat structure they provide, both in terms of complexity and heterogeneity. The examples provided give coherent results. An aggregate of COMN modules is less complex than an aggregate of CR14 modules. At the village scale, we can see the interesting effect of the heterogeneity, the village of the Larvotto reserve with BOSK modules still presents a higher complexity index, but compared to the village of the Cap d'Agde that presents two different types of module, this village has no heterogeneity of modules.

Conclusion

This first evaluation of modules of artificial reefs and module composition, proves to be promising. Indeed, we have been able to develop a method distinguishing the artificial reefs according to 4 numerical variables and to classify them according to their structure from the module until the different possible module combinations. Some improvements could be done in order to better characterize the porosity and the surface appearance according to its exposure to light and/or waves. However, this first evaluation of ARs could be expanded and used in the future to evaluate designs of ARs before their production and immersion. The collection of monitoring data on different type of artificial reefs would make it possible to assess the efficiency of this method. It would be possible to determine type of profile according their structural parameter that could favour the recruitment of juveniles or adults, or maybe species of economical or ecological interest. Some perspectives for the evaluation of natural habitat structures are also feasible. Indeed, with photogrammetry technology, it is now possible to reproduce the structure of natural habitats in marine environment (Bryson et al. 2017, Riera et al. 2019), our method could be used on 3D CAD models created by photogrammetry. The comparison of AR with the natural environment and the value of their different complexity parameters could help to design structures that best mimic natural habitat for restoration purposes and for targeting species of interest according to their natural habitat.

PART 2: LINK BETWEEN MICROTOPOGRAPHY AND PHOTOSYNTHETIC BIOFILM PHYSIOLOGY AT DIFFERENT SCALES

To be submitted

Autors : Riera E., Munerol A., Androuin T., Prins A., Jesus B., Carlier A., Dubois S., Francour P. & Hubas C.

Résumé

Dans les 2 premiers chapitres, la microtopographie du matériau a été soulevée comme un paramètre susceptible d'influencer l'activité physiologique des communautés de biofilm. La présente étude propose d'adapter, à l'échelle microscopique des matériaux, les indices utilisés pour déterminer la complexité des modules de récifs artificiels. L'adaptation de ces indices permettrait de relier les paramètres de complexité à l'activité physiologique des communautés photosynthétiques. Cette étude a été menée dans le cadre d'un stage de Master 2 effectué par Axel Munerol et co-encadré par Cédric Hubas et moi-même. Nous avons émis l'hypothèse que les caractéristiques paysagères du matériau seraient susceptibles d'influencer la physiologie et l'abondance des organismes photosynthétiques du biofilm.

L'utilisation d'un scanner surfacique a permis de reconstituer un modèle 3D de la surface des matériaux afin d'en calculer la complexité grâce aux indices développés dans la section précédente (Chap.3, Part.1, p 110). A l'aide d'un Imaging Pam nous a pu caractériser l'activité des micro-organismes photosynthétiques des communautés de biofilm.

Les indices utilisés à l'échelle macroscopique s'adaptent très bien à l'étude de la complexité à l'échelle microscopique. Nous avons pu démontrer que la micro-complexité a une influence positive sur l'abondance des espèces, cependant cette relation doit être étudiée à l'échelle appropriée. Par ailleurs, l'orientation de la surface joue un rôle clé dans la physiologie et peut-être dans le comportement du biofilm qui montre une adaptation conservatrice face à l'incidence lumineuse.

La micro-complexité du matériau semble constituer diverses niches pour les micro-organismes, qui induisent une distribution et une activité différentes des communautés microbiennes au sein du biofilm.

Abstract

The present study proposes to adapt indexes used to determine the complexity of artificial modules to the microscale of the materials used to build artificial reefs. The aims is to be able to relate these complexity parameters to the physiological activity of photosynthetic communities. We have hypothesized that the landscape characteristics of the material are likely to influence the physiology and abundance of photosynthetic organisms in the biofilm. The use of a surface scanner made it possible to reconstruct a 3D model of the surface of the materials in order to calculate its complexity. We characterize the activity of photosynthetic microorganisms in biofilm communities by Imaging Pam. The indices used at the macroscopic scale are efficient to the study of complexity at the microscopic scale. We have been able to demonstrate that micro-complexity has a positive influence on the abundance of species. Moreover, the orientation of the surface plays a key role in the conservative adaptation to the incidence of light. The micro-complexity of the material seems to constitute various niches for micro-organisms, which induce a different distribution and activity of the microbial communities within the biofilm.

1. Introduction

The biofilm formation is linked to the chemical parameters of the substrate and the surrounding environment (Callow & Callow 2002, Salta et al. 2013). Motile bacteria are known to sense the surface and to be able to choose to adhere or not to a substrate (Wahl 1989, Cooksey & Wigglesworth-Cooksey 1995, Callow & Callow 2006); whereas diatoms sink on it by change and adhere to substrate by secreting large amount of EPS (Cooksey & Wigglesworth-Cooksey 1995, Wetherbee et al. 1998). The attachment of these microorganisms depends directly on the physical aspect of the substrate (Hunt & Parry 1998, Patil & Anil 2005, Teughels et al. 2006, Truong et al. 2010, Cui et al. 2010). Indeed, a flat surface gives fewer anchoring points than a rough surface (Huang et al. 2018). However, the increase of surface roughness on a very small scale (50 to 300 nm) enhance the surface wettability of hydrophilic surface (Singh et al. 2011) that prove to decrease cell bacteria attachment (Cooksey & Wigglesworth-Cooksey 1995, Cerca et al. 2005). The aspect of the surface can influence also the diversity of microorganisms and their physiology; the more the surface area of contact will be diverse, the more organisms with different body size would settle (Battin et al. 2007, Myan et al. 2013, Huang et al. 2018).

The objective of this study is to determine if the physiology of photosynthetic microorganisms is linked or not with microtopography of the associated substrate. According to the topography of the substrate, we hypothesized that (i) the photosynthetic organisms will aggregate on the surface and (ii) might have different physiological responses.

2. Materiel & method

2.1. Substrates of artificial reefs and natural rock

Three different substrates used for artificial reefs have been tested: the rock, mainly used for dikes and rockfills; the concrete, mainly used to build classical module of artificial reefs nowadays; and a substrate based on dolomite sand and white cement made by the Boskalis industry and used to build artificial reef with giant 3d print made by D-Shape, this substrate will be named “dolomite”. Five cobblestones of each substrate sized 1.5x2x5 cm. The samples have been placed in a basket at 1m dept at the Concarneau harbour (N 47°52’ 16.395” (+47°52’ 16.395”) W 3°54’ 52.2354” (-3°54’ 52.2354”). Nine of them has been retrieved after one week of immersion and six after two weeks of monitoring.

2.2. Characterization of the surface topography

2.2.1. Surface scanner

Before immersion, each cobblestone was scanned by a surface scanner to digitize its topography. These topographies can take several forms: first a mesh (in format .PLY for Polygon File Format or Stanford Triangle Format) but also a cloud of points with, for each point, its coordinates x, y, z. The software MeshLab ©, (Cignoni et al. 2008) is used to manipulate the different PLY and CloudCompare © software, is used to sample meshes in scatter plots at a very fine resolution (1000 point per unit squared) to defines more precisely the surface for indexes that are sensible to resolution (fractal dimension (D) and roughness (R)). Each mesh has been processed so that the different surfaces can be compared to one another by making a mean plane: the orientation of the 3D objects in the space has been standardized, the area of interest has been extracted from each brick and then used to define the origin of the z axis (altitude) of each 3D model.

2.2.2. Index of complexity to define microtopography

As far as possible, we used the same complexity indices developed in the previous part (chapter XX section XX). Some adaptations were necessary for the Topo index, and the poro index was not calculated in this study as it requires a volume and cannot be computed on surfaces.

Roughness "R"

The Topo index was not easy to determine at this finer scale. Then we used a different approximation of the rugosity by taking into account the variations of the continuity of the surface. For this, the "roughness" function of the R "Seewave" package (Sueur et al. 2008) makes it possible to calculate an index easily. This function calculates the integral of the second squared derivative.

EQUATION 11: $r = \int_b^a D^2x(t)^2dt$

t: is the x-axis and a and b being the cloud of points.

To enable this function to operate, it is necessary to transform the point cloud into a continuous line in order to calculate its integral. For this, the x values of the points have been rounded to the tenth. Each level of x will therefore have a cloud of points on a two-dimensional axis y z. The curves thus represented can give a roughness index via the package R. The average of all the indices harvested is then considered as the average roughness of the mesh treated with the levels of x. The same operation is repeated by rounding the values of y instead of x. A precise idea of the roughness of the surface can be approximated by averaging between the roughness of the levels of x and levels of y previously calculated.

Fractal dimension

The fractal dimension is calculated for a surface then the fractal dimension of an object in a surface ranges between 1 and 2: 1 is a flat surface and 2 a surface highly folded. We normalized the results between 0 and 1 with the following equation:

EQUATION 12: $D_n = 1 - (2 - D)$

Vector dispersion "ik"

At this scale, a previous study highlights the efficiency of the vector dispersion "ik" which measures the uniformity in angles of a surface (Carleton & Sammarco 1987) instead of SDnz. We thus decided to use both indexes to compare them. Mathematically, "ik" estimates vector variance for all normal vectors of individual planar surfaces. It is a value between 0 and 1, where 0 indicates a flat plane and a number closer to 1 indicates a more complex surface, with a highly

irregular orientation. As SDnz, this index is based on the directional cosines of each triangle's normal vector (cos_x, cos_y, and cos_z). it is determined by the following equations:

EQUATION 13: $$R1 = \sqrt{\left(\sum_1^i cos_x\right)^2 + \left(\sum_1^i cos_y\right)^2 + \left(\sum_1^i cos_z\right)^2}$$

EQUATION 14: $$1/k = (i - R1)(i - 1)^{-1}$$

i: is the number of points.

cos_x: is the directional cosine of a point's normal vector in the X direction.

cos_y: is the directional cosine of a point's normal vector in the Y direction.

cos_z: is the directional cosine of a point's normal vector in the Z direction.

2.3. Analyse of biofilm activity by Imaging PAM

After the preliminary test, only the samples retrieved after one week has been retained for the analyses because the others showed a high abundance of organic matter that saturate the Imaging Pam. The measurement is made on each pixel of the image provided by the imaging PAM. Each pixel therefore represents a set of fluorescence measurements as a function of light intensity. Pulse saturation imaging PAM (Pulse Amplitude Modulation) makes it possible to quantify several parameters relating to the photosynthetic activity of an organism. The Imaging Pam is composed of an actinic light that radiates in wavelengths allowing photosynthesis, and a fluorometer. The measurements are taken in an enclosure preventing the external light from interfering with the signal.

Use of total light energy

The fluorometer measures the fluorescence yield measured briefly before application of a Saturation Pulse (F), the minimal fluorescence yield of dark-adapted sample with all photosystems II (PS II) centers open (F0), the maximal fluorescence yield of dark-adapted sample with all PS II centers closed (Fm), the maximal fluorescence yield of illuminated sample with all PS II centers closed (Fm') . The photochemical conversion quantum yield (Y (II)) is expressed by the following relationship.

EQUATION 15: $Y(II) = (Fm' - F)/Fm' = \Delta F/Fm'$

This index provides information on the efficiency of the use of light by photosynthetic organisms. It is also complementary to Y(NO), the quantum efficiency of energy dissipation by non-photochemical and unregulated pathways, and Y(NPQ), the quantum efficiency of energy dissipation by non-photosynthetic regulated pathways. The indices Y(NO) and Y(NPQ) are calculated by the following equations:

EQUATION 16: $Y(NO) = F/Fm$

EQUATION 17: $Y(NPQ) = (F/Fm') - (F/Fm)$

These three indices make it possible to apprehend the different aspects of photosynthesis of organisms and their relation to light (Klughammer and Schreiber, 2008).

Each index is therefore a proportion of use of total light energy. Indeed, the cumulation of these three parameters is always equal to 1, and is calculated by the following equation:

EQUATION 18: $Y(II) + Y(NO) + Y(NPQ) = 1$

Relative electron transporting rate "Ek" & maximal saturation brightness values ETRmax

The rETR (relative Electron Transport Rate) is calculated by the following formula:

EQUATION 19: $rETR = Y(II) \times PAR \times 0.84 \times 0.5$

This formula takes into account the quantum yield as well at a given light intensity (PAR in µl quantat.m-2.s-1). 0.84 is the average ratio of light absorbed by a leaf and does probably not reflect that of our biofilm. It is necessary to divide by two to obtain the rETR because there are two photosystems and we make the assumption that the two photosystems have the same efficiency. Different rETR are calculated at each intensity of light which gives. a curve of photosynthetic activity (rETR) as a function of light intensity also called light curves (*Figure IV-8*). A model (Eilers & Peeters 1988) is applied to the data to retrieve different photosynthetic parameters such as maximum rETR and the light saturation parameter (Ek) (Figure IV-8). Light saturation values (Ek) determine the light intensity, for which photosynthesis efficiency (rETR) reach a plateau. This parameter makes it possible to determine if the biofilms are adapted to strong or low luminosity. A high Ek value defines individuals acclimated to a strong irradiance.

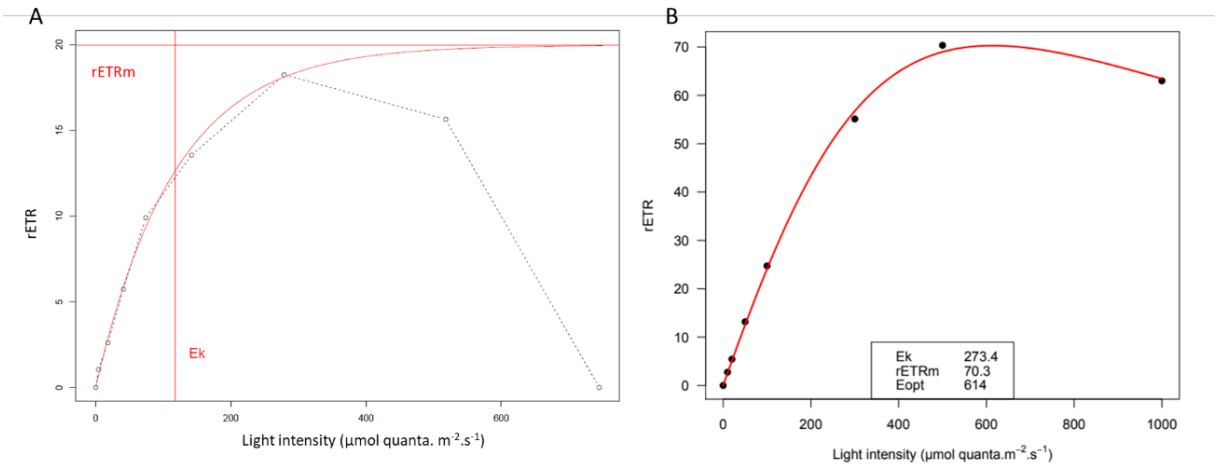

Figure IV-8: Example of a light curve (A) fited with the model of Eilers and Peeters (B) used to find the values of Ek and ETRmax

2.4. scale

Even if in the previous study we identified no significant differences in biofilm communities between substrates (Chap. 1 & Chap. 2). We showed however that the use of chemically different substrates has an impact on biofilm formation according to their chemical and physical characteristics which is coherent with results from Teughels et al. (2006).

In the present study, several patches were selected within the same substrate at different scales. This allowed determining if the change of topography within the same substrate (which imply same chemical characteristics) influences the distribution and the physiology of the communities. The different scale selected and the number of patches is described below:

4. Medium scale (0.55 cm) : 10 patches per samples (total of 30 patches per substrate)
5. Small scale (0.25 cm): 20 patches per samples (total of 60 patches per samples)

3. Results

3.1. Characterisation of the surface of substrates at the global scale

Table IV-4: Mean of the complexity indices on the three substrates (concrete, dolomite, rock) on the total surface

Substrate	R		p	ik		p	D		p	SDnz		p
	mean	*sd*	*	mean	*sd*	*	mean	*sd*	*	mean	*sd*	*
Concrete	4.112	*1.743*	*a*	0.053	*0.009*	*b*	0.908	*0.001*	*b*	0.182	*0.028*	*a*
Dolomite	3.724	*0.105*	*a*	0.092	*0.003*	*a*	0.952	*0.007*	*a*	0.154	*0.003*	*a*
Rock	0.099	*0.041*	*b*	0.001	*0.000*	*c*	0.890	*0.010*	*c*	0.009	*0.002*	*b*

Overall the set of indexes shows coherent value to characterize the surface of the substrate (*Table IV-4*). Indeed, dolomite and concrete that show complex surface compared to the smooth surface of the natural rock, showed the highest value for all the parameters (*Table IV-4* & *Figure IV-9*). Concrete and dolomite showed equivalent roughness (R) and variation of the orientation of the surface according the Z axis (SDnz). However, the two surfaces are very different, dolomite shows a homogeneous roughness due to the grain size of the dolomite sand, whereas concrete shows a heterogeneous roughness linked to a smooth surface punctuated by relatively deep holes due to the various air bubbles present during its manufacture. These differences are well described by the vector dispersion (ik) and the normalized fractal dimension (Dn). Indeed, higher value of ik expresses a more diverse orientation of the faces; and higher fractal dimension expresses a self-repeated aspect or a more refolded surface. These two indexes highlight these aspects of dolomite due to the grain size.

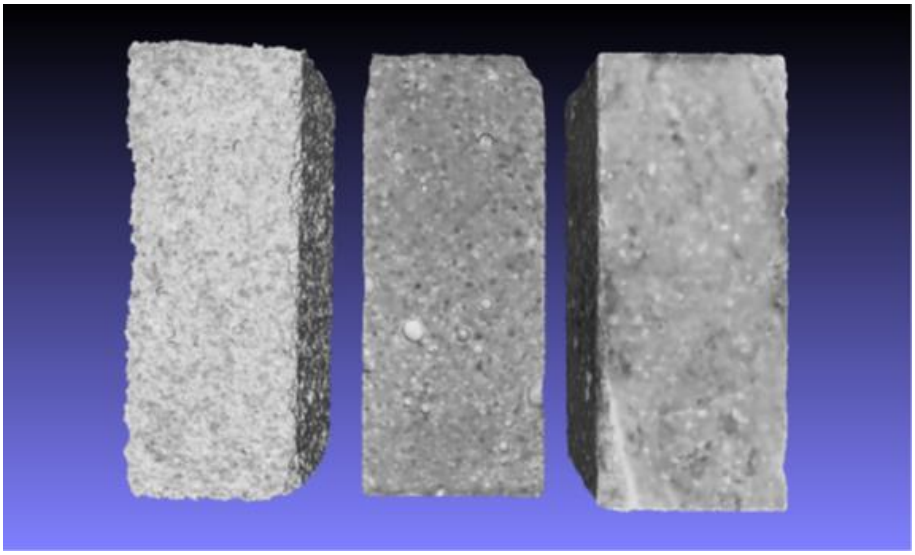

Figure IV-9: Surface scan image of the different substrates (from left to right: dolomite, concrete, rock)

3.2. Characterisation of the biofilm activity with Imaging PAM and correlation with complexity indexes

The activity of the organisms resulting from the Imaging Pam showed that the absorbance was significantly stronger on the natural rock than on the other two substrates (Waerden Van der test: $p < 0.05$; post hoc test: C-D: > 0.05, C-R: < 0.05, R-D: < 0.05) (*Figure IV-10*).

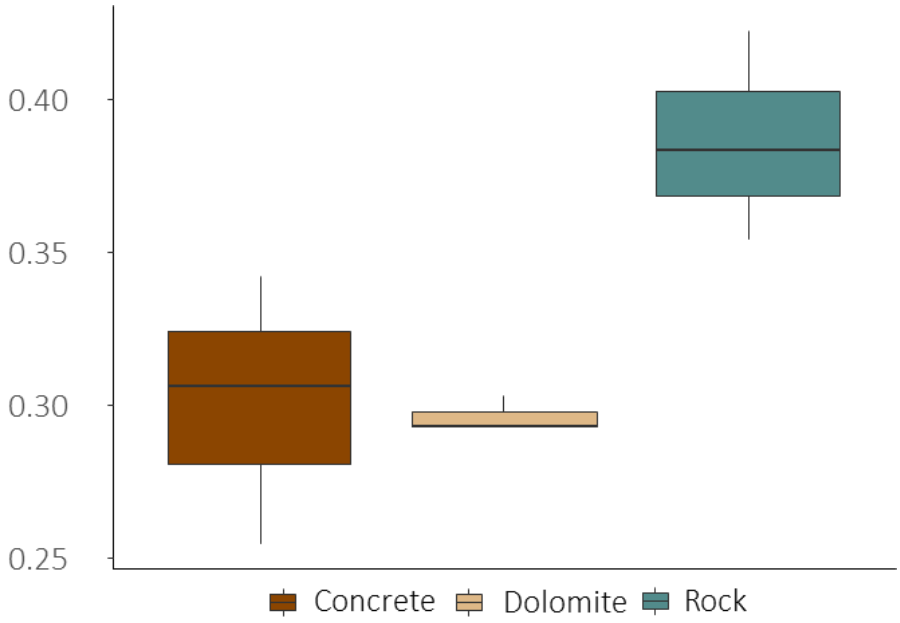

Figure IV-10: Absorbance of the biofilm by imaging PAM on the different substrates (concrete, dolomite & rock)

We also noticed a high heterogeneity of the measured parameters at the surface of concrete samples. The photographs of the PAM imaging (*Figure IV-11*) show a non-homogeneous distribution of individuals according to the different indices. The absorbance related to the abundance of communities shows that the entire surface is colonized. However, the cavities welcome fewer abundance compare to smooth surfaces. This differences of abundance in the cavities are related to high rETR, low photochemical efficiency Y(II), and high Y(NO) and Y(NPQ)

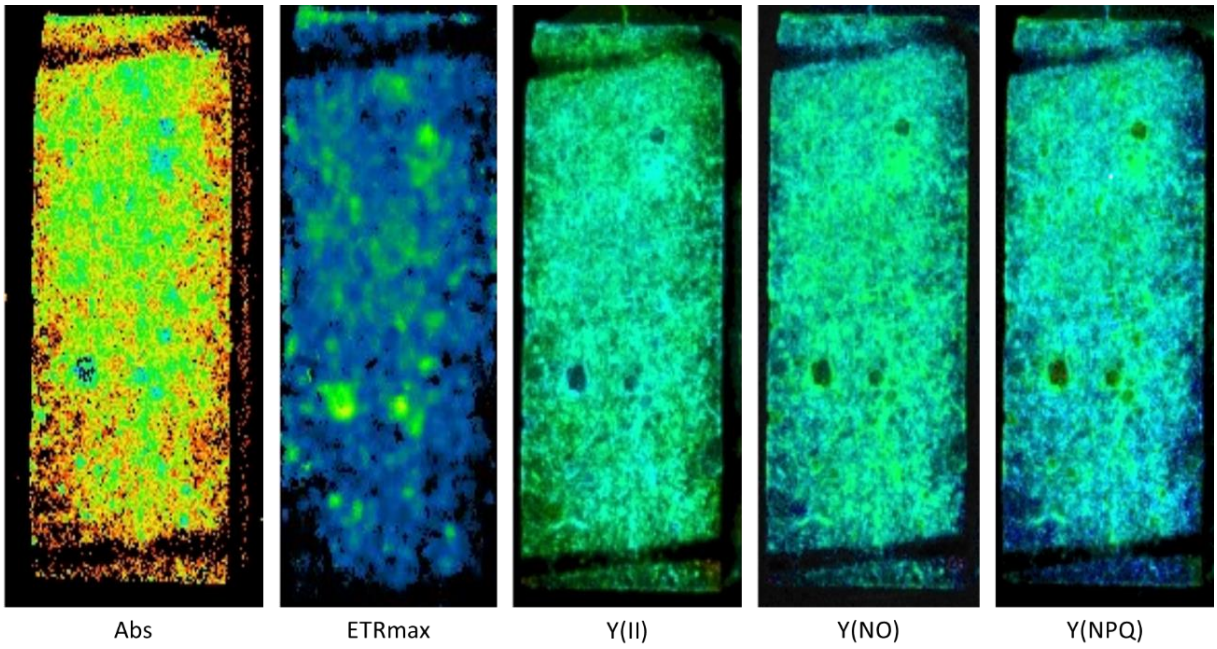

Figure IV-11: Different Imaging PAM-parameters on cobblestone number 3 of concrete

On dolomite, absorbance did not show any relation with the complexity indexes neither at the medium or small scale. However, indexes related to the photosynthetic activity and adaptation to high irradiance (Y(II), Ek, and ETRmax), show a positive correlation with almost all the indexes of complexity at medium scale (*Figure IV-12*). At small scale, these relations decrease and are significant only with the indexes related to surface orientation (ik and SDnz). Moreover, the non-photochemical quenching Y(NPQ) (which reflects the extent to which the algae are inhibited by high irradiance) is negatively correlated with these last indexes of complexity. On the other substrates, at medium scale, roughness (concrete) or high fractal dimension (rock) were negatively correlated with absorbance. However, this relation shift to positive correlation at smaller scale. Moreover, on rock fractal dimension is related to photosynthetic activity and adaptation to high irradiance. On Concrete, surface orientation is related to high absorbance and high photosynthetic activity (positive correlation with Y(II), Y(NO), rETRmax, Ek, and negatively with Y(NPQ)). It is noted that, on average, significant correlations rarely exceed 50%.

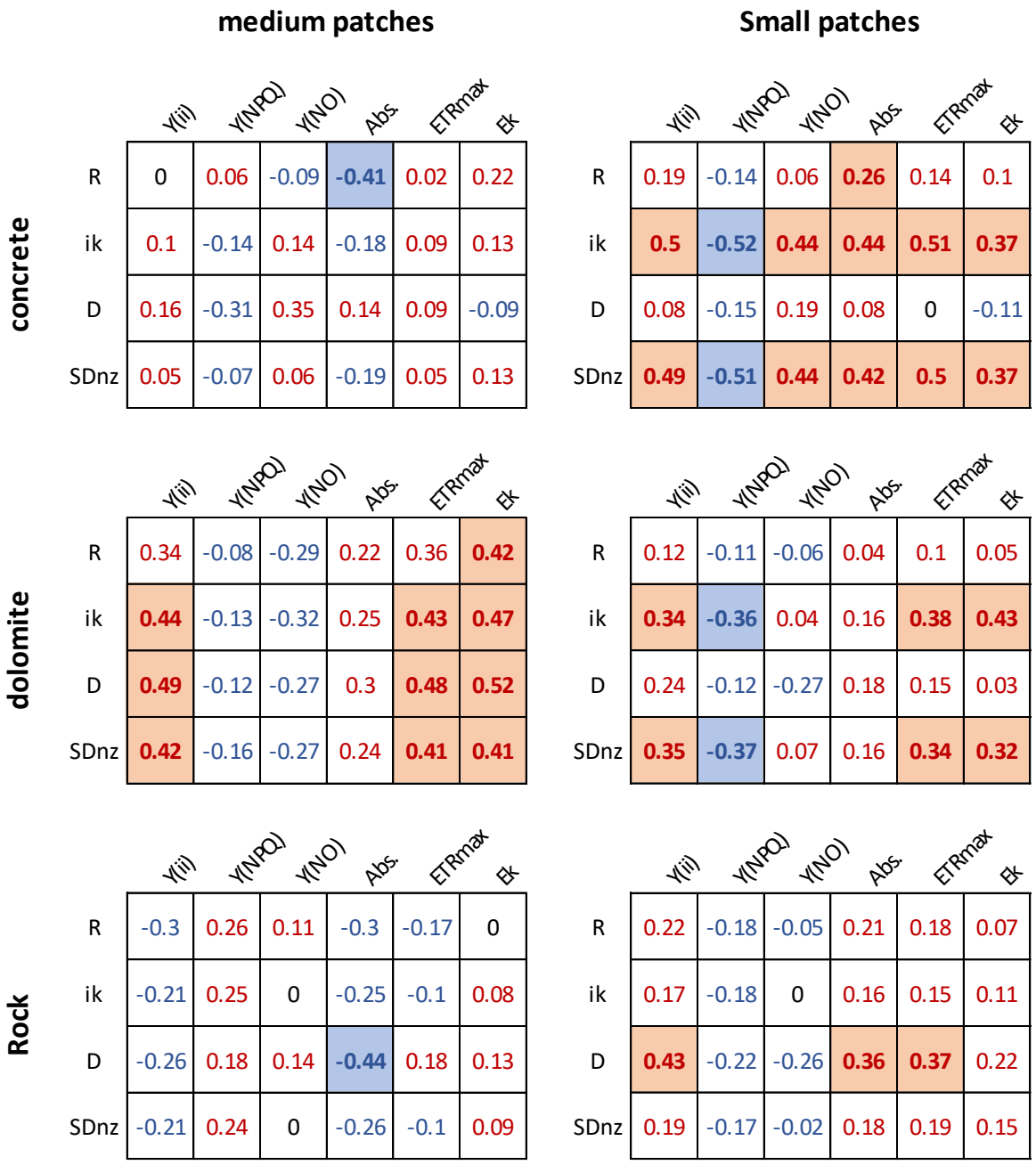

Figure IV-12: Correlogram of the microtopography complexity indices and the Imaging Pam indices on the three substrates (concrete, dolomite, rock) according to the three scale scales studied (Small, medium, big), the gradient scale corresponds to the correlations, from the red to blue from negative to positive, framed values show significant correlations at p <0.05

4. Discussion

In the present study, the use of Imaging Pam to characterize the physiological parameters of the photosynthetic biofilm communities, allowed to determine if the change of structure complexity of the surface within the same substrate influences the distribution and the physiology of the communities. At first sight, the three substrates have very different topographies. The vector dispersion (ik) and fractal dimension (D) where the index that revealed differences between each substrate, while the variation of normal to the z axis (SDnz) and roughness (R) separates the rock from the other two substrates. However, the use of different indexes helps to define the broad spectrum of surface profile, giving information about the surface orientation, its roughness aspect, how the surface is self-repeated and refolded in the space and highlight different correlations with imaging pam indexes. The indexes related to normals (ik and SDnz) proved to be redundant as they show similar correlation on concrete and dolomite with photosynthetic activity. In the previous section, SDnz was used because it was more adapted to 3D volume object (Chap.3, Part I). However, Carleton and Sammarco, (1987), had shown that ik was the best indexes to describes link between coral settlement and substratum irregularity compared to SDnz. Young et al., (2017), used it also with success on coral reef 3D photogrammetric models. Then according to the type of object study (3D surface, 3D volume object) ik or SDnz could be used and could give equivalent information related to the orientation of the surface. On the other hand, the fractal dimension (D) and the roughness index (R) has to be used with caution, because their computation is very sensible to the chosen resolution. Indeed, the number of points to define a surface must be at the highest possible resolution to truly mimic the surface, otherwise the spaces between the points may induce computational errors at very small scales. However, increasing the resolution will highly impact the computation time process. These two indices should therefore be used with caution and indicate precisely the resolutions used and the calculation methods to be able to compare the results with future studies.

Depending on the substrates, we observed that the activity of the biofilm did not respond to the same complexity parameters and that these relationships could also change from one scale to another. At first glance, smooth surface hosts more abundant communities, but when looking at small scale, within rock and concrete that present smoother area compare to dolomite, this relation is shifted. These results imply that even on a very smooth surface,

when focusing on the smallest scale, the micro topography influence positively the abundance of individuals. This is in accordance with modern ecological concepts which state that ecological niches of microorganisms are influenced by the landscape that corresponds to their body size (Battin et al. 2007). Indeed, at the µm scale, grooved surface instead of flat surface increase biomass by giving anchor point and shelter from disturbance (Huang et al. 2018), and between different topographies, some with high isotropy, provide less surface of contact and decline attachment of cells (Myan et al. 2013).

Regarding photosynthetic activity and light saturation, whatever the substrates type or scale, when correlation was significant, they were positive. Organisms show a higher yield of photosynthetic activity and adaptation to high irradiance (i.e. hight Ek and low NPQ) when the surface orientation is more irregular. It can be explained by the fact that organisms may not receive the same light dose during their lifetime as they are not always oriented in the direct axis of light (Iluz & Dubinsky 2013). It is likely that they adapt their photosynthetic apparatus to the highest light conditions they are potentially exposed to in order to avoid photoinhibition. In the microphytobenthos, biofilm diatoms are known to do vertical migration and to use physiological mechanisms as xanthophyll cycle and modulation of rETR to prevent damage from high irradiance (Cartaxana et al. 2011, Serôdio et al. 2012). It is, therefore, possible for diatoms to migrate similarly within the protected valleys conferred by topography or to simply adapt their physiology to the light intensity according to their niche provides.

Conclusion

Taking together, these results suggest that with some adaptations indexes used at macroscale can characterized the microscale and revealed some differences according these different parameters. Indeed, micro-complexity have positive influence on the abundance of species, but this relation has to be studied at the appropriate scale. Moreover, the surface orientation plays a key role the physiology and perhaps in the behaviour of the biofilm that show preservative adaptation to light. The micro-complexity of the substrate constitutes various niches for microorganisms, that induce the distribution and activity of the different microbial communities within the biofilm.

V. DISCUSSION GENERALE

Le travail effectué au cours de ces trois années offre des réponses à des besoins fondamentaux dans le domaine des récifs artificiels et permet de proposer l'esquisse d'un cadre scientifique afin d'évaluer leurs caractéristiques intrinsèques (matériaux & structures).

Les résultats relatifs à la première partie de la thèse (Chap. 1 & 2) sur le suivi comparatif du biofouling (biofilm & macrofouling) se développant sur différents matériaux révèlent que l'identification simple de la structure des communautés n'est pas un indicateur suffisant pour évaluer la qualité d'un matériau. En effet, outre sa diversité et son abondance, il est important de déterminer si ce premier maillon du réseau trophique des récifs artificiels est sain et ne séquestre pas de contaminants liés au matériau utilisé pour leur construction. Nous avions émis l'hypothèse que la pollution serait susceptible de provenir du matériau lui-même, mais nos résultats suggèrent finalement qu'au cours de cette première année la stabilité physico-chimique des matériaux n'est pas altérée par la bio-érosion. Cependant, nous avons pu montrer que malgré sa stabilité, le béton qui est le matériau le plus utilisé de nos jours pour la conception de récifs artificiels – est susceptible de favoriser indirectement la séquestration des métaux lourds présents dans l'environnement. Les mécanismes fins induisant cette séquestration restent encore à élucider. Il est possible que la sécrétion d'exopolymères (EPS) par le biofilm – plus importante sur le béton que sur les autres matériaux étudiés – en soit le vecteur et que ces composés contaminent par la suite le macrofouling (Bhaskar & Bhosle 2006). La micro-complexité du matériau, étudié dans la deuxième partie du chapitre 3 (Chap. 3. Part. 2), nous donne peut-être quelques éléments d'explication. En effet, si l'on suit la logique de l'étude de Huang et al. (2018) sur l'analyse de la microtopographie (de 100 à 200µm) selon un gradient d'impression de vagues angulaires (0°, 20°, 30°, 45°, 60°), les biofilms se développant sur des surfaces aux angles droits détiennent une matrice d'EPS plus épaisse et plus robuste face aux perturbations d'un flux laminaire que ceux se développant sur des surfaces lisses ou sur des surfaces dont les angles sont plus aigus ou plus obtus. A première vue, l'aspect lisse de la roche, très acéré de la dolomite, et les microcavités plus larges que présente le béton pourraient confirmer ces précédents résultats. La vérification de cette hypothèse nécessiterait de s'affranchir de la nature chimique bien différente de ces trois matériaux. A ce titre, il est probable que le pH des matériaux joue un rôle dans ces différences. Le béton a un pH très basique (11-13 pH) tandis que le matériau à base de sable de dolomite a un pH proche de celui de la mer (8.2 pH, selon les concepteurs des récifs) ; la roche calcaire composée principalement

de carbonate de calcium devrait avoir un pH basique (autour de 9.9 pH). Dans une étude sur l'influence du pH sur les sécrétions du biofilm, il a été démontré qu'un pH bas favorise une structuration des EPS plus dense et homogène qu'un pH neutre. Par ailleurs, la séquestration des métaux lourds par les EPS s'avère plus importante à pH basique qu'à pH acide (Comte et al. 2008). L'effet combiné d'une topographie favorable à la sécrétion d'EPS et d'un pH favorisant la séquestration des métaux lourds pourrait expliquer ces résultats sur le béton. De plus amples investigations sur ces différents paramètres sont nécessaires pour vérifier cette hypothèse.

Malgré ces questions en suspens, le suivi du biofilm a permis de déceler une probable pollution sur le long terme dans le macrofouling. Il s'agit donc d'un bon indicateur pour valider la qualité d'un matériau utilisé pour un récif artificiel, peu coûteux et facile à mettre en place. Un suivi du biofilm sur 3 semaines (correspondant à la maturité du biofilm dans nos deux études Chap. 1 & 2), et une analyse de son contenu en métaux lourds –complétée par la détection d'autres composés, tels que les polluants organiques persistants (POP) comprenant en particulier les dioxines, les polychlorobiphényles (PCB), les hydrocarbures aromatiques polycycliques (HAP) et les pesticides – permettrait d'identifier rapidement si le matériau utilisé est susceptible de favoriser ou non la séquestration des diverses pollutions anthropiques du milieu marin. Sachant que ces résultats peuvent être fluctuants en fonction du site d'exposition, il serait intéressant de répliquer l'expérience dans différents sites présentant un gradient de pollution afin de voir si la séquestration dans le biofilm dépasse les normes environnementales. Si l'étude n'a pas pu mettre en évidence des différences structurelles au sein des communautés de biofouling entre les matériaux, il est possible que la séquestration des polluants, plus importante au sein des communautés se développant sur béton, ait avec le temps un impact sur leur évolution ainsi que sur l'ensemble du réseau trophique des récifs artificiels par des phénomènes de bioaccumulation. La vérification de cette hypothèse pourrait s'effectuer en suivant des espèces cibles du macrofouling correspondant au régime alimentaire de certaines espèces mobiles inféodées aux récifs artificiels telles que des blennies, des serrans ou encore des sparidés.

La variété des méthodes expérimentales et des terminologies utilisées pour l'étude de la structure de l'habitat révèle l'aspect très complexe de son analyse (McCoy & Bell 1991). En se focalisant sur trois dimensions (complexité, hétérogénéité, échelle) comme le suggèrent Bell

& McCoy, il semble plus facile d'aborder son étude. Nous avons ainsi pu mettre au point la première méthode standardisée pour évaluer la structure des récifs (Chap. 3). Une étude *in situ* sur le suivi de différents récifs artificiels et/ou la collection de données de recensement sur les communautés mobiles permettrait de vérifier la validité de cette méthode pour évaluer l'efficacité de la colonisation des récifs artificiels selon leur macrostructure. Cette méthode nécessite cependant encore des vérifications terrain. L'immersion en 2017, dans la réserve du Larvotto (Monaco), des nouveaux récifs artificiels conçus par impression 3D, ne permet pas d'avoir suffisamment de recul sur les suivis mis en place pour déterminer un lien entre leurs structures et les espèces recrutées sur ces nouveaux habitats. Au terme des 4 premières années de suivi de ces récifs, ces données ainsi que le regroupement de données de recensement sur d'autres récifs artificiels, permettraient de définir un cadre scientifique pour lier les différents paramètres de complexité proposés à des mesures de gestion des ressources marines inféodées aux récifs artificiels. Outre les améliorations à apporter à la méthode qui ont déjà été discutées dans le chapitre 3, il serait intéressant d'ajouter une évaluation de leur connectivité qui influence la dynamique de recrutement des communautés (Koeck et al. 2011, De Bie et al. 2012). A l'échelle globale du champ de récifs, le programme des récifs du Prado avait positionné des modules intermédiaires pour assurer des corridors entre les villages ainsi qu'avec les habitats naturels (roche et posidonie) (Charbonnel et al. 2011). Dans la partie 1 du chapitre 3, le paramètre "V" correspondant au volume occupé sur la totalité du champ d'occupation peut être un moyen d'évaluer cette connectivité. Plus le ratio est faible, plus la distance entre les éléments est faible, impliquant potentiellement une plus forte connectivité structurelle sur l'ensemble du site. Par ailleurs, les premiers essais à l'échelle du matériau sur les communautés de biofilm ont donné quelques résultats encourageants. Nous avons pu observer que différentes variables de complexité ont des relations positives avec l'abondance du biofilm, son activité photosynthétique ou encore des mécanismes de photo-adaptation. Il serait intéressant de poursuivre des tests similaires sur un matériau de même nature en faisant varier les différents paramètres étudiés à différentes échelles afin d'analyser plus finement les réponses du biofilm à ces variations et à ces niveaux d'échelles qui semblent déterminants pour étudier ce type de relations.

Outre ces considérations appliquées au domaine des récifs artificiels, ces résultats nous ont permis de suivre l'évolution temporelle des communautés de biofouling sur une période

d'un an. Afin de discuter plus amplement de la stabilité des communautés du macrofouling, un suivi sur plusieurs années aurait été souhaitable. Néanmoins, nous avons pu étudier les premières étapes de colonisation d'un habitat, ce que seule l'immersion de nouvelles structures telles que les récifs artificiels peut permettre. Alors que les populations de poissons semblent se stabiliser rapidement (2-3 mois), il est difficile d'observer une stabilité des assemblages de macrofouling après deux ans d'immersion. Ceci serait lié à des perturbations physiques fréquentes auxquelles les assemblages de macrofouling seraient plus sensibles (Cummings 1994). En effet, un certain équilibre au sein des communautés serait atteint au bout de 4 ans (Ardizzone et al. 2000, Falace & Bressan 2000). Il semble malgré tout difficile de prédire précisément les mécanismes qui définissent l'établissement des communautés. Nous avons pu observer des successions d'assemblages avec le biofilm comme premier maillon, suivi par des communautés algales monospécifiques, et enfin des communautés plus diverses composées de brouteurs, filtreurs et suspensivores. Ce schéma suit la « *fouling sequence* » expliquée par (Wahl 1989) et est conforme aux successions écologiques relatives à la théorie du climax (Clements 1936). Cependant, la dynamique temporelle des différentes étapes de succession concernant le macrofouling semble très variable selon les sites d'immersion (Chap. 2). Il est donc très probable que la diversité des communautés soit avant tout déterminée par les conditions environnementales locales qui influent majoritairement sur le recrutement des larves et des spores (Svane & Petersen 2001). Les diverses étapes de succession des communautés seront fonction des perturbations physiques du milieu, des événements aléatoires météorologiques voire anthropiques, ou encore des interactions liées à la compétition interspécifique (Cummings 1994, Svane & Petersen 2001). L'ensemble de ces perturbations imprévisibles nous éloigne de l'établissement d'une communauté selon le schéma d'une succession atteignant un climax, et nous rapproche d'une théorie plus moderne prenant en compte la dynamique de ces événements stochastiques (Meiners et al. 2015). Si l'on se focalise sur la dynamique des communautés de biofilm, on observe un schéma similaire quels que soient les sites et les matériaux utilisés. Cela implique que malgré l'aspect stochastique de l'implantation des microorganismes révélé par notre étude, certains cycles sont conservés dans l'évolution d'un biofilm (i.e. adhésion, production d'EPS, ...). Par ailleurs, il est possible que la temporalité sur laquelle nous nous sommes focalisés soit trop longue pour observer des préférences de matériau. En effet, ces interactions se jouent au cours des premières heures d'immersion de la structure pour les microorganismes du biofilm (Wahl 1989,

Callow & Callow 2006, Salta et al. 2013). Après une semaine, il est possible que la colonisation des espèces pionnières ait déjà modifié largement les propriétés de surface des matériaux et que les seules différences observables soient liées à l'adaptation des communautés par la mise en place de leur matrice extracellulaire (Wahl et al. 2012, Dang & Lovell 2016). Cependant, une identification plus précise des diatomées, par microscopie ou par métagénomique, aurait pu révéler des différences au sein des communautés du biofilm. En effet, les diatomées représentent près de 80% de la biomasse des biofilms marins photosynthétiques et sont responsables de la majorité des sécrétions d'EPS (Salta et al. 2013). Des différences au sein de leur structure auraient pu expliquer cette dynamique temporelle et ces différences entre les sites et les matériaux.

L'ensemble de ces résultats suggère que l'angle de vue et les méthodes que nous adoptons pour observer ces communautés détermine largement les conclusions que nous pouvons émettre sur les différences potentielles en fonction de certaines conditions. L'échelle temporelle et spatiale choisie ne correspond pas toujours idéalement à celle que nous devrions adopter pour identifier les mécanismes fins qui impliquent le recrutement des espèces puis leur établissement dans le temps (Chap 3. Part. 2). Les relations changeantes observées entre les échelles ouvrent une question fondamentale sur la façon dont nous étudions le lien entre les organismes et leur paysage. L'importance de l'échelle pour déterminer ces relations a déjà été soulignée par McCoy & Bell (1991). Tokeshi & Arakaki (2012) ont également souligné que l'échelle géographique implique des relations différentes selon que notre question se focalise sur l'échelle globale, régionale, locale ou sur celle des micro-habitats. *In fine*, il semble primordial de définir l'échelle en fonction du niveau d'organisation correspondant à la taille de l'organisme étudié (Farjalla et al. 2012), Chap. 3 Part. 2). Cependant l'étude de la structure de l'habitat selon les échelles ne nous permet pas d'identifier si les relations observées à une échelle peuvent avoir un impact sur les échelles supérieures. Y a-t-il une continuité ou une rupture dans les relations ? Y a-t-il des émergences de mécanismes nouveaux en fonction du niveau d'organisation ? Ou bien comme le présente Kupiec (1983) dans ses travaux sur l'application de la théorie de l'évolution à l'échelle cellulaire, le vivant "bricole- t-il" toujours afin d'améliorer sa *fitness* en fonction des lois physiques dont l'influence peut changer selon l'échelle ? Il est bien connu que des espèces dites ingénieurs comme les castors, les fourmis, ou encore les termites modifient considérablement leur environnement à leur profit,

impliquant des conséquences sur les écosystèmes et les organismes qu'ils côtoient (Jones et al. 1994). Par ailleurs, nous connaissons bien les effets *top down* des prédateurs et *bottom up* des producteurs primaires qui régulent les populations des niveaux trophiques intermédiaires. A ces égards, le biofilm peut être considéré comme une communauté ingénieure qui construit son écosystème grâce à ses sécrétions extracellulaires et qui par ce biais influence le recrutement des larves et des spores des espèces de macrofouling (Flemming & Wingender 2010). Il est également le producteur primaire des communautés benthiques offrant une source d'éléments nutritifs aux communautés de macrophytes et aux micro-brouteurs. Il influe ainsi sur tout l'écosystème benthique et son réseau trophique. Au regard de ces mécanismes observés au niveau du biofilm et des échelles supérieures ainsi que des autres exemples cités, il est donc justifié de se demander si ces relations inter-échelles sont susceptibles d'être récurrentes dans les écosystèmes.

Conclusion

Les caractéristiques extrinsèques des récifs artificiels (RA), liées au site d'immersion, constituent le facteur de réussite le plus déterminant car elles conditionnent la diversité des espèces et les conditions environnementales. Mais les caractéristiques intrinsèques des RA jouent également un rôle important.

L'étude des matériaux, à travers le suivi du biofouling et plus particulièrement du biofilm, permet de tester rapidement la qualité d'un matériau et son influence sur les communautés. Les résultats révélés sur le béton nous conduisent à nous interroger sur l'impact écologique de toutes les structures artificielles immergées le long des côtes. Il est fort probable que dans des environnements particulièrement pollués, le béton favorise une bioaccumulation de métaux lourds ou d'autres polluants. Si, comme nous le supposons, la séquestration est favorisée par le pH du matériau, il est envisageable de produire des matériaux en béton ayant un pH plus proche de l'environnement marin.

L'étude de la structure des RA par le biais de la méthode mise en place permettrait de construire des RA de façon plus rigoureuse, si tant est qu'il soit possible de relier ces paramètres structuraux au recrutement de certaines espèces. Malgré tout, la mise au point de cette méthode d'évaluation semble efficace pour proposer une classification intéressante des différents modules existants. Elle permet en effet de distinguer les structures selon leurs objectifs d'immersion. Pour la première fois, il est possible d'utiliser une méthode standardisée qui permettra d'évaluer *in situ* l'influence des paramètres structuraux des RA sur le recrutement, l'abondance, la distribution et/ou la diversité.

Enfin, les récifs immergés dans la réserve du Larvotto (Monaco), représentent l'une des structures les plus complexes et le matériau à base de sable de dolomite utilisé pour les concevoir ne favorise pas la séquestration de polluants au sein du biofouling et semble accueillir des communautés tout aussi diverses que les autres matériaux. Cette évaluation positive de ces caractéristiques intrinsèques laisse envisager un avenir prometteur pour ce type de structure afin de concevoir des RA répondant aux directives actuelles de l'UNEP.

Pour compléter les travaux initiés au cours de cette thèse et donner des réponses aux questions encore en suspens, nous pouvons envisager différentes perspectives :

(i) Un suivi comparatif de différents types de béton (en faisant varier leur pH et leur microtopographie), des sécrétions du biofilm et de divers polluants séquestrés par le biofilm, permettrait d'isoler les paramètres les plus influents sur les sécrétions d'EPS et la séquestration de polluants.

(ii) Une étude comparative des communautés épibenthiques et mobiles de différents designs de récifs RA permettrait de déterminer l'influence de la structure des RA sur les communautés à l'aide de la méthode d'évaluation de la structure des RA.

(iii) Sur la base de la structure des habitats naturels qui peuvent être reproduits par photogrammétrie, des mesures de restauration et /ou compensation pourraient voir le jour. L'utilisation de la méthode d'évaluation de la structure sur ces habitats naturels, permettrait d'imiter leur complexité et leur hétérogénéité et de produire des récifs biomimétiques.

(iv) L'impact des RA sur les milieux naturels qu'ils recouvrent est très peu étudié. L'étude de la sédimentation, de la production de matière organique et de l'activité de la méiofaune à leurs abords permettrait de disposer de nouveaux éléments relatifs à l'influence des RA.

Les résultats de ces différentes recherches permettraient d'améliorer les directives de UNEP sur les RA afin de proposer des moyens de choisir le matériau, la structure et d'émettre des limitations d'immersion en fonction de leur impact sur le milieu naturel. Un récif artificiel constitue un outil d'ingénierie écologique intéressant à condition qu'il respecte l'environnement.

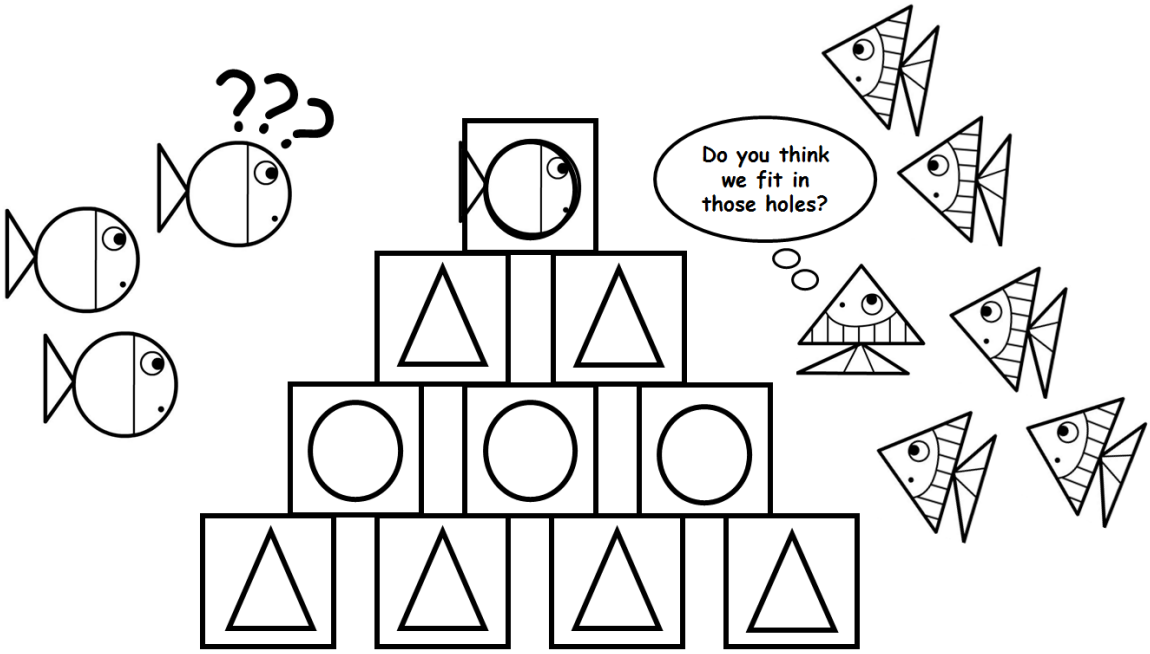

© Elisabeth Riera

RÉFÉRENCES

Abed RMM, Al Fahdi D, Muthukrishnan T (2019) Short-term succession of marine microbial fouling communities and the identification of primary and secondary colonizers. Biofouling 0:1–15.

Achternbosch M, Bräutigam K (2003) Heavy Metals in Cement and Concrete Resulting from the Co-incineration of Wastes in Cement Kilns with Regard to the Legitimacy of Waste Utilisation.

Aguilera MA, Broitman BR, Thiel M (2014) Spatial variability in community composition on a granite breakwater versus natural rocky shores: Lack of microhabitats suppresses intertidal biodiversity. Mar Pollut Bull 87:257–268.

Anderson MJ (2001) A new method for non-parametric multivariate analysis of variance. Austral Ecol 26:32–46.

Antsulevich AE (1994) Artificial reefs project for improvement of water quality and environmental enhancement of Neva Bay (St. Petersburg County region). Bull Mar Sci 55:1189–1192.

Ardizzone G, Somaschini A, Belluscio A (2000) Prediction of Benthic and Fish Colonization on the Fregene and other Mediterranean Artificial Reefs. In: *Artificial Reefs in European Seas*, 2000th ed. Jensen, Al. E (eds) Kluwer Academic Publishers, p 113–128

Bao W-Y, Satuito CG, Yang J-L, Kitamura H (2007) Larval settlement and metamorphosis of the mussel Mytilus galloprovincialis in response to biofilms. Mar Biol 150:565–574.

Barnabe G, Charbonnel E, Marinaro J-Y, Ody D, Francour P (2000) Artificial Reefs in France: Analysis, Assessments and Prospects. In: *Artificial Reefs in European Seas*. p 167–184

Barnabé G, Charbonnel E, Ody D, Francour P (2000) Artificial reef in France : analysis , assessments and prospects. In: *Artificial Reefs in European Seas*, Springer S. Jeansen AC, Collins KJ, Lockwood APM (eds) p 167–184

Battin TJ, Sloan WT, Kjelleberg S, Daims H, Head IM, Curtis TP, Eberl L (2007) Microbial landscapes: New paths to biofilm research. Nat Rev Microbiol 5:76–81.

Beck MW (1998) Comparison of the measurement and effects of habitat structure on gastropods in rocky intertidal and mangrove habitats. Mar Ecol Prog Ser 169:165–178.

Beck MW (2000) Separating the elements of habitat structure: independent effects of habitat complexity and structural components on rocky intertidal gastropods. J Exp Mar Bio Ecol 249:29–49.

BETOCIB (2000) Constituants : Ciment Blanc. In: *Les Bétons à base de Ciment Blanc. Prescriptions Techniques*. p 10–23

Bhaskar P V., Bhosle NB (2006) Bacterial extracellular polymeric substance (EPS): A carrier of heavy metals in the marine food-chain. Environ Int 32:191–198.

Bhosle NB, Garg A, Fernandes L, Citon P (2005) Dynamics of amino acids in the conditioning film developed on glass panels immersed in the surface seawaters of Dona Paula Bay. Biofouling 21:99–107.

Bhosle NB, Wagh AB (1997) Amino acids in biofilm material on aluminium panels immersed in marine waters. Biofouling 11:37–41.

De Bie T, De Meester L, Brendonck L, Martens K, Goddeeris B, Ercken D, Hampel H, Denys L, Vanhecke L, Van der Gucht K, Van Wichelen J, Vyverman W, Declerck SAJ (2012) Body size and dispersal mode as key traits determining metacommunity structure of aquatic organisms. Ecol Lett 15:740–747.

Bixler GD, Bhushan B (2012) Biofouling: lessons from nature. Philos Trans R Soc A 370:2381–2417.

Blouet S, Chéré É, Grandrive RD de la, Foulquié M, Scourzic T, Dalias N, Lenfant P, Jarraya M, Trougan M, Cucurrullo

P (2011) Suivi scientifique des récifs artificiels au large de la commune d'Agde.

Bodilis P, Dombrowski E, Grillon P, Moulin A, Francour P (2008) Suivi des peuplements ichtyologiques des récifs artificiels des zones marimes protégées des Alpes-Maritimes.

Bodilis P, Seytre C, Charbonnel E, Patrice F (2011) Monitoring of the artificial reef fish assemblages of golfe juan marine protected area (France, North-Western Mediterranean). Brazilian J Oceanogr 59:167–176.

Bohnsack JA (1989) Are high densities of fishes at artificial reefs the results of habitat limitation or behavioural preference? Bull Mar Sci 44:631–645.

Bohnsack JA (1991) Habitat structure and the design of artificial reefs. In: *Habitat Structure*. p 412–426

Bohnsack JA, Sutherland DL (1985) Artificial reef research: a review with recommendations for the future prorities. Bull Mar Sci 37:11–39.

Bombace G (1989) Artificial reefs in the Mediterranean Sea. Bull Mar Sci 44:1023–1032.

Brian-Jaisson F, Ortalo-Magné A, Guentas-Dombrowsky L, Armougom F, Blache Y, Molmeret M (2014) Identification of Bacterial Strains Isolated from the Mediterranean Sea Exhibiting Different Abilities of Biofilm Formation. Microb Ecol 68:94–110.

Briand J-F, Djeridi I, Jamet D, Coupé S, Bressy C, Molmeret M, Le Berre B, Rimet F, Bouchez A, Blache Y (2012) Pioneer marine biofilms on artificial surfaces including antifouling coatings immersed in two contrasting French Mediterranean coast sites antifouling coatings immersed in two contrasting. Biofouling 28:453–463.

Briand JF, Barani A, Garnier C, Réhel K, Urvois F, LePoupon C, Bouchez A, Debroas D, Bressy C (2017) Spatio-Temporal Variations of Marine Biofilm Communities Colonizing Artificial Substrata Including Antifouling Coatings in Contrasted French Coastal Environments. Microb Ecol 74:585–598.

Brochier-Armanet C, Gribaldo S, Forterre P (2012) Spotlight on the Thaumarchaeota. ISME J 6:227–230.

Brotas V, Plante-Cuny MR (2003) The use of HPLC pigment analysis to study microphytobenthos communities. Acta Oecologica 24:109–115.

De Brouwer C, Wolfstein K, Stal J (2002) Physical characterization and diel dynamics of different fractions of extracellular polysaccharides in an axenic culture of a benthic diatom. Eur J Phycol 37:37–44.

Brown CJ (2005) Epifaunal colonization of the Loch Linnhe Artificial Reef : Influence of substratum on epifaunal assemblage structure . Biofouling 21:73–85.

Brown MR (1991) The amino-acid and sugar composition of 16 species of microalgae used in mariculture. J Exp Mar Bio Ecol 145:79–99.

Bruckner CG, Bahulikar R, Rahalkar M, Schink B, Kroth PG (2008) Bacteria associated with benthic diatoms from Lake Constance: Phylogeny and influences on diatom growth and secretion of extracellular polymeric substances. Appl Environ Microbiol 74:7740–7749.

Bryan PJ, Qian PY (1998) Induction of larval attachment and metamorphosis in the abalone Haliotis diversicolor (Reeve). J Exp Mar Bio Ecol 223:39–51.

Bryson M, Ferrari R, Figueira W, Pizarro O, Madin J, Williams S, Byrne M (2017) Characterization of measurement errors using structure-from-motion and photogrammetry to measure marine habitat structural complexity. Ecol Evol 7:5669–5681.

Burt J, Bartholomew A, Bauman A, Saif A, Sale PF (2009) Coral recruitment and early benthic community

development on several materials used in the construction of arti fi cial reefs and breakwaters. J Exp Mar Bio Ecol 373:72–78.

Caddy JF, Stamatopoulos C (1990) Mapping Growth and Mortality Rates of Organisms onto a Perforated Surface: The Relevance of 'Cover' to the Carrying Capacity of Natural and Artificial Habitats. Estuar Coast Shelf Sci 31:87–106.

Caliński T, Harabasz J (1974) A dendrite method for cluster analysis. Commun Stat 3:1–27.

Callow JA, Callow ME (2006) Biofilms. In: *Antifouling Compound. Marine Molecular Biotechnology, vol 42.*, 2006th ed. N. Fusetani ASC (ed) Springer-Verlag Berlin Heidelberg, Berlin, p 141–169

Callow ME, Callow JA (2002) Marine biofouling : a sticky problem. Biologist 49:1–5.

Camacho-Chab JC, Lango-Reynoso F, Castañeda-Chávez del Refugio M, Galaviz-Villa I, Hinojosa-Garro D, Otto Ortega-Morales B (2016) Implications of Extracellular Polymeric Substance Matrices of Microbial Habitats Associated with Coastal Aquaculture Systems. Water 8:1–21.

Carleton JH, Sammarco PW (1987) Effects of substratum irregularity on success of coral settlement: quantification by comparative geomorphological techniques. Bull Mar Sci 40:85–98.

Cartaxana P, Ruivo M, Hubas C, Davidson I, Serôdio J, Jesus B (2011) Physiological versus behavioral photoprotection in intertidal epipelic and epipsammic benthic diatom communities. J Exp Mar Bio Ecol 405:120–127.

de Carvalho CCCR (2018) Marine biofilms: A successful microbial strategy with economic implications. Front Mar Sci 5:1–11.

Cépralmar R-L-R (ed) (2015) Guide pratique d'aide à l'élaboration, l'exploitation et la gestion des récifs artificiels en Languedoc-Roussillon.

Cerca N, Pier GB, Vilanova M, Oliveira R, Azeredo J (2005) Quantitative analysis of adhesion and biofilm formation on hydrophilic and hydrophobic surfaces of clinical isolates of Staphylococcus epidermidis. Reasearch Microbiol 156:506–514.

Charbonnel E, Harmelin J-G, Carnus F, Direac'h L Le, Ruitton S, Lenfant P, Beurois J, 1*Parc (2011) Artificial Reefs in Marseille : From Complex Natural Habitats to Concepts of Efficient Artificial Reef Design. Brazilian J Oceanogr 59:177–178.

Charbonnel E, Ody D, Le Diréach L, Ruitton S (2001) Effet de la complexification de l'architecture des récifs artificiels du Parc national de Port-Cros (Méditerranée, France) sur les peuplements ichtyologiques. Sci Rep Port-Cros Natl Park Fr 18:163–217.

Charbonnel E, Serre C, Ruitton S, Harmelin J, Jensen A (2002) Effects of increased habitat complexity on fish assemblages associated with large artificial reef units (French Mediterranean coast). ICES J Mar Sci 59:208–213.

Chung HC, Lee OO, Huang Y, Mok SY, Kolter R (2010) Bacterial community succession and chemical profiles of subtidal biofilms in relation to larval settlement of the polychaete Hydroides elegans. ISME J 4:817–828.

Cignoni P, Callieri M, Corsini M, Dellepiane M, Ganovelli F, Ranzuglia G (2008) MeshLab : an Open-Source Mesh Processing Tool. Eurographics Ital Chapter Conf.

Clemens PV, Mark S, Markus R, Markus B (2018) The regional assessment report on Biodiversity and Ecosystem

Services for Europe and Central Asia. Mark Rounsevell, Markus Fischer, Amor Torre-Marin Rando AM (ed).

Clements FE (1936) Nature and Structure of the Climax. J Ecol 24:252.

Collins KJ, Jensen AC, Albert S (1995) A Review of Waste Tyre Utilisation in the Marine Environment. Chem Ecol 10:205–216.

Comte S, Guibaud G, Baudu M (2008) Biosorption properties of extracellular polymeric substances (EPS) towards Cd, Cu and Pb for different pH values. J Hazard Mater.

Cooksey KE, Wigglesworth-Cooksey B (1995) Adhesion of bacteria and diatoms to surfaces in the sea : a review. Aquat Microb Ecol 9:87–96.

Costerton JW, Lewandowski Z, Caldwell DE, Korber DR, Lappin-scott HM (1995) Microbial biofilms. Annu Rev Microbiol 49:711–745.

Costerton JW, Lewandowski Z, Debeer D, Caldwell D, Korber D, James G (1994) MINIREVIEW Biofilms, the Customized Microniche. J Bacteriol 176:2137–2142.

Cui Y, Yuan WW, Pei Z (2010) International Manufacturing Science and Engineering Conference. In: *Effects of Carrier Material and Design on Microalgae Attachment for Biofuel Manufacturing: A Literature Review*. American Society of mechanical engineers, Erie, Pennsylvania, USA, p 525–540

Cummings SL (1994) Colonization of a nearshore artificial reef at Boca Raton (Palm Beach County), Florida. Bull Mar Sci 55:1193–1215.

D'Souza F, Garg A, Bhosle NB (2005) Seasonal variation in the chemical composition and carbohydrate signature compounds of biofilm. Aquat Microb Ecol 41:199–207.

Dahms H, Dobretsov S, Qian P (2004) The effect of bacterial and diatom biofilms on the settlement of the bryozoan Bugula neritina. J Exp Mar Bio Ecol 313:191–209.

Dang H, Li T, Chen M, Huang G (2008) Cross-Ocean Distribution of Rhodobacterales Bacteria as Primary Surface Colonizers in Temperate Coastal Marine Waters. Appl Environ Microbiol 74:52–60.

Dang H, Lovell CR (2000) Bacterial Primary Colonization and Early Succession on Surfaces in Marine Waters as Determined by Amplified rRNA Gene Restriction Analysis and Sequence Analysis of 16S rRNA Genes. Appl Environ Microbiol 66:467–475.

Dang H, Lovell CR (2016) Microbial Surface Colonization and Biofilm Development in Marine Environments. Microbiol Mol Biol Rev 80:91–138.

Dang H, Lovell CR (2002) Numerical Dominance and Phylotype Diversity of Marine Rhodobacter Species during Early Colonization of Submerged Surfaces in Coastal Marine Waters as Determined by 16S Ribosomal DNA Sequence Analysis and Fluorescence In Situ Hybridization. Appl Environ Microbiol 68:496–504.

Das N, Vimala R, Karthika P (2008) Biosorption of heavy metals - An overview. Indian J Biotechnol 7:159–169.

Dash HR, Mangwani N, Chakraborty J, Kumari S, Das S (2013) Marine bacteria: Potential candidates for enhanced bioremediation. Appl Microbiol Biotechnol 97:561–571.

Decho AW, Gutierrez T (2017) Microbial Extracellular Polymeric Substances (EPSs) in Ocean Systems. Front Microbiol 8:1–28.

Dexter SC (1979) Influence of Substratum Critical Surface Tension on Bacterial Adhesion--in. J Colloid Interface Sci 70:346–354.

Dexter SC, Sullivan JD, Iii JW, Watson SW (1975) Influence of Substrate Wettability on the Attachment of Marine Bacteria to Various Surfaces. Appl Microbiol 30:298–308.

Dillon PS, Maki JS, Mitchell R (1989) Adhesion of Enteromorpha Swarmers to Microbial Films. Microb Ecol 47:39–47.

Dobretsov S, Abed RMM, Voolstra CR (2013) The effect of surface colour on the formation of marine micro- and macro-fouling communities. Biofouling 29:617–627.

Dobretsov S, Qian P (2006) Facilitation and inhibition of larval attachment of the bryozoan Bugula neritina in association with mono-species and-multi-species biofilms. J Exp Mar Bio Ecol 333:263–274.

Dogsa I, Kriechbaum M, Stopar D, Laggner P (2005) Structure of bacterial extracellular polymeric substances at different pH values as determined by SAXS. Biophys J 89:2711–2720.

Dray S, Dufour AB, Thioulouse J (2018) Analysis of Ecological Data: Exploratory and Euclidean Methods in Environmental Sciences. J Stat Sorftware:1–20.

Dubois M, Gilles K, Hamilton J, Rebers P, Smith F (1956) Colorimetric method for determination of sugars and related substances. Anal Chem 28:350–356.

Egeland ES, Eikrem W, Throndsen J, Wilhelm C, Zapataii M, Liaaen-jensent SZVE (1995) Carotenoids from Further Prasinophytes. Biochem Syst Ecol 23:747–755.

Eilers PHC, Peeters JCH (1988) A model for the relationship between light intensity and the rate of photosynthesis in phytoplankton. Ecol Modell 42:199–215.

Erioli Alessandro A; Z, Zomparelli Alessio A; E (2012) Emergent Reefs. Gener Des 1:329–337.

Fabi G, Spagnolo A, Bellan-santini D, Charbonnel E, Çiçek BA, García JJG, Jensen AC, Kallianiotis A, Santos MN dos (2011) Overview on artificial reefs in Europe. Brazilian J Oceanogr 59:155–166.

Faimali M, Garaventa F, Terlizzi A, Chiantore M, Cattaneo-vietti R (2004) The interplay of substrate nature and biofilm formation in regulating Balanus amphitrite Darwin , 1854 larval settlement. J Exp Mar Bio Ecol 306:37–50.

Falace A, Bressan G (2000) 'Periphyton' Colonization: Principles, Criteria and Study Methods. Artif Reefs Eur Seas 2:435–449.

Fang F, Lu WT, Shan Q, Cao JS (2014) Characteristics of extracellular polymeric substances of phototrophic biofilms at different aquatic habitats. Carbohydr Polym 106:1–6.

Farjalla VF, Srivastava DS, Marino NAC, Azevedo FD, Dib V, Lopes PM, Rosado AS, Bozelli RL, Esteves FA (2012) Ecological determinism increases with organism size. Ecology 93:1752–1759.

Finlay J a., Callow ME, Ista LK, Lopez GP, Callow JA (2002) The Influence of Surface Wettability on the Adhesion Strength of Settled Spores of the Green Alga Enteromorpha and the Diatom Amphora. Integr Comp Biol 42:1116–1122.

Flemming H, Wingender J (2010) The biofilm matrix. Nat Rev Microbiol 8:623–633.

Fletcher M, Pringle JH (1985) The Effect of Surface Free Energy and Medium Surface Tension on Bacterial Attachment to Solid Surfaces. J Colloid Interface Sci 104:5–14.

Fletcher RL, Callow ME (1992) The settlement , attachment and establishment of marine algal spores. Br Phycol J 27:303–329.

Fletchert M, Loeb GI (1979) Influence of Substratum Characteristics on the Attachment of a Marine Pseudomonad to Solid Surfaces. Appl Environ Microbiol 37:67–72.

Frau L, Marzeddu A, Dini E, Gracia V, Gironella X, Erioli A, Zomparelli A, Sánchez-Arcilla A (2016) Effects of Ultra-Porous 3D Printed Reefs on Wave Kinematics. J Coast Res 75:851–855.

Friedlander AM, Parrish JD (1998) Habitat characteristics affecting fish assemblages on a Hawaiian coral reef. J Exp Mar Bio Ecol 224:1–30.

Friedman A, Pizarro O, Williams SB, Johnson-Roberson M (2012) Multi-Scale Measures of Rugosity, Slope and Aspect from Benthic Stereo Image Reconstructions. PLoS One 7.

Frølund B, Palmgren R, Keiding K, Nielsen PH (1996) Extraction of extracellular polymers from activated sludge using a cation exchange resin. Water Res 30:1749–1758.

Frontier S (1987) Applications of fractal theory to ecology. Dev Numer Ecol G14:335–378.

Frost N. J., Burrows M.T., Johnson M.P., Hanley M.E., Hawkins S.J., Frost NJ, Burrows MT, Johnson MP, Hanley ME, Hawkins SJ (2005) Measuring surface complexity in ecological studies. Limnol Oceanogr Methods 3:203–210.

Gadd GM, Griffiths AJ (1977) Microorganisms and heavy metal toxicity. Microb Ecol 4:303–317.

García-Charton JA, Pérez-Ruzafa Á, Sánchez-Jerez P, Bayle-Sempere JT, Reñones O, Moreno D (2004) Multi-scale spatial heterogeneity, habitat structure, and the effect of marine reserves on Western Mediterranean rocky reef fish assemblages. Mar Biol 144:161–182.

Giulia ADA, Stefano G (1991) Guida alle conchiglie mediterranee, 1991st ed. Fabbri, Milano.

Gratwicke B, Speight MR (2005) The relationship between fish species richness, abundance and habitat complexity in a range of shallow tropical marine habitats. J Fish Biol 66:650–667.

Grohmann CH, Smith MJ, Riccomini C (2009) Surface Roughness of Topography : A Multi-Scale Analysis of Landform Elements in Midland Valley, Scotland. Proc Geomorphometry 2009:140–148.

Hackradt CW, Félix-Hackradt FC, Garcia-Charton JA (2011) Influence of habitat structure on fish assemblage of an artificial reef in southern Brazil. Mar Environ Res 72:235–247.

Hall-stoodley L, Costerton JW, Stoodley P (2004) Bacterial Biofilms: From the Natural Environment to Infectious Diseases. Nat Rev Microbiol 2:95–108.

Halley JM, Hartley S, Kallimanis AS, Kunin WE, Lennon JJ, Sgardelis SP (2004) Uses and abuses of fractal methodology in ecology. Ecol Lett 7:254–271.

Hamer JP (2002) The development and settlement of certain marine tubeworm (serpulidae and spirorbidae) larvae in response to biofilms

Hecky RE, Mopper K, Kilham P, Degens ET (1973) The Amino Acid and Sugar Composition of Diatom Cell-Walls. Mar Biol 19:323–331.

Hoaglang KD, Rosowski JR, Gretz MR, Poemer SC (1993) Diatom Extracellular Polymeric Substances: Function, Fine structure, Chemistry, and Physiology. J Phycol 29:537–566.

Hobson RD (1972) Surface Roughness in Topography: A Quantitative Approach. In: *Spatial Analysis in Geomorphology*, R.J., Ed. Methuen & Co (ed) Chorley, London, p 221–245

Holmström C, Kjelleberg S (1994) The effect of external biological factors on settlement of marine invertebrate

and new antifouling technology. Biofouling 8:147–160.

Huang S, Hadfield MG (2003) Composition and density of bacterial biofilms determine larval settlement of the polychaete Hydroides elegans. Mar Ecol Prog Ser 260:161–172.

Huang Y, Zheng Y, Li J, Liao Q, Fu Q, Xia A, Fu J, Sun Y (2018) Enhancing microalgae biofilm formation and growth by fabricating microgrooves onto the substrate surface. Bioresour Technol 261.

Huggett MJ, Nedved BT, Hadfield MG (2009) Effects of initial surface wettability on biofilm formation and subsequent settlement of Hydroides elegans. Biofouling 25:387–399.

Hunt AP, Parry JD (1998) The effect of substrattum roughness and river flow rate on the developpement of a freshwater biofilm community. Biofouling 12:287–303.

Hunter WR, Sayer MDJ (2009) The comparative effects of habitat complexity on faunal assemblages of northern temperate artificial and natural reefs. ICES J Mar Sci 66:641–698.

Husson F, Josse J, Le S, Mazet J (2016) Package 'FactoMineR'.

Iluz D, Dubinsky Z (2013) Quantum Yields in Aquatic Photosynthesis. Intech:135–158.

Ito S, Kitamura H (1997) Induction of larval metamorphosis in the sea cucumber Stichopus japonicus by periphitic diatoms. Hydrobiologia 358:281–284.

Jachlewski Is, Jachlewski WD, Linne U, Bräsen C, Wingender J, Siebers B (2015) Isolation of extracellular polymeric substances from biofilms of the thermoacidophilic archaeon Sulfolobus acidocaldarius. Front Bioeng Biotechnol 3:1–11.

Javaherdashti R, Nikraz H, Borowitzka M, Moheimani N, Olivia M (2009) On the impact of algae on accelerating the biodeterioration/biocorrosion of reinforced concrete: A mechanistic review. Eur J Sci Res 36:394–406.

Jeansen AC, Collins KJ, Lockwood APM (2000) Artificial Reefs in European Seas. Jeansen AC, Collins KJ, Lockwood APM (eds) Springer Science & Business Media Dordrech.

Jeffrey SW, Wright SW, Zapata M (2011) Microalgal classes and their signature pigments. In: *PHYTOPLANKTON PIGMENTS. Characterization, Chemotaxonomy and Applications in Oceanography*. Roy S, Llewellyn CA, Egeland ES, Johnsen G (eds) Cambridge University Press, p 3–77

Jenness JS (2004) Calculating landscape surface area from digital elevation models. Wildl Soc Bull 32:829–839.

Jensen A, Collins K, Lockwood P (2000) Introduction and Background to artificial Reefs in European Seas. In: *Artificial Reefs in European Seas*, 2000th ed. Al. ACJ et (ed) Kluwer Academic Publishers, p ix–xi

Johnson M. P., Frost N. J., Mosley M. W. J., Roberts M. F., Hawkins S. J. (2003) The area-independent effects of habitat complexity on biodiversity vary between regions. Ecol Lett:126–132.

Jones PR, Cottrell MT, Kirchman DL, Dexter SC (2007) Bacterial Community Structure of Biofilms on Artificial Surfaces in an Estuary. Microb Ecol 53:153–162.

Koeck B, Pastor J, Larenie L, Astruch P, Saragoni G, Jarraya M, Lenfant P (2011) Evaluation of Artificial Reefs Impact on Artisanal Fisheries: Necessity of Complementary Approaches. Glob Chang Mankind-Marine Environ Interact 59:105–113.

Kostylev VE, Erlandsson J, Mak YM, Williams GA (2005) The relative importance of habitat complexity and surface area in assessing biodiversity: Fractal application on rocky shores. Ecol Complex 2:272–286.

Kovalenko KE, Thomaz SM, Warfe DM (2012) Habitat complexity: approaches and future directions. Hydrobiologia

685:1–17.

Kratochvil D, Volesky B (1998) Advances in the biosorption of heavy metals. Trends Biotechnol 16:291–300.

Kupiec J-J (1983) A probabilist theory for cell differentiation, embryonic mortality and DNA C- value paradox. Speculations Sci Technol 6:471–478.

Lakshmi K, Muthukumar T, Doble M, Vedaprakash L, Dineshram R (2012) Influence of surface characteristics on biofouling formed on polymers exposed to coastal sea waters of India. Colloids Surfaces B Biointerfaces 91:205–211.

Lam C, Harder T, Qian P (2003) Induction of larval settlement in the polychaete Hydroides elegans by surface-associated settlement cues of marine benthic diatoms. Mar Ecol Prog Ser 263:83–92.

Lan CH, Lan KT, Hsui CY (2008) Application of fractals: create an artificial habitat with several small (SS) strategy in marine environment. Ecol Eng 32:44–51.

Leguay S, Lavoie I, LEvy JL, Fortin Cl (2016) Using biofilm for monitoring metal contamination in lotic ecosystemes: the protective effects of hardness an pH on metal bioaccumulation. Environ Toxicol Chem 35:1489–1501.

Liu L, Du R, Zhang X, Dong S, Sun S (2017) Succession and seasonal variation in epilithic biofilms on artificial reefs in culture waters of the sea cucumber Apostichopus japonicus. J Oceanol Limnol 35:132–152.

Lizarraga-Partida ML (1974) Organic pollution in Ensenada Bay, Mexico. Mar Pollut Bull.

Loke LHL, Jachowski NR, Bouma TJ, Ladle RJ, Todd PA (2014) Complexity for Artificial Substrates (CASU): Software for Creating and Visualising Habitat Complexity. PLoS One 9:1–6.

Loke LHL, Ladle RJ, Bouma TJ, Todd PA (2015) Creating complex habitats for restoration and reconciliation. Ecol Eng 77:307–313.

Loke LHL, Todd PA (2016) Structural Complexity and component type increase intertidal biodiversity independently of area. Ecology 97:383–393.

Luckhurst E, Luckhurst K (1978) Analysis of the Influence of Substrate Variables on Coral Reef Fish Communities. Mar Biol 49:317–323.

MacArthur RH, MacArthur JW (1961) On Bird Species Diversity. Ecology 42:594–598.

MacArthur RH, MacArthur JW, Preer J (1962) On Bird Species Diversity II. Prediction of Bird Census from Habitat Measurements. Am Soc Nat XCVI:167–174.

Mace G, Masundire H, Baillie J, Ricketts T, Brooks T, Hoffmann M, Stuart S, Balmford A, Purvis A, Reyers B, Wang J, Revenga C, Kennedy E, Naeem S, Alkemade R, Allnutt T, Bakarr M, Bond W, Chanson J, Cox N, Fonseca G, Hilton-Taylor C, Loucks C, Rodrigues A, Sechrest W, Stattersfield A, Rensburg BJ van, Whiteman C (2005) Biodiversity.

Mark DM, Aronson PB (1984) Scale-Dependent Fractal Dimensions of Topographic Surfaces : An Empirical Investigation , with Applications in Geomorphology and Computer Mapping. Math Geol 16:671–683.

Matias MG, Underwood AJ, Hochuli DF, Coleman RA (2010) Independent effects of patch size and structural complexity on diversity of benthic macroinvertebrates. Ecology 91:1908–1915.

McCoy ED, Bell SS (1991) Habitat structure : The evolution and diversification of a complex topic. In: *Habitat Structure*.

McCoy ED, Bell SS, Terborgh J, Petren K (1991) Habitat structure, 1991st ed. Bell SS, McCoy ED, Mushinsky HR

(eds) Springer Science & Business Media Dordrech, Suffolk.

Meiners SJ, Cadotte MW, Fridley JD, Pickett STA, Walker LR (2015) Is successional research nearing its climax? New approaches for understanding dynamic communities. Funct Ecol 29:154–164.

De Mendiburu F (2016) Package 'agricolae'''.

Miller MW (2002) Using ecological processes to advance artificial reef goals. ICES J Mar Sci 59:27–31.

Mohammed JS (2016) Applications of 3D printing technologies in oceanography. Methods Oceanogr 17:97–117.

Muhamed AP, Saly NT (2011) Bioaccumulation of Trace Metals in Biofilms Formed on Aluminium and Steel in Aquatic Environment. Fish Technol 48:25–32.

Murtagh F, Legendre P (2014) Ward's Hierarchical Agglomerative Clustering Method: Which Algorithms Implement Ward's Criterion? J Classif 31:274–295.

Musard O, Le Dû-Blayo L, Francour P, Beurier JP, Feunteun E, Talassinos L (2014) Underwater seascapes: From geographical to ecological perspectives. Musard O, Le Dû-Blayo L, Francour P, Beurier J-P, Feunteun E, Talassinos L (eds).

Muthukrishnan T, Abed RMM, Dobretsov S, Kidd B, Finnie AA (2014) Long-term microfouling on commercial biocidal fouling control coatings. Biofouling 30:1155–1164.

Myan FWY, Walker J, Paramor O (2013) The interaction of marine fouling organisms with topography of varied scale and geometry: A review. Biointerphases 8:1–13.

Myklestad S, Holm-Hansen O, Varum KM, Volcani BE (1989) Rate of release of extracellular amino acids and carbohydrates from the marine diatom Chaetoceros affinis. J Plankton Res 11:763–773.

Ochoa-Herrera V, León G, Banihani Q, Field JA, Sierra-Alvarez R (2011) Toxicity of copper(II) ions to microorganisms in biological wastewater treatment systems. Sci Total Environ 412–413:380–385.

Oksanen AJ, Blanchet FG, Friendly M, Kindt R, Legendre P, Mcglinn D, Minchin PR, Hara RBO, Simpson GL, Solymos P, Stevens MHH, Szoecs E (2017) Package 'vegan'.

Ortega-Morales BO, Chan-Bacab MJ, De la Rosa-García S del C, Camacho-Chab JC (2010) Valuable processes and products from marine intertidal microbial communities. Curr Opin Biotechnol 21:346–352.

Ozkan A, Berberoglu H (2013) Biointerfaces Cell to substratum and cell to cell interactions of microalgae. Colloids Surfaces B Biointerfaces 112:302–309.

Pais MP, Henriques S, Costa MJ, Cabral HN (2013) Improving the 'chain and tape' method: A combined topography index for marine fish ecology studies. Ecol Indic 25:250–255.

Pal A, Paul AK (2008) Microbial extracellular polymeric substances: Central elements in heavy metal bioremediation. Indian J Microbiol 48:49–64.

Pansini M, Manconi R, Pronzato R (2011) Fauna d'Italia. Vol. XLVI, Porifera. I, Calcarea, Demospongiae (partim), Hexactinellida, Homoscleromorpha, 2011th ed. Calderini, Milano.

Parada AE, Needham DM, Fuhrman JA (2016) Every base matters : assessing small subunit rRNA primers for marine microbiomes with mock communities , time series and global field samples. Environ Microbiol 18:1403–1414.

Patel P, Callow ME, Joint I, Callow JA (2003) Specificity in the settlement – modifying response of bacterial biofilms towards zoospores of the marine alga Enteromorpha. Environ Microbiol 5:338–349.

Patil JS, Anil AC (2005) Biofilm diatom community structure : Influence of temporal and substratum variability. Biofouling 21:189–206.

Pester M, Schleper C, Wagner M (2011) The Thaumarchaeota: An emerging view of their phylogeny and ecophysiology. Curr Opin Microbiol 14:300–306.

Pickering H, Whitmarsh D (1997) Artificial reefs and fisheries exploitation: A review of the 'attraction versus production' debate, the influence of design and its significance for policy. Fish Res 31:39–59.

Pickering H, Whitmarsh D, Jensen A (1998) Artificial Reefs as a Tool to aid Rehabilitation of Coastal Ecosystemes: Investigating the Potential. Mar Pollut Bull 37:505–514.

Pittman SJ, Brown KA (2011) Multi-scale approach for predicting fish species distributions across coral reef seascapes. PLoS One 6.

Pollet T, Berdjeb L, Garnier C, Durrieu G, Le C, Misson B, Briand J, Pollet T, Berdjeb L, Garnier C, Durrieu G, Poupon C Le, Pollet T, Berdjeb L, Garnier C, Durrieu G, Le C, Misson B, Briand J (2018) Prokaryotic community successions and interactions in marine biofilms : the key role of Flavobacteriia To cite this version : HAL Id : hal-02024255 Prokaryotic community successions and interactions in marine biofilms : the key role of Flavobacteriia HAL. FEMS Microb Ecol 94:1–13.

Pringle JH, Fletcher M (1986) Adsorption of Bacterial Surface Polymers to Attachment Substrata. J Gen Microbiol 132:743–749.

Qian PY, Lau SCK, Dahms HU, Dobretsov S, Harder T (2007) Marine biofilms as mediators of colonization by marine macroorganisms: Implications for antifouling and aquaculture. Mar Biotechnol 9:399–410.

Rageh MM, El-lakkani A, Ali MHM, El-fattah AMMA, Raafat AE (2009) Effect of high power ultrasound on aqueous solution of DNA. Int J Phys Sci 4:63–68.

Rahim SAKA, Li JY, Kitamura H (2004) Larval metamorphosis of the sea urchins, Pseudocentrotus depressus and Anthocidaris crassispina in response to microbial films. Mar Biol 144:71–78.

Raunkjær K, Hvitved-Jacobsen T, Nielsen PH (1994) Measurement of pools of protein, carbohydrate and lipid in domestic wastewater. Water Res 28:251–262.

Riedl R (1991) Fauna e flora del Mediterraneo. Dalle alghe ai mammiferi: una guida sistematica alle specie che vivono nel mar Mediterraneo. Muzzio F (ed) Padova.

Riera E, Lamy D, Goulard C, Francour P, Hubas C (2018) Biofilm monitoring as a tool to assess the efficiency of artificial reefs as substrates: Toward 3D printed reefs. Ecol Eng 120:230–237.

Riera E, Reveret C, Madelaine C, Pinel R, Mahamadaly V, Gautier Debernardi J, Mauroy B, Francour P (2019) An easy method to assess 3D underwater habitat complexity Riera. In: *ECSD5 2019*. p 14

Risso-de Faverney C, Guibbolini-Sabatier ME, Francour P (2010) An ecotoxicological approach with transplanted mussels (Mytilus galloprovincialis) for assessing the impact of tyre reefs immersed along the NW Mediterranean Sea. Mar Environ Res 70:87–94.

Roberts CM, Ormond RFG (1987) Habitat complexity and coral reef fish diversity and abundance on Red Sea fringing reefs. Mar Ecol Prog Ser 41:1–8.

Rodriguez-Prieto C, Trainito E, Ballesteros E, Boisset F, Afonso-Carrillo J (2015) Alghe e fanerogame del Mediterraneo, italiana a. Egigio Trainito (ed) Il Castello.

Romera E, González F, Ballester A, Blázquez ML, Muñoz JA (2007) Comparative study of biosorption of heavy metals using different types of algae. Bioresour Technol 98:3344–3353.

Rossi F, De Philippis R (2015) Role of Cyanobacterial Exopolysaccharides in Phototrophic Biofilms and in Complex Microbial Mats. Life 5:1218–1238.

Rouane-hacene O, Boutiba Z, Belhaouari B, Guibbolini-sabatier ME, Francour P, Faverney CR (2015) ScienceDirect Seasonal assessment of biological indices , bioaccumulation and bioavailability of heavy metals in mussels Mytilus galloprovincialis from Algerian west coast , applied to environmental monitoring §. Oceanologia 57:362–374.

S. Morin, Duong TT, Dabrin A, Coynel A, Herlory O, Baudrimont M, Delmas F, Durrieu G, Schäfer J, Winterton P, Blanc G, Coste M (2016) Long-term survey of heavy-metal pollution, biofilm contamination and diatom community structure in the Riou Mort watershed, South-West France. Enveronmental Pollut 151:532–542.

Salamone AL, Robicheau BM, Walker AK (2016) Fungal diversity of marine biofilms on artificial reefs in the north-central Gulf of Mexico. Bot Mar 59:291–305.

Salta M, Wharton JAA, Blache Y, Stokes KRR, Briand JFJ (2013) Marine biofilms on artificial surfaces : structure and dynamics. Environ Microbiol 15:2879–2893.

Sánchez-Caballero CAA, Borges-Souza JMM, De La Cruz-Agüero G, Ferse SCACA (2017) Links between fish community structure and habitat complexity of a rocky reef in the Gulf of California threatened by development: Implications for mitigation measures. Ocean Coast Manag 137:96–106.

Sanli K, Bengtsson-Palme J, Henrik Nilsson R, Kristiansson E, Rosenblad MA, Blanck H, Eriksson KM (2015) Metagenomic sequencing of marine periphyton: Taxonomic and functional insights into biofilm communities. Front Microbiol 6:1–14.

Schmid PE (1999) Fractal Properties of Habitat and Patch Structure in Benthic Ecosystems.

Serôdio J, Ezequiel J, Barnett A, Mouget JL, Meĺéder V, Laviale M, Lavaud J (2012) Efficiency of photoprotection in microphytobenthos: Role of vertical migration and the xanthophyll cycle against photoinhibition. Aquat Microb Ecol 67:161–175.

Seytre C, Clozza M, Bodilis P, Cottalorda J, Spennato G, Francour P, Hurel C, Nicolas M (2012) Études préalables à la mise en place de récifs artificiels dans les eaux de la Principauté de Monaco juillet 2012.

Sheng G, Yu H, Li X (2010) Extracellular polymeric substances (EPS) of microbial aggregates in biological wastewater treatment systems : A review. Biotechnol Adv 28:882–894.

Sherrard TRW (2017) Intertidal Structures: Coastal Engineering for Sustainability and Biodiversity. University of Southampton

Shikuma NJ, Hadfield MG (2006) Temporal variation of an initial marine biofilm community and its effects on larval settlement and metamorphosis of the tubeworm Hydroides elegans. Biofilms:1–8.

Shokry M, Ammar A (2009) Coral Reef Restoration and Artificial Reef Management , Future and Economic. Open Environ Eng J 2:37–49.

Singh AV, Vyas V, Patil R, Sharma V, Scopelliti PE, Bongiorno G, Podestà A, Lenardi C, Gade WN, Milani P (2011) Quantitative characterization of the influence of the nanoscale morphology of nanostructured surfaces on bacterial adhesion and biofilm formation. PLoS One 6:1–12.

Siqueiros-Beltrones D a., Voltolina D (2000) Grazing Selectivity of Red Abalone Haliotis rufescens Postlarvae on Benthic Diatom Films under Culture Conditions. J World Aquac Soc 31:239–246.

Siqueiros Beltrones DA, Valenzuela Romero G (2004) Benthic Diatom Assemblages in an Abalone (Haliotis spp.) Habitat in the Baja California Peninsula. Pacific Sci 58:435–446.

Slattery M (1992) Larval settlement and juvenile survival in the red abalone (Haliotis rufescens), an examination of inductive cues and substrate selection. Aquaculture 102:143–153.

Smith DJ, Underwood GJC (2000) The production of extracellular carbohydrates by estaurine benthic diatoms: The effects of growth phase and light and dark treatment. Jounal Phycol 36:321–333.

Späth R, Flamming HC, Wuertz S (1998) Sorption properties of biofilms. In: *Water Science and Technology*.

Staats N, De Winder B, Stal LJ, Mur LR (1999) Isolation and characterization of extracellular polysaccharides from the epipelic diatoms Cylindrotheca closterium and Navicula salinarum. Eur J Phycol 34:161–169.

Stal LJ, Défarge C (2005) Structure and Dynamics of Exopolymers in an Intertidal Diatom Biofilm. Geomicrobiol J 22:341–352.

Stone RB (1985) HISTORY OF ARTIFICIAL REEF USE IN THE UNITED STATES. In: *ARTIFICIAL REEFS Marine and Freshwater Applications*, 2018th ed. D'ltri FM (ed) CRC Press, Taylor & Francis Group, p 160–164

Strain HH, Manning WM, Hardin G (1944) Xanthophylls and Carotenes of Diatoms, Brown Algae, Dinoflagellates, and Sea-Anemones. Biol Bull 86:169–191.

Sueur J, Aubin T, Simonis C (2008) Equipment review: Seewave, a free modular tool for sound analysis and synthesis. Bioacoustics 18:213–226.

Sutherland TF, Grant J, Amos CL (1998) The effect of carbohydrate production by the diatom Nitzschia curvilineata on the erodibility of sediment. Limnol Oceanogr 43:65–72.

Svane I, Petersen JK (2001) On the Problems of Epibioses, Fouling and Artificial Reefs, a Review. Mar Ecol 22:169–188.

Sweet MJ, Croquer A, Bythell JC (2011) Development of Bacterial Biofilms on Artificial Corals in Comparison to Surface-Associated Microbes of Hard Corals. PLoS One 6:e21195.

Tagliapietra D, Sigovini M (2010) Biological diversity and habitat diversity: a matter of Science and perception. NEAR Curric Nat Environ Sci 88:147–155.

Tan EL-Y, Mayer-Pinto M, Johnston1 EL, Dafforn KA (2015) Differences in Intertidal Microbial Assemblages on Urban Structures and Natural Rocky Reef. Front Microbiol 6:1–14.

Taneez M, Hurel C, Mady F, Francour P (2018) Capping of marine sediments with valuable industrial by-products: Evaluation of inorganic pollutants immobilization. Environ Pollut.

Telford T (1999) Portland cement : Composition, production and properties, 2nd editio. Bye GC, Telford T (eds) Thomas Telford, London.

Tessier A, Francour P, Charbonnel E, Dalias N, Bodilis P, Seaman W, Lenfant P (2015) Assessment of French artificial reefs: due to limitations of research, trends may be misleading. Hydrobiologia 753:1–29.

Teughels W, Van Assche N, Sliepen I, Quirynen M (2006) Effect of material characteristics and/or surface topography on biofilm development. Clin Oral Implants Res 17:68–81.

Tews J, Brose U, Grimm V, Tielborger K, Wichmann M, Schwager M, Jeltsch F (2004) Animal species diversity driven

by habitat heterogeneity/diversity: the importance of keystone structures. J Biogeogr 31:79–92.

Thierry JM (1988) Artificial reefs in Japan - A general outline. Aquac Eng 7:321–348.

Tokeshi M, Arakaki S (2012) Habitat complexity in aquatic systems : fractals and beyond. Hydrobiologia 685:27–47.

Trapido-Rosenthal HG, Morse DE (1985) L-α, ω-Diamino acids facilitate GABA induction of larval metamorphosis in a gastropod mollusc (Haliotis rufescens). J Comp Physiol B 155:403–414.

Truong VK, Lapovok R, Estrin YS, Rundell S, Wang JY, Fluke CJ, Crawford RJ, Ivanova EP (2010) The influence of nano-scale surface roughness on bacterial adhesion to ultrafine-grained titanium. Biomaterials 31:3674–3683.

Turner CH, Ebert EE, Given RR (1969) Man-Made Reef Ecology. UC San Diego Libr – Scripps Collect Fish bulle:15–16.

Underwood GJC (2010) Exopolymers (Extracellular Polymeric Substances) in Diatom: Dominated Marine Sediment Biofilms. In: *Microbial Mats: Modern and Ancient Microorganisms in Stratified Systems*, 2010th ed. Seckbach J, Oren A (eds) Springer Science+Business Media, p 287–300 DOI

Underwood GJC, Fietz S, Papadimitriou S, Thomas DN, Dieckmann GS (2010) Distribution and composition of dissolved extracellular polymeric substances (EPS) in Antarctic sea ice. Mar Ecol Prog Ser 404:1–19.

Underwood GJC, Paterson DM (2003) The Importance of Extracellular Carbohydrate Production by Marine Epipelic Diatoms. Adv Bot Res 40:1–58.

Underwood GJC, Smith DJ (1998) Predicting Epipelic Diatom Exopolymer Concentrations in Intertidal Sediments from Sediment Chlorophyll. Microb Ecol 35:116–125.

UNEP (2009) An introduction to Artificial Reefs. In: *London Convention and Protocol/UNEP: Guidelines for the Placement of Artificial Reefs*. International Maritime Organization, London, p 1–8

UNEP MAP (2005) Guidelines for the placement at sea of matter for purpose other than the mere disposal (Construction of artificial reefs). Athens.

Wahl M (1989) Marine epibiosis. I. Fouling and antifouling: some basic aspects. Mar Ecol Prog Ser 58:175–189.

Wahl M, Goecke F, Labes A, Dobretsov S, Weinberger F (2012) The second skin : ecological role of epibiotic biofilms on marine organisms. Front Aquat Microbiol 3:1–21.

Warfe DM, Barmuta LA, Wotherspoon S (2008) Quantifying habitat structure : surface convolution and living space for species in complex environments. OIKOS 117:1764–1773.

Wetherbee R, Lind JL, Burke J, Quatrano RS (1998) The first kiss: Establishment and control of initial adhesion by raphid diatoms. J Phycol 34:9–15.

Wickham H, Winston C (2019) Create Elegant Data Visualisations Using the Grammar of Graphics. Packag 'ggplot2'.

Wilding TA, Palmer EJL, Polunin NVC (2010) Comparison of three methods for quantifying topographic complexity on rocky shores. Mar Environ Res 69:143–151.

Williams TW (2006) Sinking Poor Decision Making With Best Practicices - A Case Study of Artificial Reef Decision-Making in the Florida Keys. Virginia Commonwealth University

Willis SC, Winemiller KO, Lopez-Fernandez H (2005) Habitat structural complexity and morphological diversity of fish assemblages in a Neotropical floodplain river. Oecologia 142:284–295.

Xiao MEL (2014) Influence of Surface Topography on Marine Biofouling

Young GC, Dey S, Rogers AD, Exton D (2017) Cost and time-effective method for multiscale measures of rugosity, fractal dimension, and vector dispersion from coral reef 3D models. PLoS One 12:1–18.

Zardus JD, Nedved BT, Huang Y, Tran C, Hadfield MG (2008) Microbial Biofilms Facilitate Adhesion in Biofouling Invertebrates. Biol Bull 214:91–98.

ANNEXES

Annexe 1: Schéma résumant les différentes étapes de la récupération du model 3D au calcul des paramètres de complexité

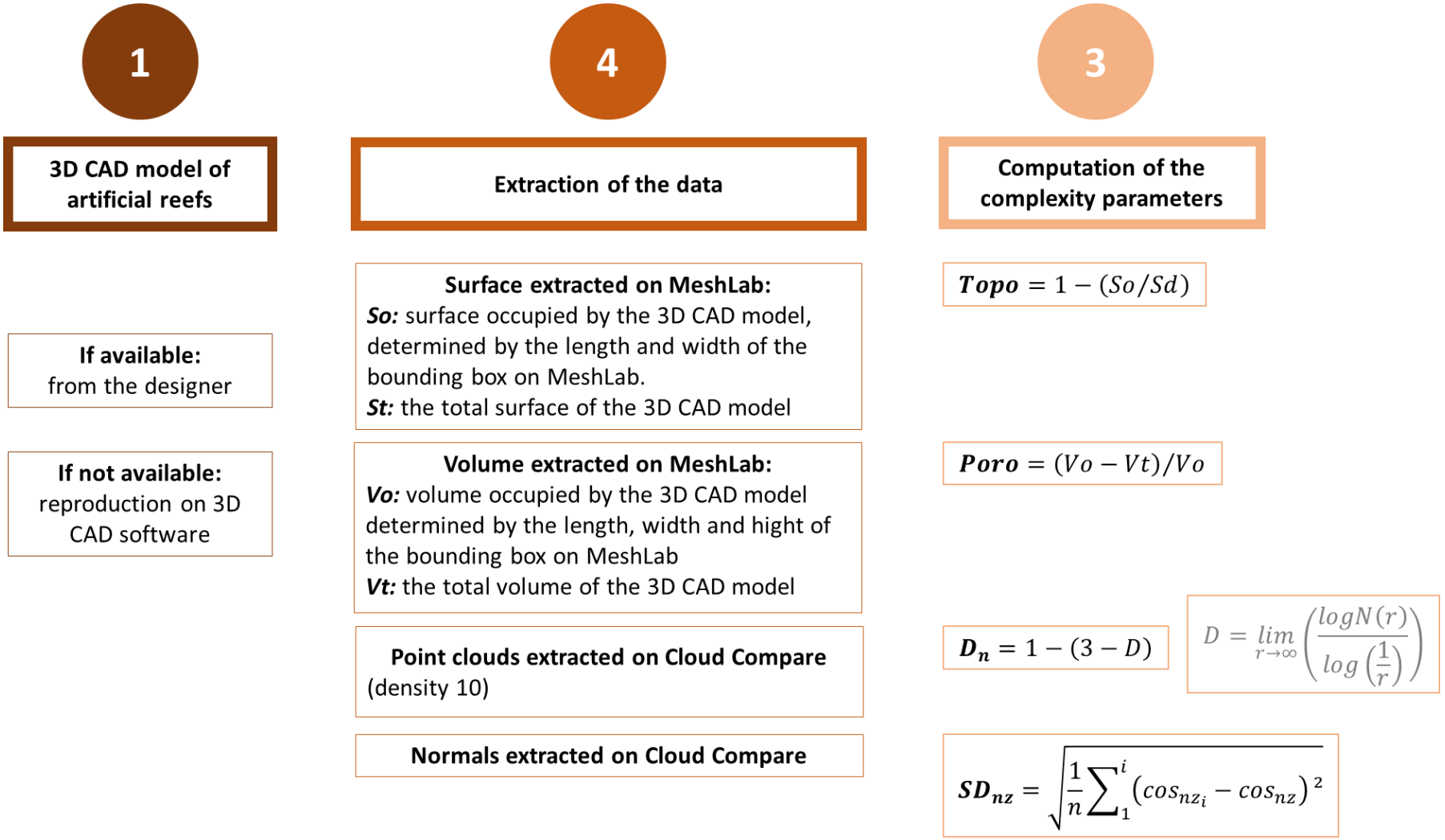

Annexe 2: Extraction des données sur MeshLab et Cloud Compare

Etape 1 : Ouvrir le modèle numérique au format STL sur Meshlab 

Etape 2 : Utiliser l'outil ''Compute Geometric Measures'' (barre de menu -> Filters -> Quality Measure and Computations -> Compute Geometric Measures)

Etape 3 : Dans la fenêtre en bas à droite récupérer les données : Mesh Bounding Box Size, Mesh Surface Area, Mesh Volume pour calculer les différents indices Poro & Topo. Veiller à contrôler l'échelle des modèles numériques (ci-après un lien vers un tutoriel pour redéfinir l'échelle sur Meshlab : https://www.youtube.com/watch?v=6psAppbOOXM)

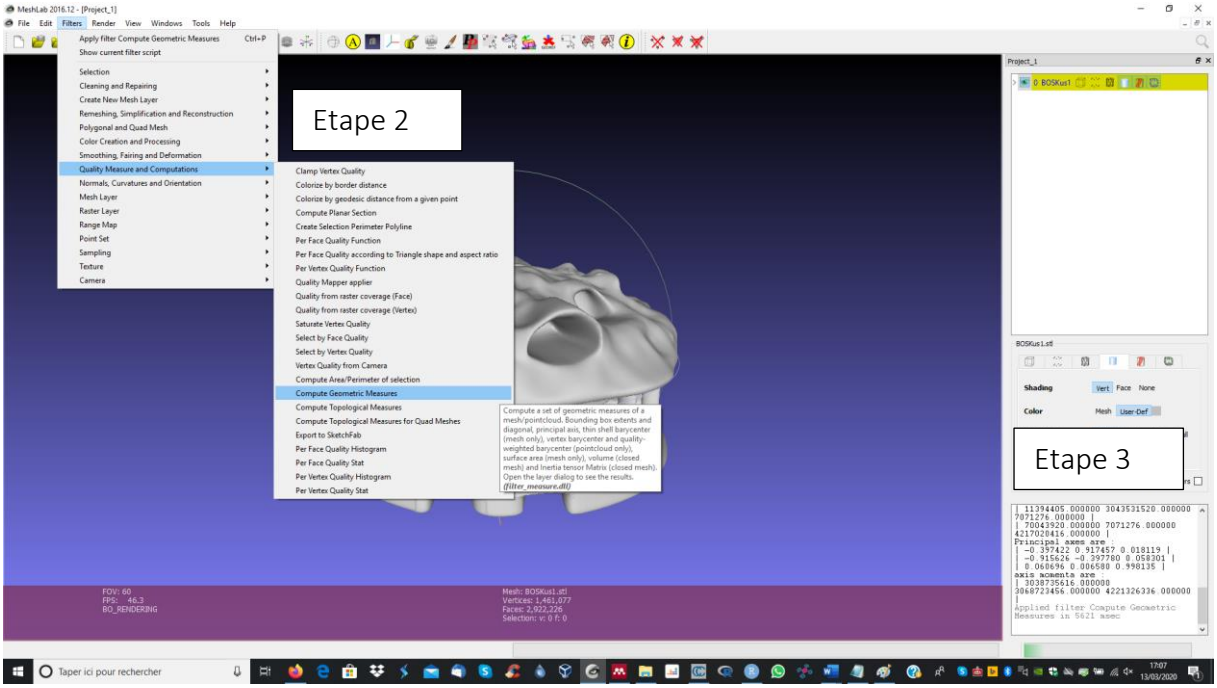

Etape 4 : Ouvrir le modèle numérique au format STL sur cloud compare  .

Etape 5 : A l'aide de l'outil "sample point on a mesh"  , extraire un nuage de points et les normales du modèle numérique. Définir le nombre de points en densité de 10 selon nos recommandations (il est important que cette densité soit la même pour tous les modèles étudiés). Cocher "generates normals" et décocher "get color from RGB or from material/texture if available" (ces données ne sont pas utiles aux calculs qui suivent).

Etape 2 : Sélectionner les nuages de points et les normales générées à partir des fichier STL 

et les sauvegarder  au format "ASCII cloud (*txt,….)".

Annexe 3 : Script R pour le calcul des paramètres de complexité

Les scripts présentés ci-dessous peuvent être utilisés pour faire le calcul de différents indices de complexité (D, ik, SDnz, et R) sur les modules numériques des récifs artificiels ou sur les surfaces des matériaux reconstitués par scanner surfacique. Au préalable il est nécessaire d'extraire à partir d'un fichier STL les nuages de points et les normales des modèles comme présenté dans l'Annexe 3.

ANNEXE 3.1 : SCRIPT RELATIF AU CHAPITRE 3 PARTIE 1 : ETUDE DE LA COMPLEXITE DES MODULES DE RECIFS ARTIFICIELS

```
# prepare the envrionment
setwd("C:/MyFile") # path where are the table with the point clouds and normal
initial.wd=getwd() # gives the address where I work
list=list.files(initial.wd) # name list of all the tables

# libraries
library(Rdimtools) # for fractal dimension

output=NULL # create an empty object « output » in which all the indexes will be combined

### create a loop to process all the indexes in a row for each table ###
for (i in 1:length(list)) {
cat(paste0("--- ",Sys.time(),"processing_",list[i]," ---/n")) # to monitor the processing time for each table.
M=read.table(paste0(initial.wd,"/",list[i]), h=T, sep=" ") # read each table of the list
P=M[,1:3] # extraction of the points from the table
N=M[,4:6] # extraction of the normal from the table

# processing of Dn
outputD=est.boxcount(P, nlevel=100, cut = c(0.1,0.9)) # the result of the function est.boxcount
Dn=1-(3-outputD$estdim)# compile the fractal dimension normalized between 0 and 1

# processing of SDnz
SDn=as.matrix(apply(N,2,sd)) # processing of the standard deviation on the director cosines
SDnz=SD[3] # SD[3] must correspond to the director cosines on the Z axe.

# compilation of the indexes in the object "output"
output=rbind(output,c(Dn,SDnz))

}

# save the data
row.names(output)=list # rename the row with the names of the AR modules
colnames(output)=c("Dn","SDnz") # rename the columns with the names of the index
write.csv2(output,"Complexity_Modules.csv")
```

ANNEXE 3.2 : SCRIPT RELATIF AU CHAPITRE 3 PARTIE 2 : ETUDE DE LA MICROTOPOGRAPHIE

```
# prepare the envrionment
setwd("C:/MyFile ") # path where are the table with the point clouds and normal
initial.wd=getwd() # gives the address where I work
list=list.files(initial.wd) # name list of all the tables

# libraries
library(Rdimtools) # for fractal dimension
library(seewave) # for rugosity

# create a function to process the squared of the number
```

```
square <- function(x){
  squared <- x*x
  return(squared)
}

### create a loop to process all the indexes in a row for each table ###
for (i in 1:length(list)) {
cat(paste0("--- ",Sys.time(),"processing_",list[i]," ---/n")) # to monitor the processing time for each table.
M=read.table(paste0(initial.wd,"/",list[i]), h=T, sep=" ") # read each table of the list
P=M[,1:3] # extraction of the points from the table
N=M[,4:6] # extraction of the normal from the table

# computation of Dn
outputD=est.boxcount(P, nlevel=100, cut = c(0.1,0.9)) # the result of the function est.boxcount
Dn=1-(3-outputD$estdim) # compile the fractal dimension normalized between 0 and 1

# computation of SDnz
SDn=as.matrix(apply(N,2,sd)) # processing of the standard deviation on the director cosines
SDnz=SD[3] # SD[3] must correspond to the director cosines on the Z axe.

# computation of ik
cos=as.matrix(apply(N,2, sum)) # sum of the director cosines on each axis
i=length(N$Nx) # number of normal
R1= sqrt((cos[1,]^2)+(cos[2,]^2)+(cos[3,]^2)) # equation of R1
ik=(i-R1)*(i-1)^-1 # equation of ik

# compuation of R
P$X2=as.factor(round(P[,1], 1)) # round the points on the X axis
vecx=aggregate(M$Z,by=list(P$X2),roughness) # the derivative second of Z curve on the X axis
meanVecx=mean(vecx$x) # mean of the derivative second of Z curve on the X axis
P$Y2=as.factor(round(P[,2], 1)) # round the points on the Y axis
vecy=aggregate(M$Z,by=list(P$Y2),roughness) # the derivative second of Z curve on the y axis
meanVecy=mean(vecy$x) # mean of the derivative second of Z curve on the Y axis
R=(meanVecx+meanVecy)/2 # computation of R

# compilation des indices dans “output”
output=rbind(output,c(ik,Dn, SDnz, R))


}

# sauvegarde du tableau au format csv
row.names(output)=list # noms des lignes du tableau correspondant aux modèles numériques
colnames(output)=c("ik","Dn","SDnz","R") # rename the columns with the names of the index
write.csv2(output,"Complexity_Surface.csv")
```

Annexe 4: Descriptif des récifs artificiels étudiés dans le chapitre 3, partie 1

Ce tableau regroupe : les noms des récifs artificiels étudiés (‘‘Module names’’), leurs noms de code (‘‘Code names’’), les références utilisées (‘‘References’’), le volume (‘‘Total volume (m3)’’), la surface (‘‘Total area deployed (m2)’’) et le volume occupé (‘‘Bounding box’’) récupérés sur Meshlab.

Code names	Module names	References	Total area deployed (m^2)	Total volume (m3)	Bounding box
BONN	Bonna	Duval - Melon 1987	158.02	10.81	6*6*4.4
BONP	Bonna pipe	© G.Fourneau	7.73	0.27	1.2*1.2*1
BOSK	3D reef	© Boskalis	27.14	1.04	2*2*1
COMN	Comin	© M.Foulquié	18.99	0.59	2.3*2.3*2.3
CR01	Cubic reef of 1m3	Charbonnel et Serre 1999	3.92	0.10	1*1*1
CR02	Cubic reef of 2m3	Charbonnel et Serre 1999	10.39	0.33	1.7*0.9*1.25
CR14	Cubic reef of 1.4m3	Charbonnel et Serre 1999	8.19	0.31	1.2*1.2*1
DALO	Dalot	© Cépralmar	33.13	2.97	2*2*2
FAKR	Fakir electri piles	Charbonnel et Bachet 2010	26.21	2.69	2.5*2.5*1.6
KHEO	Kheops	Charbonnel & Bachet 2010	25.18	1.17	2.3*2.4*1.7
NEGR	Negri column	Charbonnet et Bachet 2010	21.54	2.64	2.5*2.5*1.6
PIPE	Pipe	© M.Foulquié	46.10	1.97	2.5*1.9*1.9
SALB	Sabla	© M.Foulquié	7.70	0.29	1.2*1.2*1.2
SEAR	Sea rock	Charbonnel et Bachet 2010	11.79	1.36	2*2*1.3
STBS	Steel basket	© M.Foulquié	237.68	9.48	4*3*3.5
TIPY	Typi	© G.Fourneau	95.39	14.34	4.6*4.6*4.6

Annexe 5 : Participation à la 5ème conférence européenne sur la plongée scientifique

Cette étude présente l'utilisation de la première méthode développée pour évaluer quantitativement la structure de récifs artificiels sur la base de modèles numériques 3D (cette méthode a par la suite évolué pour correspondre à celle présentée au chapitre 3). Pour appliquer cette méthode sur le milieu naturel, il est possible d'avoir recours à la méthode de reconstruction 3D par photogrammétrie. Celle-ci permet d'effectuer des mesures à partir de photographies pour déduire la géométrie 3D d'un site à partir d'un ensemble de photographies non ordonnées. Le processus technique de photogrammétrie implique le calcul des positions, des orientations et des informations de profondeur de plusieurs images 2D pour recréer une projection 3D. Pour tester si la photogrammétrie est un moyen efficace d'accéder à la structure 3D de l'habitat, nous avons comparé le modèle numérique conçu pour l'impression 3D et le modèle numérique généré par photogrammétrie. Les premiers résultats montrent que la photogrammétrie est une méthode relativement rapide et efficace pour reconstituer près de 40% de la structure avec une seule campagne d'échantillonnage photographique en plongée sous-marine. Avec un effort d'échantillonnage plus important, le recours à cette méthode permettra d'envisager l'étude de la complexité de l'habitat de façon quantitative.

Accessible via :
https://www.researchgate.net/publication/334262796_An_easy_method_to_assess_3D_underwater_habitat_structure_Application_on_Artificial_Reef